Neutronic Design and Fuel Cycle Analysis of a Commercial-Scale Fluoride Salt-cooled High-Temperature Reactor (FHR)

Dissertation

Presented in Partial Fulfillment of the Requirements for the Degree Doctor of Philosophy in the Graduate School of The Ohio State University

By

Zuolong Zhu

Graduate Program in Nuclear Engineering

The Ohio State University

2022

Dissertation Committee

Professor Dean Wang, Advisor

Professor Tunc Aldemir

Professor Marat Khafizov

Professor Richard Vasques

Abstract

A fluoride-salt-cooled high-temperature reactor (FHR) is a novel reactor concept that combines the fuel designed for high-temperature gas-cooled reactors (HTGRs) and liquid salt coolant developed for molten salt reactors (MSRs). This combination created a reactor with high output temperatures and operating capability at atmospheric pressures makes it a leading candidate for the next generation of nuclear power plants.

This study begins by exploring and characterizing the available design space for a commercial-scale FHR. The core employs tristructural-isotropic (TRISO) particle fuel within prismatic graphite blocks as the basic fuel form, FLiBe ($2\ ^{7}LiF\text{-}BeF_2$) as the primary coolant, and a three-batch fuel cycle scheme. Numerous detailed core parameters are evaluated to determine configurations that offer acceptable neutronic performance and meet all design goals, such as assembly size, fuel channel pitch, reflector layers, and composition of burnable poison. Several core designs with different power levels are developed to meet the needs of various markets. Among the various design options, 165MWth small core design's fuel cycle is evaluated in detail (cycle length, fuel burnup, power distribution, temperature coefficients, etc.). It was found that a larger fuel channel pitch (FCP) would have a relatively harder neutron spectrum, and yield a relatively longer cycle length, lower power peaking factor (PPF), better fuel temperature coefficient (FTC), moderator temperature coefficient (MTC), and fuel and moderator temperature coefficient

(FMTC). Burnable poison (BP), Er_2O_3, can effectively reduce PPF, hold down the multiplication factor, and more importantly it can improve the MTC. The preliminary design of control blades is also presented in this paper. This stage of work provides a useful reference for applying design alternatives to improve feasible designs at the next stage.

In the second stage, on the basis of the proposed 165MWth core, this work proposes a novel core design which incorporates "fuel inside radial moderator (FIRM)" assemblies, movable moderator, and movable burnable poison. FIRM assembly provided the flexibility for adopting the movable moderator design concept. Movable moderator concept is only applied around the fresh fuel assemblies to reduce the local excess reactivity and minimize the neutron leakage. Meanwhile, a suppressed excess reactivity led to a reduced requirement for BP. An updated BP management scheme in conjunction with the movable moderator is also presented in this work. This new design can extend the fuel cycle length by approximately 45 days for an 18-month fuel cycle. Improvements were also found in PPF, discharge burnup, and temperature coefficients. In addition, various design alternatives, such as coolant, moderator, and fuel form, are tested. Each design alternative has specific advantages. However, the original design, comprising FLiBe as a coolant, graphite as a moderator, and TRISO as a fuel, has the best neutronic performance.

Dedication

For their selfless help and support throughout this journey, I dedicate this achievement to my beloved parents, teachers, families and friends.

Acknowledgments

I would like to express my sincere thanks to the many wonderful people who have supported, accompanied and encouraged me on my journey. It is a pleasure to work with my advisor, Dr. Dean Wang, who is very kind and helpful to me. There are not enough words to express my gratitude to him. His advice and guidance were a beacon of light throughout my research. It was he who taught me a great deal of principles in both research and life, and who made me a better person. There is no greater treasure in my life than these. Please accept my sincere thanks, Dr. Wang.

Also, I would like to thank my dissertation committee members – Dr. Tunc Aldemir, Dr. Marat Khafizov, and Dr. Richard Vasques. The support they have given me includes not only the kind revisions and valuable suggestions made to this dissertation, but also the help they provided in the classroom, in my work, and in other aspects of my life. I will miss that.

My sincere thanks also belong to Khizar Nasir, Pengcheng Luan, Wenyi Zhou, and Xingfeiyue Liu (don't be jealous, the names are listed alphabetically). They are the ones who provide me with the most selfless company. In my darkest and most helpless moments, they give me hope and strength. I want you to know our friendship means a lot to me. May our friendship last forever.

In addition, I would like to express my gratitude to my parents. In gratitude for the way they raised me, the unselfish love they showed, and the consistent support they gave even when my choices were seemingly innocent or willful. I know, raising a son like me can be difficult. Thank you for being so patient and perfect. I love you both!

Thank you, thank you for all the people and things I encounter, whether happy or sad, comfort or suffering, success or failure, reunion or separation... This is what I am today and have the courage to face a new world.

Vita

2010 - 2014……	B.S. Nuclear Engineering, Nanhua University
2014 – 2017……	M.S. Nuclear Engineering, University of Science and Technology of China
2018 – 2022……	Graduate Research Associate, Department of Mechanical and Aerospace Engineering, The Ohio State University

Publications

D. Wang and Z. Zhu, "A Revisit to CMFD Schemes: Fourier Analysis and Enhancement," *Energies*, vol. 14, no. 2, p. 424, Jan. 2021, doi: 10.3390/en14020424.

Z. Zhu and D. Wang, "Neutronic Design and Fuel Cycle Analysis of a Fluoride Salt-Cooled High Temperature Reactor (FHR)," *Proceedings of PHYSOR 2022*, pp. 368–377, May 2022.

Z. Zhu and D. Wang, "A Novel Core Design with Movable Moderator for a High Temperature Fluoride Salt-cooled Reactor," *Nuclear Science and Engineering*, 2022, (Accepted).

Fields of Study

Major Field: Nuclear Engineering

Table of Contents

Abstract ii
Dedication iv
Acknowledgments v
Vita vii
List of Tables xi
List of Figures xiii
List of Acronyms xvii
1. Introduction 1
1.1 Background and Motivation 1
1.2 Thesis Objective 4
1.3 Organization of the Thesis 5
2. FHR Technology Background 7
2.1 AHTR 7
2.1.1 Small modular AHTR (SmAHTR) 7
2.1.2 Full-size AHTR 13
2.2 Mark-I Pebble-bed (PB) FHR 17
2.3 FHR Test Reactor (FHTR) 21
2.4 FHR Demonstration Reactor (DR) 24
3. Design Exploration and Optimization 27
3.1 Component Description 27
3.1.1 Graphite 28
3.1.2 TRISO particle 29
3.1.3 FLiBe 31
3.2 Serpent and Calculation Setup 32
3.2.1 Serpent 32

3.2.2 Calculation setup 34
3.3 Assembly Design 36
3.3.1 Assembly design baseline 36
3.3.2 Assembly size 37
3.3.3 Coolant channel radius 38
3.3.4 Fuel channel pitch (FCP) 39
3.4 Core Design 41
3.4.1 Reflector design 41
3.4.2 Burnable poison design 43
3.4.3 Three core design schemes 46
3.5 165 MWth Small Core Design 55
3.5.1 Refueling and shuffling scheme 59
3.5.2 Cycle length 60
3.5.3 Power peaking factor 62
3.5.4 Discharge burnup 63
3.5.5 Temperature coefficient 64
3.5.6 Shutdown margin 68
4. Design Alternatives 71
4.1 A Novel Core Design with Movable Moderator 71
4.1.1 Moderator and BP configuration 73
4.1.2 Updated cycle length 75
4.1.3 Updated power peaking factor 76
4.1.4 Updated discharge burnup 77
4.1.5 Updated temperature coefficients 77
4.2 Alternative Coolant Salts 79
4.2.1 $NaF\text{-}ZrF_4$ 81
4.2.2 $^{7}LiF\text{-}ZrF_4$ 82
4.2.3 $NaF\text{-}BeF_2$ 82
4.3 Alternative Moderator or Fuel Composition 82
4.3.1 SiC 83
4.3.2 Metal hydrides 84
4.3.3 FCM 89

5. Conclusion 92
5.1 Summary 92
5.2 Recommendations for Future Work 94
Bibliography 96

List of Tables

Table 2-1. SmAHTR design parameters 8

Table 2-2. AHTR design parameters 16

Table 2-3. Mk1 PB-FHR design parameters 20

Table 2-4. Early-stage FHTR design parameters 22

Table 2-5. FHR DR design parameters 26

Table 3-1. Graphite matrix density 29

Table 3-2. Typical dimensions of TRISO particle 31

Table 3-3. Basic assembly parameters 37

Table 3-4. Major reactions that affect neutron balance 41

Table 3-5. Core parameters 48

Table 3-6. Small core design parameters 59

Table 3-7. Cycle length (days) for each scenario in stage 2 61

Table 3-8. Power peaking factors 63

Table 3-9. Accumulated discharge burnup (MWd/kgHM) 64

Table 3-10. CSDM of different control blade length 70

Table 4-1. Updated power peaking factors 77

Table 4-2. Updated accumulated discharge burnup (MWd/kgHM) 77

Table 4-3. Properties of FLiBe and the potential alternative coolant salts 80

Table 4-4. Salt density equations 80

Table 4-5. Replacing graphite with SiC, k_{inf} at BOC 84

Table 4-6. Properties of metal hydrides have potential application in FHR design 85

Table 4-7. The impact of ZrH_2 density on neutronic performance 86

Table 4-8. The impact of $YH_{1.92}$ density on neutronic performance 87

Table 4-9. Combined moderator strategy 89

List of Figures

Figure 2-1. Assembly design of SmAHTR, solid cylindrical fuel 9

Figure 2-2. The core design of SmAHTR, solid cylindrical fuel 10

Figure 2-3. Front and isometric views of a single annular fuel bead 11

Figure 2-4. Assembly design of SmAHTR, annular fuel 11

Figure 2-5. Assembly design of SmAHTR, plank fuel 12

Figure 2-6. The core design of SmAHTR, plank fuel 13

Figure 2-7. Assembly design of full-size AHTR 14

Figure 2-8. Transverse cross-section of a fuel plate 15

Figure 2-9. Cross-sectional view of the reactor vessel 16

Figure 2-10. A PB-FHR pebble fuel element 18

Figure 2-11. Mk1 pebble core geometry showing fuel pebble (green) and graphite reflector pebble (yellow) regions 19

Figure 2-12. Mk1 pebble injection channels schematic 19

Figure 2-13. Early-stage assembly design of FHTR 22

Figure 2-14. FIRM assembly design of FHTR 23

Figure 2-15. The preliminary FIRM core design of FHTR 24

Figure 2-16. Assembly design of FHR DR 25

Figure 2-17. Layout of design of FHR DR 26

Figure 3-1. Illustrative cutaway drawing of a TRISO fuel particle 30

Figure 3-2. Sensitivity analysis of model height 34

Figure 3-3. Distribution of fuel and coolant channels 37

Figure 3-4. Sensitivity study of assembly size..... 38

Figure 3-5. Sensitivity analysis of coolant channel radius 39

Figure 3-6. Fuel & coolant channels distribution of four scenarios (a) FCP = 1.78 cm; (b) FCP = 2.18 cm; (c) FCP = 2.58 cm; (d) FCP = 2.88 cm. 40

Figure 3-7. Neutron spectrum and cycle length..... 40

Figure 3-8. The number of reflector layers for the small core design (a) Layer = 0; (b) Layer = 1; (c) Layer = 4; (d) Final choice. 42

Figure 3-9. Sensitivity analysis of the number of reflector layers..... 43

Figure 3-10. Distribution of fuel, coolant, and BP channels 44

Figure 3-11. Er-167 absorption cross section 45

Figure 3-12. Sensitivity analysis of Er_2O_3 weight fraction..... 46

Figure 3-13. Three power levels of core design 47

Figure 3-14. Small core run-in cycles for both w/ and w/o 5% BP cases..... 50

Figure 3-15. Power distribution of the small core design..... 51

Figure 3-16. Medium core run-in cycles for both w/ and w/o 5% BP cases 52

Figure 3-17. Power distribution of the medium core design 53

Figure 3-18. Large core run-in cycles for both w/ and w/o 5% BP cases..... 54

Figure 3-19. Power distribution of the large core design..... 54

Figure 3-20. Updated sensitivity analysis of assembly size 56

Figure 3-21. Updated sensitivity analysis of the weight fraction of Er_2O_3 56
Figure 3-22. Fuel assembly and core design 58
Figure 3-23. Three-batch refueling and shuffling scheme 60
Figure 3-24. Refueling and shuffling of the first 7 cycles (Stage 1) 61
Figure 3-25. Power distribution of FCP = 2.88 cm 63
Figure 3-26. Temperature coefficients of the 165MWth FHR design 66
Figure 3-27. Assembly k_{inf} vs. delta T at different operating stages 67
Figure 3-28. Full core k_{eff} vs. delta T at different operating stages 68
Figure 3-29. Cold zero power keff vs. control blade length 69
Figure 4-1. Movable moderator configurations (black regions indict moderator withdrawn) 74
Figure 4-2. Comparing the k_{eff} vs. time for the equilibrium cycles 75
Figure 4-3. U-235 and Pu-239 mass density vs. time in fresh fuel assembly 76
Figure 4-4. Updated FTC, MTC, and FMTC of the FHR design (FCP = 2.0 cm) 79
Figure 4-5. Neutronic performance of different coolant alternatives 81
Figure 4-6. Cross-section of C-nat and Si-28 84
Figure 4-7. Cross-section of H-1 and Zr-90 86
Figure 4-8. Cross-section of Y-89 88
Figure 4-9. Combined moderator strategy (a) No replacement; (b) 6 cells replaced; (c) 18 cells replaced; (d) 30 cells replaced 89
Figure 4-10. Dimensional change contrast of CVD SiC and FCM fuel with nuclear graphite ATR-2E and matrix graphite 90

Figure 4-11. Neutronic performance of FCM fuel... 91

List of Acronyms

AGR	Advanced Gas-Cooled Reactor
AHTR	Advanced High-Temperature Reactor
AS	Assembly Size
BOC	Beginning of Cycle
BOL	Beginning of Life
BP	Burnable Poison
CSDM	Cold Shutdown Margin
CTC	Coolant Temperature Coefficient
CZP	Cold Zero Power
DOE	Department of Energy
EOC	End of Cycle
EOL	End of Life
FCM	Fully Ceramic Micro-encapsulated fuel
FCP	Fuel Channel Pitch
FHR	Fluoride salt-cooled High-temperature Reactor
FHR DR	FHR Demonstration Reactor
FHTR	FHR Test Reactor
FIRM	Fuel Inside Radial Moderator

FLiBe	Li_2BeF_4
FMTC	Fuel and Moderator Temperature Coefficient
FPs	Fission Products
FTC	Fuel Temperature Coefficient
GE	General Electric
GT	Gas Turbine
HTGR	High Temperature Gas-cooled Reactor
INL	Idaho National Laboratory
IPyC	Inner layer of Pyrolytic Carbon
KP	Kairos Power
LWR	Light Water Reactor
MHC	Molybdenum Hafnium Carbide
MIT	Massachusetts Institute of Technology
Mk1 PB-FHR	Mark-I Pebble-Bed FHR
MM	Movable Moderator
MSR	Molten Salt Reactor
MSRE	Molten Salt Reactor Experiment
MTC	Moderator Temperature Coefficient
MWd/kgHM	MWd per kg HM, equivalent to GWD per MTHM
NACC	Nuclear Air-Brayton Combined Cycle
OPyC	Outer layer of Pyrolytic Carbon
ORNL	Oak Ridge National Laboratory

pcm	per cent mille (10^{-5})
PB-AHTR	Pebble-Bed AHTR
PPF	Power Peaking Factor
PSG	Probabilistic Scattering Game
SDM	Shutdown Margin
SiC	Silicon Carbide
Sm-AHTR	Small Modular AHTR
SNAP	Systems Nuclear Auxiliary Power program
SNL	Sandia National Laboratories
TCR	Transformational Challenge Reactor program
TRIGA	Training, Research, Isotopes, General Atomic reactors
TRISO	TRi-structural ISOtropic
UCB	University of California at Berkeley
VC	Void Coefficient
w/	with
w/o	without
wt%	weight percent
YHx	Yttrium hydride
ZrHx:	Zirconium Hydride

1. Introduction

1.1 Background and Motivation

Fluoride-salt-cooled high-temperature reactors (FHRs) comprise a class of Gen-IV reactor designs that use graphite as a moderator and low-pressure liquid fluoride salt as a coolant with a high degree of inherent safety. It combines the advantages of prior reactor classes and thermal power plants within a single design. The basic fuel form used in FHRs is TRi-structural ISOtropic (TRISO) particle fuel within graphite moderators, which was originally designed for high-temperature gas-cooled reactors (HTGRs). For heat removal, FHRs use a liquid fluoride salt coolant, which is similar to the carrier salt in molten salt reactors, except that there is no fuel dissolved in it [1]. Compared to conventional high temperature gas-cooled reactors (HTGRs) or British advanced gas-cooled reactors (AGRs) concepts, molten salt coolant allows the FHR designs to have higher thermal efficiency, higher volumetric heat capacities, better thermal conductivity, and near atmospheric pressure operational advantages. The high-temperature operation of FHRs enables high thermodynamic efficiency for power conversion. Additionally, the atmospheric pressure operation of FHRs allows for cheaper components and prevents depressurization during accidents, enhancing safety.

The FHR technology can be traced back to the concept of molten salt reactor (MSR) proposed by Oak Ridge National Laboratory (ORNL) in the late 1940s. The MSR was then

demonstrated by the Aircraft Reactor Experiment in 1950s [2], and the graphite-moderated Molten Salt Reactor Experiment (MSRE), which was built and operated successfully between 1965 and 1969 at ORNL [3], [4]. Since 2000's there has been a renewed interest in FHRs. Forsberg et. al. proposed a molten-salt–cooled advanced high-temperature reactor, which can provide very high-temperature (750 to 1000^{o}C) heat to enable efficient production of hydrogen (H_2) or production of electricity [5]. ORNL developed a pre-conceptual design of a 125MWt fluoride-salt-cooled Small Modular Advanced High-Temperature Reactor (Sm-AHTR) [6] and a full-size 3400MWt AHTR [7], [8]. Both AHTR core designs employ the plank-type fuel and lithium-beryllium fluoride (FLiBe) coolant with 99.95% Li-7. Sm-AHTR was designed to operate for at least three years, whereas the AHTR baseline core was sized for a two-year, single-batch refueling scheme. Investigations for increasing the fuel burnup, multiple fuel batches, and lower fuel enrichments were also performed. A negative reactivity coefficient for the overall average temperature can always persist for these designs, but the moderator temperature coefficient still has the potential to become positive. Georgia Institute of Technology investigated the FHR design with plank-type fuel geometry to assist in the verification and validation of the core physics modeling and simulation methods [9]–[11]. A spectral shift technique, which can extend FHRs' cycle length and burnup was also proposed in recent years [12], [13]. Most recently, the University of California at Berkeley developed the Mark 1 pebble-bed FHR (Mk1 PB-FHR) based on previous pre-conceptual designs [14], [15], under the support of the U.S. Department of Energy (DOE) Nuclear Energy University Program (NEUP). This design can achieve around 130 MWd/kgHM burnup. The Mk1 PB-FHR has

been designed with negative fuel, moderator, and coolant temperature feedbacks, and also allows the reactor to co-fire with natural gas and utilize the nuclear air-Brayton combined cycle (NACC) system to enhance revenue. FHR designs adopting features from the British AGR and alternative decay heat cooling systems have been proposed in recent years [16]–[18]. The Massachusetts Institute of Technology (MIT) has recently proposed a prismatic graphite block type of FHR test reactor (FHTR) with a "fuel inside radial moderator (FIRM)" assembly design, which utilizes fuel manufacturing capabilities derived from HTGR experiences and incorporates operating experiences from AGR communities [19]–[21]. With the FIRM assembly design, the core is able to (1) physically separate the fuel-bearing region and central fuel cluster region and provide the flexibility to control these two areas independently; (2) reduce the amount of graphite in the spent nuclear fuel. ORNL has proposed the FHR demonstration reactor (FHR DR) as another potential near-term viable design option [22], [23], using the same fuel form and type of assembly developed for the FHTR. In addition, it should be mentioned that the Shanghai Institute of Applied Physics (SINAP) of the Chinese Academy of Sciences (CAS) has been working on an experimental liquid fuel thorium-based molten salt reactor since 2011. A 2MWt prototype, called TMSR-LF1, is currently being built in northwest China [24]. The TMSR-LF1 reactor will use a mixture of uranium and thorium as fuel (uranium in the form of UF_4 enriched in uranium-235 to less than 20% and a thorium load of about 50 kg), and a blanket of lithium-beryllium fluoride (FLiBe) with 99.95% Li-7.

In the past decades, the feasibility of FHRs as low-cost, near-term systems while maintaining full passive safety has been widely investigated. It has been demonstrated at a

pre-conceptual level that high-power liquid salt cooled reactors are feasible for FHRs with alternative fuel configurations [25]–[27]. The prismatic graphite matrix structure is one of the promising designs, offering the advantage of precise control over fuel, moderator, and coolant ratios (in contrast to pebble-bed design), as well as proven manufacturing capabilities (in contrast to plank-type design) which derive from HTGR.

1.2 Thesis Objective

The primary objective of this work is to create a feasible design for a commercial-scale FHR using the prismatic type of fuel assembly. To assess baseline performance and scalability, the initial core sizing and fuel loading design are based on TRISO particle fuel and Li_2BeF_4 (FLibe) salt coolant. Core parameters similar to the FHR DR design are referred as the starting point to do the investigation. The following tasks are performed to achieve the objective:

- Crucial core design parameters such as core size, fuel loading pattern, burnable poison design, and reflector design, are investigated in stages.
- Several core designs are proposed with varying power levels to meet market requirements.
- Detailed fuel cycle of the core designs is evaluated from different perspectives: cycle length, fuel burnup, power distribution, temperature coefficient, etc.
- Benefits of multi-batch fuel cycle are assessed.

A comprehensive technical assessment of the viable alternatives is necessary before any conclusions can be drawn about the design space and technology of a commercial-

scale FHR. Therefore, the second objective of the work is to perform sensitivity and design-alternative studies for a better understanding of the FHR design space to enable better-optimized designs in the future. In this part,

- An innovative core design incorporating FIRM assembly, movable moderator, multi-batch strategy, and burnable poison management scheme is proposed and demonstrated, and improvements are observed in all aspects of the fuel cycle analysis.
- Several alternative salt coolants such as $NaF\text{-}ZrF_4$, $^7LiF\text{-}ZrF_4$, and $NaF\text{-}BeF_2$, are investigated, and their neutronics performance is compared with the reference salt FLiBe to determine the optimal coolant option for the FHR.
- Silicon Carbide (SiC) and metal hydride are tested as moderator alternatives. Due to the fact that the prismatic type of fuel assembly has a moderating region that is physically and mechanically separate from the fuel array, alternative moderator materials are possible in the FHR design.
- Fully ceramic micro-encapsulated fuel (FCM) has potentially similar performance as TRISO coated particle fuel, however, it can be manufactured at a lower cost. This work examined replacing the TRISO fuel with this alternative as a cost-saving measure.

1.3 Organization of the Thesis

The technical content of the thesis is based on the two objectives identified in the previous section. Chapter 2 briefly reviews of the evolution of FHRs and describes existing

FHR design options and their neutronic characteristics. In chapter 3, the available design space of a commercial-scale FHR system is identified by evaluating different dimensional parameters, assembly configurations, core configurations, reflector configurations, fuel cycle parameters, etc., in the pursuit of a preliminary design that could be accepted. In section 4.1 of chapter 4, a novel core design incorporating FIRM assembly, movable moderator multi-batch strategy, and burnable poison management scheme is proposed based on the commercial-scale FHR reactor design explored in the previous chapter. Furthermore, in chapter 4, testing of alternative design options such as molten salts, moderator materials, and fuel forms is discussed. The thesis concludes with a summary and recommendations for future work in chapter 5.

2. FHR Technology Background

There have been a number of studies that provide early exploration of the potential for FHR systems and are contributing to the understanding of the possible design space for FHR systems. Chapter 2 delivers general information about a few of the existing FHR designs and provides descriptions about their basic neutronic characteristics.

2.1 AHTR

2.1.1 Small modular AHTR (SmAHTR)

The FHR design space was explored in 2010 by Oak Ridge National Laboratory (ORNL) with its pre-conceptual design for a small modular (Sm) FHR, called SmAHTR [6]. The thermal output of SmAHTR was designed to be 125 MW. It served as a reliable source of heat and power for high-temperature processes from a small and portable plant that can be easily transported to and installed at remote locations. Crucial design parameters are summarized in Table 2-1 [6].

Table 2-1. SmAHTR design parameters

Variable	**Value**
Reactor power	125 MWth
Primary coolant salt	FLiBe
Core cooling mode	Forced convection
Fuel type	TRISO
TRISO packing factor	50% or 40%
Fuel enrichment	19.75 wt%
Core uranium loading at BOL	1600–2020 kg
Core life	3–4.19 years
Moderator material	Graphite
Number of fuel assemblies	19
Core height	4 m
Core diameter	~2.2 m
Vessel height	9 m
Vessel diameter	3.5 m
Vessel wall thickness	2.5 cm

While the design evolution process was underway, various graphite-structure assembly designs were investigated. The assembly designs included solid cylindrical fuel "pins" in stringer fuel, "hollow annular fuel pins" in stringer fuel assemblies, and "solid plate" or "plank"-type fuel elements.

In the cylindrical fuel option, the enrichment of U-235 in TRISO particles with UCO kernel was 19.75 wt%, and TRISO particles were packed 50% volumetrically. The cylindrical fuel core comprised five prismatic blocks stacked vertically containing stringer fuel bundles. On each prismatic fuel block, 72 fuel pins and 19 graphite pins were present, 80 cm in height and 45 cm in width (see Figure 2-1 [6]). The graphite and fuel pins had the same radius of 1.4 cm. In the process of cooling, coolant salt filled the gap between the pins and separated them from the enclosing graphite block.

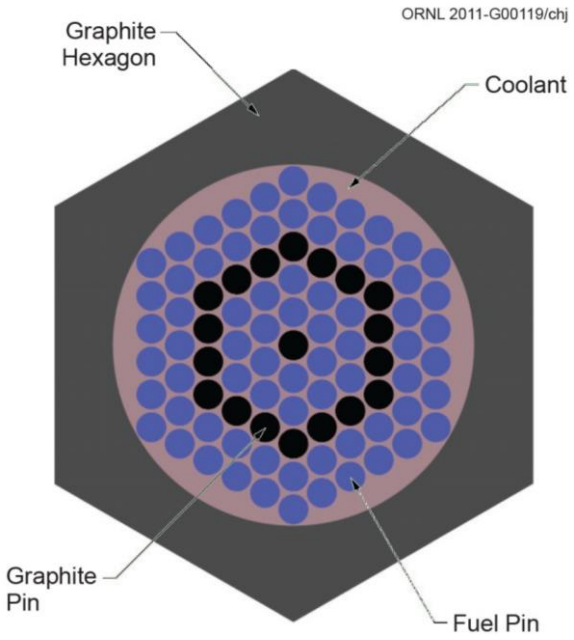

Figure 2-1. Assembly design of SmAHTR, solid cylindrical fuel

A SmAHTR core consists of 19 hexagonally close-packed fuel blocks, as shown in Figure 2-2 [6]. Based on the depletion calculations, it was estimated that this design could maintain reactivity above zero for 3.52 years. Moreover, the fuel and coolant temperature coefficients were maintained in the negative range. Nevertheless, the temperature coefficient of the moderator (graphite) was approximately greater than zero.

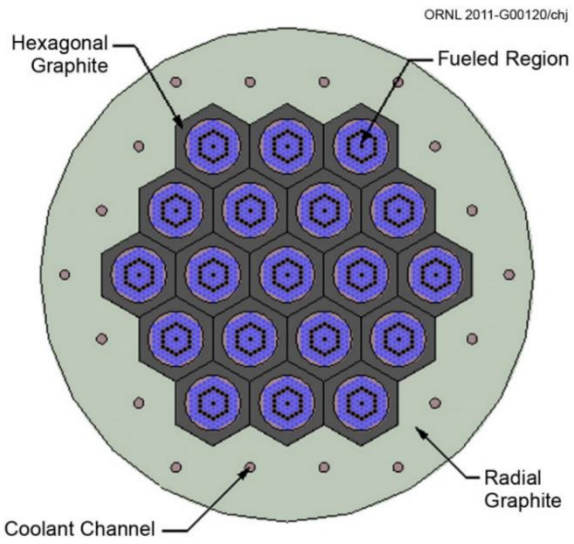

Figure 2-2. The core design of SmAHTR, solid cylindrical fuel

The geometry of an annular SmAHTR fuel core is similar to that of a cylindrical fuel, and it uses the same 80 cm high hexagonal fuel blocks stacked five high on top of each other. The major difference is that instead of using cylindrical fuel pins, the updated design adopts a fuel form that is configured into annular compacts. The annular fuel beads are approximately 5 cm high with an inner radius of 1.1 cm and an outer radius of 3.25 cm, as depicted in Figure 2-3 [6]. The fuel beads are strung vertically on a carbon-carbon composite vertical tie rod. The same graphite hexagonal block is used to enclose 15 annular fuel rods and 4 solid graphite rods (see Figure 2-4 [6]). Based on the design, 1,806.7 kg of uranium was loaded into the reactor, which was 16.1% higher than the amount of uranium required by the solid cylindrical fuel design (1,556.4 kg). In addition, the annular fuel core variant was calculated to become subcritical after 4.19 years. Nevertheless, the moderator temperature coefficient remains slightly above zero.

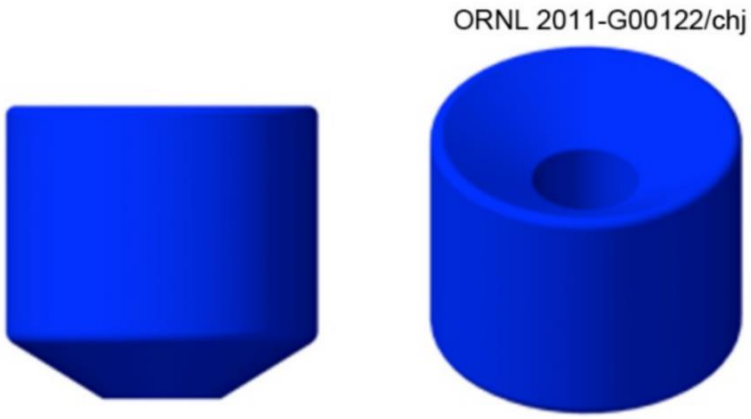

Figure 2-3. Front and isometric views of a single annular fuel bead

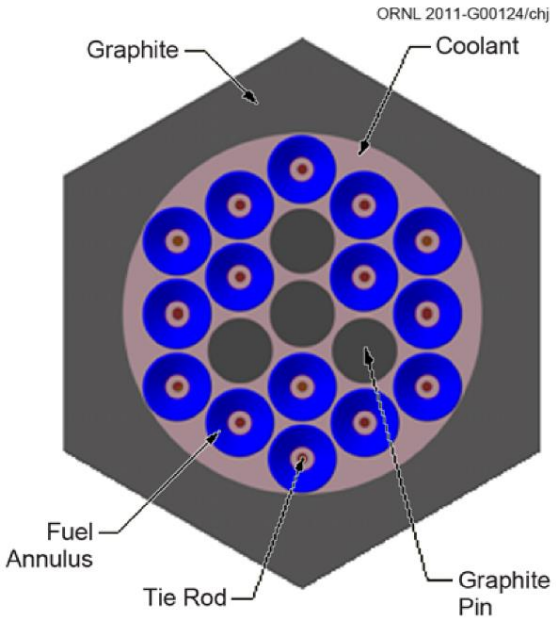

Figure 2-4. Assembly design of SmAHTR, annular fuel

Compared with the first two assembly design geometry evaluations, the third assembly design geometry evaluated for SmAHTR was significantly different. As shown in Figure 2-5 [6], the fuel is configured into full core height (4 m) planks mounted on a

carbon-carbon composite frame that maintains a flat-to-flat width of 45 cm. Three fuel blocks were included in each assembly, with six fuel plates contained in each block. The length and thickness of the fuel slab were 23.4 and 2.8 cm, respectively. A 2 mm thick unfueled sleeve covered the whole slab to protect it from erosion. Flow-induced vibration was eliminated by using unfueled spacer ridges spanning the length of each fuel plate. Sensitivity analyses were conducted by altering the fuel loading on the planks and the number and thickness of the planks. With a volumetric packing fraction of 40% and a loading of 15.4 kg of uranium (19.75 wt % U-235), the longest cycle length was 3.08 years. Figure 2-6 shows the layout of the plank-fuel core [6].

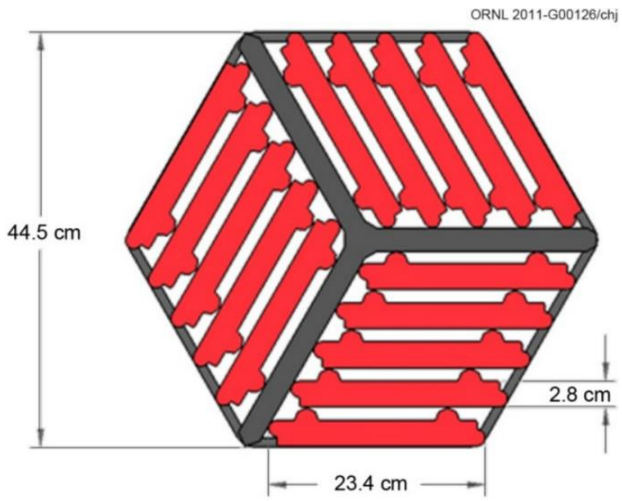

Figure 2-5. Assembly design of SmAHTR, plank fuel

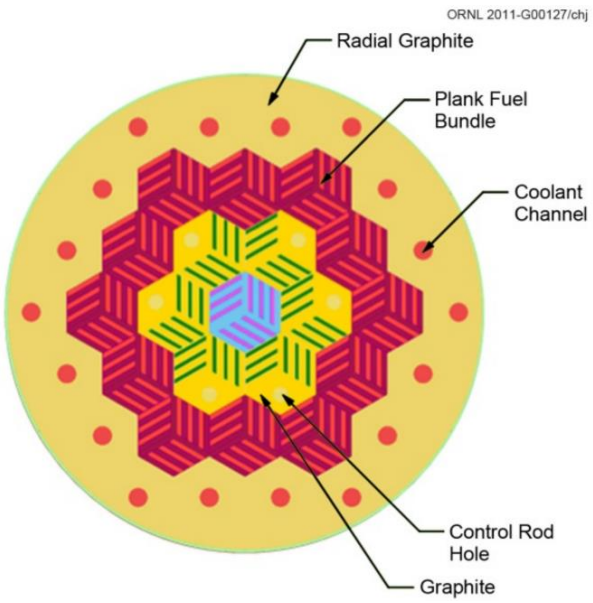

Figure 2-6. The core design of SmAHTR, plank fuel

2.1.2 Full-size AHTR

Full-sized AHTR [7] is a scaled-up version of SmAHTR that produces 3400 MWth and is intended to be used as a centralized electricity generating facility. Full-size AHTR uses FLiBe as its primary coolant salt and a plank-type assembly as its reference assembly configuration, similar to that described in the previous section. The major changes to the structure were that the control rod no longer occupied the space of the fuel slabs, and the full-size AHTR induced a Y-shaped control blade slot at its center (see Figure 2-7 [7]).

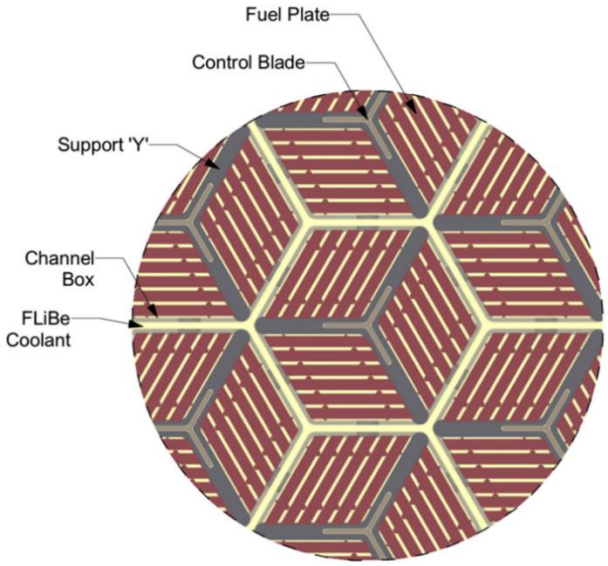

Figure 2-7. Assembly design of full-size AHTR

Moreover, the fuel plate's design changed significantly. The SmAHTR design embedded the TRISO particles uniformly in the graphite compact, regardless of the fuel design. For the full-size AHTR, two distinct regions were present on the fuel plate: a fuel stripe and a central matrix (Figure 2-8 [7]). The updated design provided increased moderation and could improve the core's thermal-hydraulic performance due to better cooling.

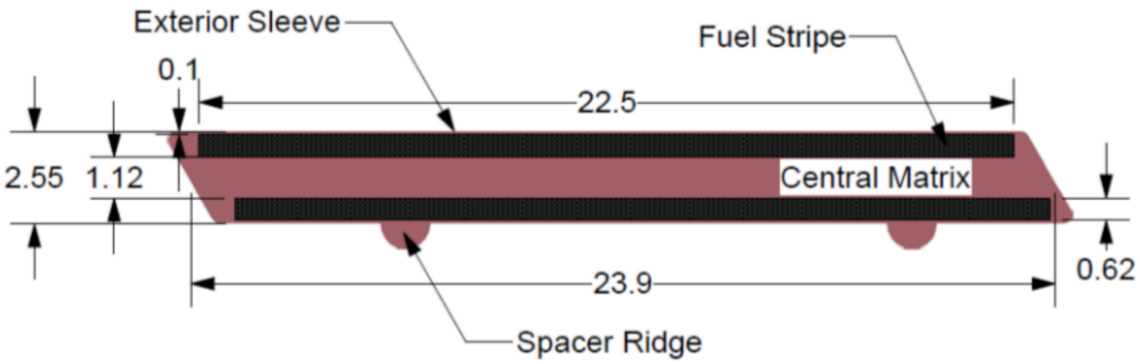

Figure 2-8. Transverse cross-section of a fuel plate

The height of the fuel assembly was 6 m, of which 5.5 m was the active fuel region. Assembly widths remained at 45 cm, while gaps between adjacent assemblies increased to 1.7 cm and were filled with coolant salt. The reference core for the 3400 MWh AHTR consisted of 252 fuel assemblies arranged in a hexagonal lattice with approximately cylindrical shapes (see Figure 2-9 [7]). Table 2-2 summarizes the design parameters of full-size AHTR [7].

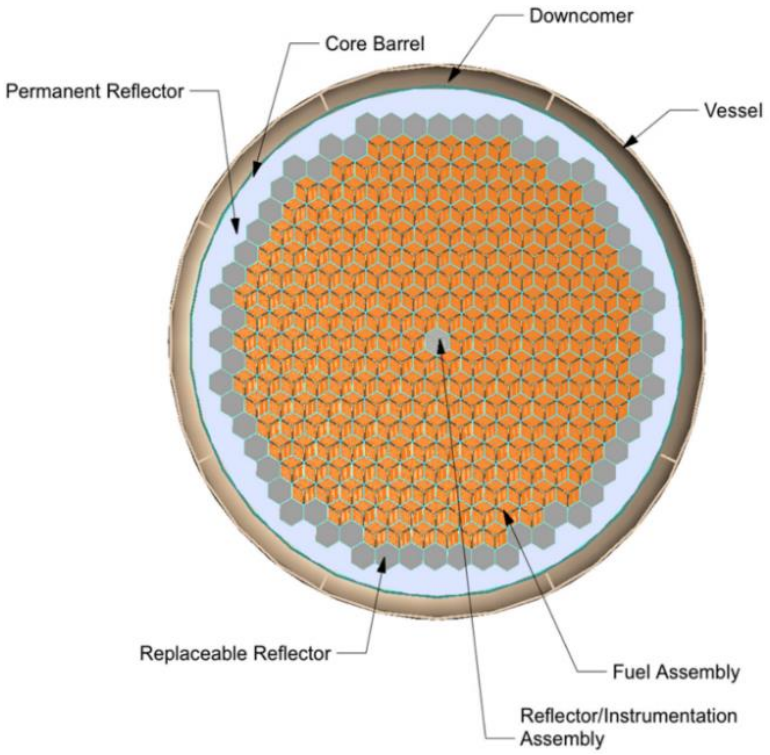

Figure 2-9. Cross-sectional view of the reactor vessel

Table 2-2. AHTR design parameters

Variable	Value
Reactor power	3400 MWth
Exterior vessel diameter	10.48 m
Vessel height	17.7 m
Equivalent core diameter (fueled region)	7.81 m
Core height (fueled region)	5.5 m
Primary coolant salt	FLiBe
Fuel type	TRISO
TRISO packing factor	40%
Fuel enrichment	19.75 wt%
Mass of fissile	6.5 MT
Fuel cycle length (once-through)	2.2 years
Moderator material	Graphite
Number of fuel assemblies	252
Inlet coolant temperature	650 ℃
Outlet coolant temperature	700 ℃

2.2 Mark-I Pebble-bed (PB) FHR

The University of California, Berkeley (UCB) developed a pre-conceptual design of the Mark-I pebble-bed (PB) FHR in 2014 [14], [15]. The utilization of a nuclear air-Brayton combined cycle (NACC) based on a modified general electric (GE) 7FB gas turbine (GT) is a significant innovative element of this design compared to other FHR systems. For of power reactors operating solely with nuclear heat, the power output was 100 MW (electric). However, when natural gas was injected (co-firing), the power output increased by a factor of 1.5 (242 MW). Additionally, due to the high thermal efficiency of the NACC system, the steam-bottoming condenser of the Mk1 PB-FHR required 60% less cooling water than a conventional light water reactor (LWR), and due to this feature, the Mk1 PB-FHR could be used in water scarce areas.

Fuel pebbles were 3.0 cm in diameter in the Mk1 PB-FHR, half the size of those used in conventional helium-cooled PB reactors. Fuel particles were uniformly distributed in the spherical shell area of the fuel pebbles. Furthermore, pebbles had a high-density graphite surface and a low-density graphite core, as shown in Figure 2-10 [14]. In each Mk1 pebble, 1.5 g of uranium (19.9 wt% U-235) was encased in 4730 coated particles. Fuel layers were packed at a volumetric fraction of 40%.

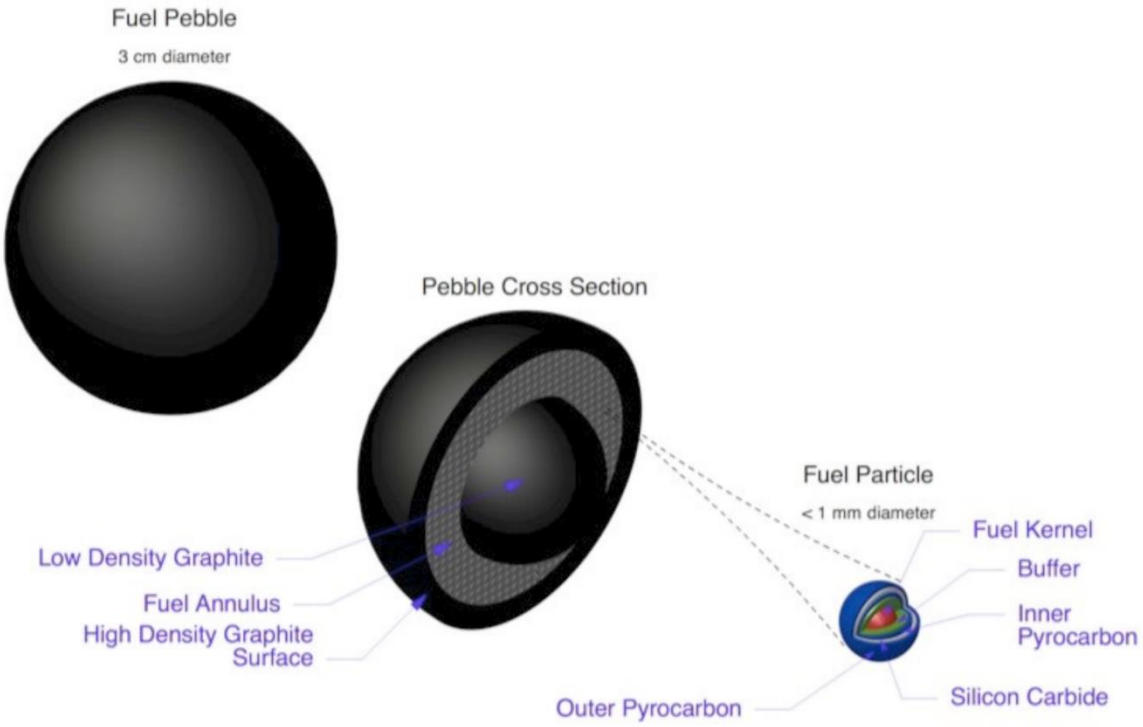

Figure 2-10. A PB-FHR pebble fuel element

An annular pebble-bed core geometry was used in the Mk1 PB-FHR, which consisted of two radial layers, an inner area of fuel pebbles homogeneously mixed, and a thinner outer region of graphite reflector pebbles (see Figure 2-11 [14]). Four-pebble injection channels were placed at the bottom of the core because the density of coolant salt was higher than that of fuel and reflector pebbles (see Figure 2-12 [14]). As the fuel was continuously injected, the pebbles moved upward slowly during the operation, and the average residence time was 2.1 months. Over time, the spent fuel was removed from the core through an annular slot located at the top.

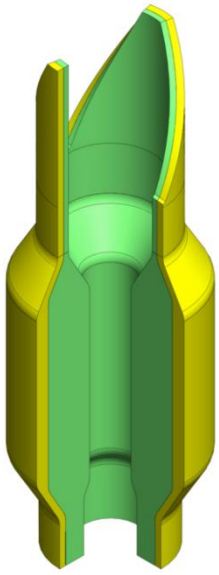

Figure 2-11. Mk1 pebble core geometry showing fuel pebble (green) and graphite reflector pebble (yellow) regions

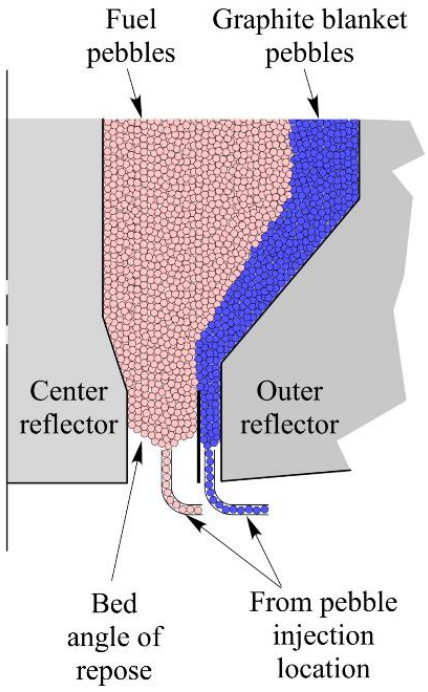

Figure 2-12. Mk1 pebble injection channels schematic

A summary of the key design parameters of the Mk1 PB-FHR is presented in Table 2-3 [14], [15]. With the co-firing capability of the Mk1 design, its most significant feature is to change the value proposition for nuclear power. The new value proposition appeared from additional revenues earned by providing flexible grid support services in addition to base-load electrical power generation.

Table 2-3. Mk1 PB-FHR design parameters

Variable	Value
Thermal power	236 MWth
Base-load net electrical power output	100 MWe
Base-load thermal efficiency	42.5%
Co-firing net electrical power output	241.8 MWe
Co-firing efficiency (gas-to-peak-power)	66.4%
Fuel enrichment	19.90%
Fuel discharge burnup	180 MWt-d/kg
Fuel full-power residence time in core	1.38 years
Reactor vessel diameter	3.5 m
Reactor vessel height	12.0 m
Inner reflector radius	0.35 m
Outer radius of fuel pebble region	1.05 m
Outer radius of graphite pebble region	1.25 m
Volume of active fuel region	10.4 m^3
Primary coolant salt	FLiBe
Fuel type	TRISO
TRISO packing factor	40%
Moderator material	Graphite
Inlet coolant temperature	600 ℃
Outlet coolant temperature	700 ℃
Number of fuel pebbles in core and defueling chute	470,000
Number of graphite pebbles in core and defueling chute	218,000

2.3 FHR Test Reactor (FHTR)

A design for an FHR test reactor (FHTR) was developed by the Massachusetts Institute of Technology (MIT) in 2016 [20], [21]. It was intended to be the first step toward developing a commercially viable FHR design. Therefore, the materials used and other parameters were largely derived from technologies that had been successfully demonstrated. The FHTR's objectives were to: (1) demonstrate the technical viability of an FHR, (2) develop the safety and licensing basis for a commercial FHR, and (3) test structures, fuels, and coolants.

The prismatic-block graphite matrix structure was selected for use in the FHTR since it allows for very precise and consistent control of the fuel, moderator, and coolant volume fractions within the core (in contrast to pebble fuel). Similar graphite assembly structures had been manufactured and operated successfully with HTGRs for many years (as opposed to plate-type fuel). At the early stages of the design of the FHTR, the reactor was designed to generate 20 MW of thermal power. Furthermore, TRISO fuel with UCO kernel embedded within a cylindrical graphite matrix is the basic fuel form. The packing fraction of TRISO particles is 35 vol%, while the uranium-235 enrichment is 19.5 at%. Furthermore, FHTR aims to achieve a six-month cycle length. The key aspects of the early stage FHTR core are summarized in Table 2-4 [20], [21]. Furthermore, the assembly design of the FHTR is illustrated in Figure 2-13 [20], where light blue represents salt coolant, gray represents graphite, and black and purple represent the fuel rod.

Table 2-4. Early-stage FHTR design parameters

Variable	Value
Thermal power	20 MWth
Fuel form	UCO-kernel TRISO
Assembly type	Prismatic graphite block
Fuel enrichment	19.5 a% U-235
Core outlet temperature	700 ℃
Number of fuel assemblies	54
Assembly flat-to-flat width	24.8 cm
Assembly pitch	25 cm
Fuel/coolant channel radius	8 mm
Fuel/coolant channel pitch	1.8 cm
Active core height	1.35 m
Outer reflector thickness	0.25 m
Inner reflector thickness	0.25 m
Axial reflector thickness	0.15 m
Core width (flat-to-flat)	2.45 m
Core height	1.65 m

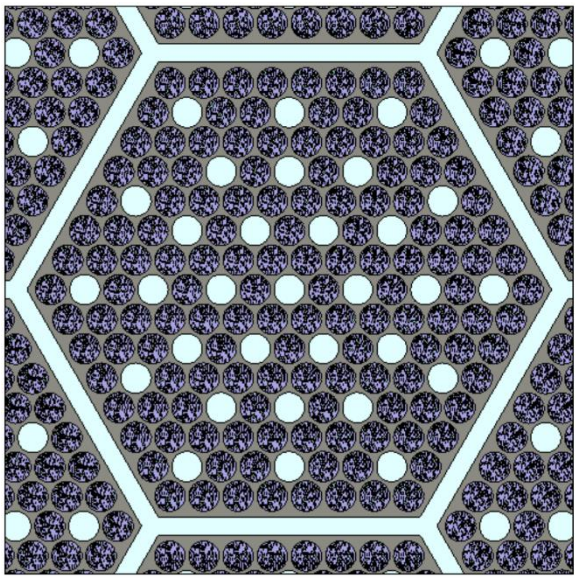

Figure 2-13. Early-stage assembly design of FHTR

The fuel inside radial moderator (FIRM), which geometrically separates the fuel from the moderator, was introduced later (see Figure 2-14 [20]). The FIRM design increased the volumetric fraction of the moderator graphite in each assembly while condensing all channels (fuel and coolant) into the center to ensure structural separation between the fuel and moderator. Additionally, the number of fuel channels was reduced from 138 to 60, and the number of coolant channels was reduced from 31 to 24. For additional cooling, irradiation, and remote manipulation purposes, a central hole of radius 2.1 cm was added to assemblies. To reduce the power peaking factor at the fuel beginning of life (BOL), the enrichment of the innermost ring of fuel assemblies was reduced to 9.75 wt%. The layout of the preliminary FHTR core is shown in Figure 2-15 [20].

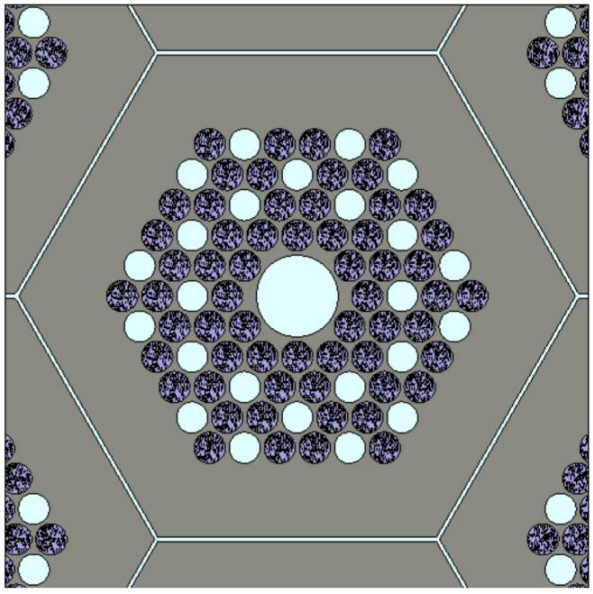

Figure 2-14. FIRM assembly design of FHTR

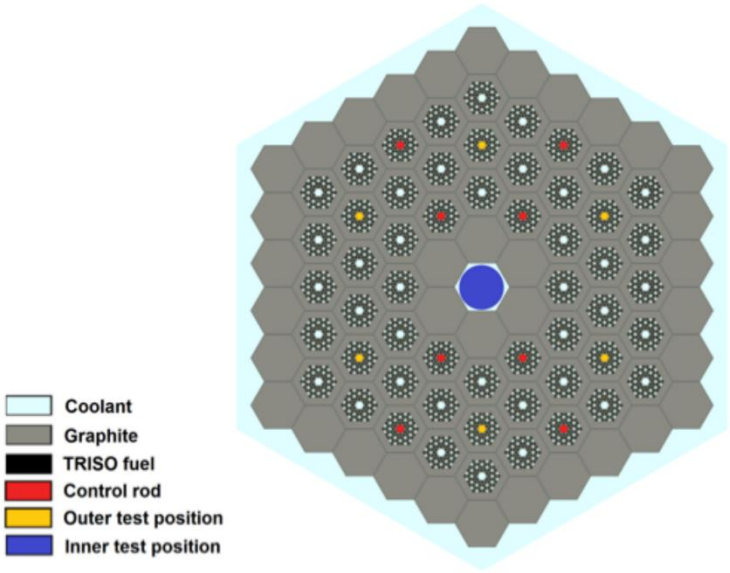

Figure 2-15. The preliminary FIRM core design of FHTR

2.4 FHR Demonstration Reactor (DR)

A demonstration reactor design for FHRs was developed by Oak Ridge National Laboratory in 2017 [22], [23]. This design aims to build a low-cost, near-term system for demonstrating technology solutions. Similar to the FHTR design, this design incorporates low-risk technologies that have been identified from previous experimental and design efforts. This plant is designed to produce 100 MWth thermal output, using hexagonal fuel arrangements with TRISO fuel in compacts within a graphite matrix as the primary fuel form and FLiBe as the primary coolant. Moreover, FHR DR should have the flexibility to be capable of testing different types of coolant salts and fuel forms within the core.

Similar to FHTR, FHR DR utilized the same fuel form, consisting of TRISO fuel with a UCO kernel embedded within a cylindrical graphite matrix with a packing factor of 35%. In addition, the enrichment of uranium-235 reduced from 19.9% to 15.5%. The width

of the FHR DR's fuel assembly (from face-to-face) was 46 cm, containing 180 fuel compacts, 109 coolant channels, 6 burnable poison rods, and 3 structural tie rods (Figure 2-16 [22]). The core was composed of 18 hexagonal fueling positions and one central irradiation position. The reflector assemblies may be converted into test positions as required. Figure 2-17 illustrates the layout of the FHR DR core [22]. Table 2-5 summarizes the primary reactor parameters [22], [23].

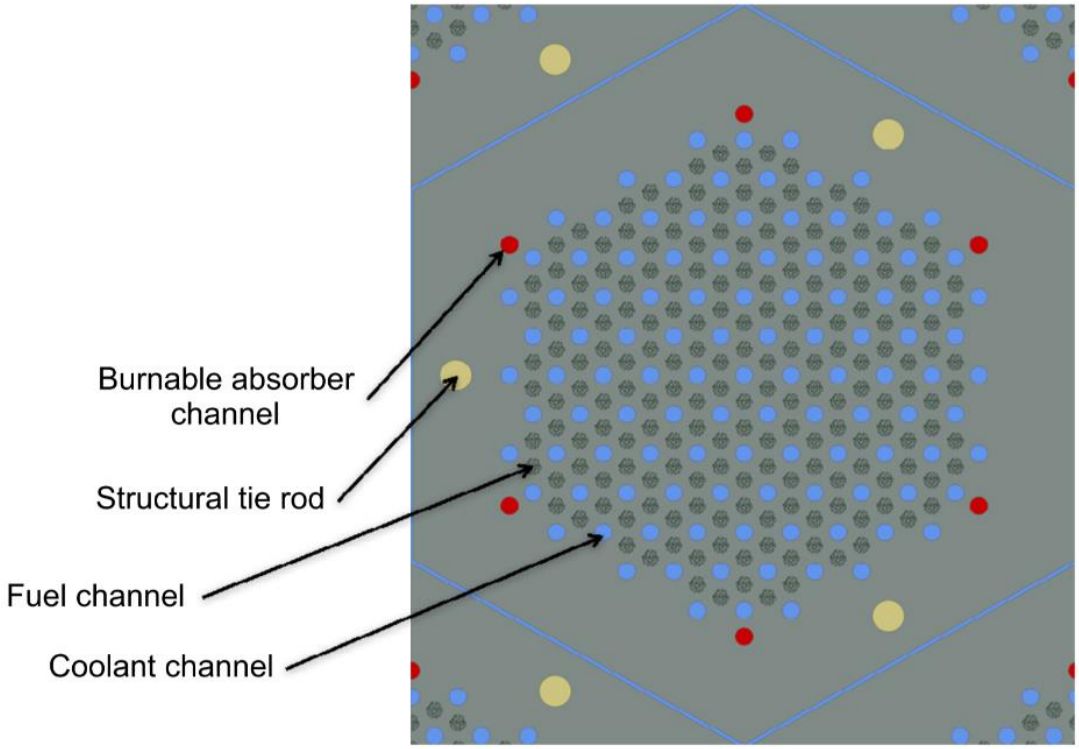

Figure 2-16. Assembly design of FHR DR

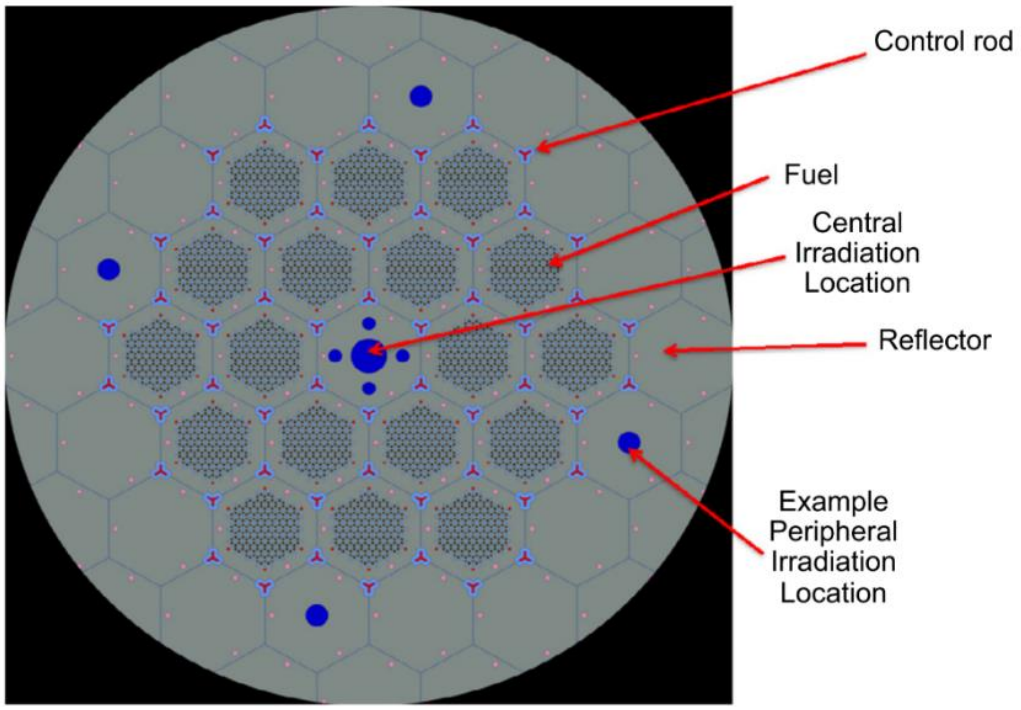

Figure 2-17. Layout of design of FHR DR

Table 2-5. FHR DR design parameters

Variable	Value
Reactor power	100 MWth
Targeted net thermal efficiency	42 %
Primary coolant	FLiBe
Lithium-7 enrichment level	99.995 %
Fuel type	$UC_{0.5}O_{1.5}$ coated particle
Fuel packing	30-40 %
^{235}U enrichment	15.5 % (baseline)
Reflector material	Graphite
Core structural material	C/C composites
Typical refueling interval	12-18 months
Mixed mean core outlet temperature	701 ℃
Core inlet temperature	660 ℃
Number of fuel assemblies	18 fueled
Core fueled height	2.61 m
Core pressures drop for normal operation	60 kPa

3. Design Exploration and Optimization

To arrive at a preliminary design that can be accepted, Chapter 3 identifies the available design space of a commercial-scale FHR system. Section 3.1 of this chapter describes the physical properties of major components in order to ensure an accurate model of the reactor core. Section 3.2 contains information regarding the simulation tool Serpent as well as the calculation setup used in this study. Detailed sensitivity analyses of multiple dimensional parameters are presented in section 3.3. Three core design schemes with varying levels of power are presented in section 3.4. In section 3.5, an in-depth analysis of small core design is presented.

3.1 Component Description

The FHR integrates several existing technologies in a novel manner. Accurately modeling the primary components of the core is essential for producing the neutronic behavior of the core reliably. Additionally, first, their physical properties should be described to model them and gain a deeper understanding of the results obtained with the code.

3.1.1 Graphite

In FHR designs, graphite is an integral part of the fuel elements and provides thermal and neutron shielding, channeling for fuel, coolant, and control and safety shut-off devices. Several exceptional nuclear physical properties of graphite, including its high moderating and reflecting properties, relatively low atomic mass, low neutron absorption cross-section, high mechanical strength, chemical stability, thermal shock resistance, high machinability, and lightweight, make it an ideal moderator for FHRs.

Crystallographically perfect graphite has a density of 2.266 g/cc [28]. The density of synthetic graphite, however, rarely exhibits a density of $>$ 2.0 g/cc, particularly for large graphite blocks used in nuclear reactors. In this work, graphite is assumed to have an isotropic structure. A great deal of research has been conducted on graphite-moderated reactor designs. Data on the density of graphite blocks used in various studies are summarized in Table 3-1. The benchmark value of the high-temperature gas-cooled moderator graphite is 1.75 g/cc [29], which is selected as the reference density in the preliminary study in sections 3.3 and 3.4.

Based on a study conducted by Idaho National Laboratory (INL) in 2016 [30], [31], high-density graphite moderators can be an alternative option for graphite-moderated reactors in the future. With high-density graphite moderators, fuel-to-moderator ratios can be achieved in a relatively smaller volume, allowing for a more compact fuel assembly and core structure. The reference graphite density for detailed 165 MWth small FHR core design (section 3.5) at T_0 =22.6℃ is ρ_0 =1.8885 g/cc. The change in density with temperature can be calculated by using the following formula [30]:

$$\alpha(T) = 4.812 \times 10^{-6} + 1.145 \times 10^{-9}(T + 30), \quad (3\text{-}1)$$

$$\varepsilon(T) = \alpha(T) \cdot (T - T_0), \quad (3\text{-}2)$$

$$\rho(T) = \frac{\rho_0}{(1+\varepsilon(T))^3}, \quad (3\text{-}3)$$

Where, α is the mean thermal expansion coefficient, ε is the thermal strains, and ρ is the density.

Table 3-1. Graphite matrix density

Countries	**Density of Matrix Graphite (g/cc)**
USA	1.75 [29], [32], near 1.8 [33], 1.76-1.78 [34], 1.85 [35], 1.89 [30]
UK	1.805 [36], 1.81 [37]
China	1.781 [38], 1.70-1.85 [39]
Germany	1.78 [40]
South Korea	1.6-1.76 [41]
Japan	1.70 [42]

3.1.2 TRISO particle

Heavy metal loads are carried by TRi-structural ISOtropic (TRISO) fuel. Additionally, TRISO particle comprises five distinct regions, as shown in Figure 3-1 [43]. A fuel kernel containing nuclear fuel is located at the center of a particle, which typically can be oxide, carbide, or oxycarbide. Kernels are encapsulated by four concentric layers: a porous graphite buffer, an inner layer of pyrolytic carbon (IPyC), a ceramic layer of silicon carbide (SiC), and an outer layer of pyrolytic carbon (OPyC). The porous graphite layer attenuates recoiling fission particles and accommodates internal fission gas accumulation and kernel dimension changes. The SiC layer acts as the particle's primary pressure vessel, enduring stresses due to internal gas pressure increases, as well as acting as a diffusion

barrier to prevent gaseous and metallic fission products (FPs) from escaping. The PyC layers protect the SiC layer from chemical attack during TRISO particle operation, while the IPyC layer protects the fuel kernel from corrosive gases used to deposit the SiC layer [43]. Each micro-sphere acts as a mini-pressure vessel, adding robustness to the reactor fuel system.

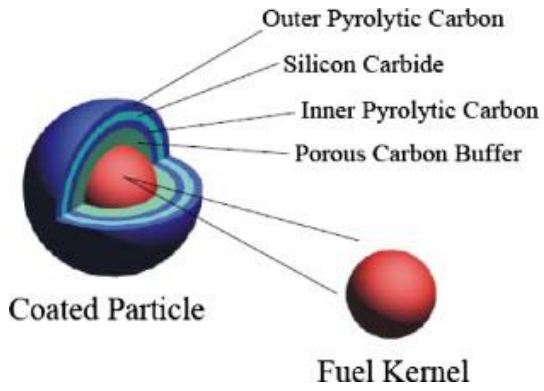

Figure 3-1. Illustrative cutaway drawing of a TRISO fuel particle

The fuel form studied in this work consists of TRISO particles embedded within cylindrical graphite compacts with packing fractions of 0.35. Additionally, TRISO kernel is composed of 9.5% enriched $UC_{0.5}O_{1.5}$. The features mentioned in the previous paragraph make TRISO fuels structurally superior to traditional reactor fuels in terms of resistance to neutron irradiation, corrosion, oxidation, and high temperatures. Each particle functions as its own containment system, allowing them to function safely under extreme reactor operating conditions. More than 70 projects are underway in the United States. The

dimensions of TRISO particles are summarized in Table 3-2. The dimensions referred to in this study are obtained from the benchmark specifications for HTGR [29].

Table 3-2. Typical dimensions of TRISO particle

Item	[29]	[35]	[43]	[44]	[45], [46]
Outer radius (mm)	0.455	0.425	0.460	0.425	0.425
Fuel Kernel radius (mm)	0.25	0.21	0.25	0.21	0.21
Coating materials	Buffer/IPyC/SiC/OPyC				
Coating thickness (mm)	0.09/0.04/0.035/0.04	0.1/0.04/0.035/0.04	0.095/0.04/0.035/0.04	0.1/0.04/0.035/0.04	0.1/0.04/0.035/0.04
Coating densities (g/cc)	1.05/1.9/3.18/1.9	1.05/1.9/3.19/1.9	1.1/1.7/3.2/1.7	1.05/1.9/3.19/1.9	1.05/1.9/3.19/1.9

3.1.3 FLiBe

Molten salt FLiBe (2 ^{7}LiF-BeF_2) is used as the primary coolant in this study. As this study focuses on the neutronic characteristics of the salt instead of its thermal and hydraulic properties, only single-phase liquid salt conditions were considered throughout the simulation.

FLiBe (2 ^{7}LiF-BeF_2), with melting and boiling points of 458 and 1400 ℃, respectively, allows for a substantial margin of safety for nominal operating conditions (650 ℃ inlet / 700 ℃ outlet) of the FHR design. Additionaly, FLiBe is characterized by high passive safety, atmospheric operating pressure, high thermal efficiency, high moderating ratio, and high heat capacity. Moreover, FLiBe can act as a neutron moderator

due to its relatively low average atomic mass. Therefore, both the coolant temperature coefficient (CTC) and void coefficient (VC) are either negative or negligible [47], [48]. Li^7 in FLiBe is enriched to 99.995 % to minimize the challenge of tritium production, and it is required to develop a tritium management technology that is cost-effective and technically feasible to deploy commercial FHRs.

A combination of experimental data and precise constitutive relationships can be used to characterize the density of FLiBe salt liquids [49]. The temperature-dependent liquid density of FLiBe was precisely measured with an error of < 0.05 % for the temperature range from 514.5 to 820.3 ℃. The density of FLiBe linearly depends on temperature, and the relationship can be calculated by the following equation [49]:

$$\rho(T) = -0.4884 \cdot T + 2413, \tag{3-4}$$

Where ρ is the density of FLiBe, in kg/m^3, and T is the temperature, in K.

When the reciprocal temperature increased, FLiBe's viscosity decreased exponentially. The following equation [49] describes an experimentally determined correlation, although its uncertainty is approximately 20%.

$$\mu(T) = 1.16 \times 10^{-4} \cdot e^{\frac{3755}{T}}, \tag{3-5}$$

Where μ is the viscosity of FLiBe, in Pa · s, and T is the temperature, in K.

3.2 Serpent and Calculation Setup

3.2.1 Serpent

Serpent is a multi-purpose three-dimensional continuous-energy Monte Carlo neutron and photon transport code, developed at VTT Technical Research Centre of

Finland since 2004 [50]. The predecessor of Serpent is known as the "probabilistic scattering game (PSG)" from 2004 to 2008 [51]. Several universities and research organizations first implemented the pre-release version of Serpent in October 2008. Afterward, the stable version Serpent 1.0.0 was submitted to the OECD/NEA Data Bank for public distribution and released in May 2009. RSICC distribution to North America started one year later.

Nevertheless, Serpent 1's limitations became increasingly apparent over time. First, Serpent 1 employed a methodology developed over a short period without a systematic approach. Continual additions of new calculation routines made it challenging to maintain the program structure. Second, parallelization based on distributed memory MPI became a major limitation [52]. To solve these issues, research activities for Serpent 2 were started in 2010. The primary objective for the development of Serpent 2 was to extend the applicability of the method from 2D assembly-level calculations to 3D full-core issues with hundreds of thousands of depletion zones without imposing any limits on parallelization. Various optimization modes introduced for small- and large-scale burnup calculations, and shared memory techniques (OpenMP) were employed to distribute the neutron histories between CPU cores without increasing overall memory requirements.

Currently, Serpent 2 is used in various applications such as (1) reactor modeling, (2) generation of group constants, (3) coupled multi-physics applications and Kraken Framework, and (4) radiation transport and fusion applications [52]. The newest stable version 2.2.0 was released in May 2022. Currently, three major components of Serpent 2 are under development: (1) advanced methods for spatial homogenization, (2) coupled

multi-physics simulations, and (3) new applications in fusion neutronics and radiation transport.

3.2.2 Calculation setup

The calculations are performed by using the Monte Carlo code Serpent 2 version 2.1.31 [50]. To achieve convergence and reliable results, a large number of sampling particles are required. A sensitivity analysis of the model's height was performed in advance to reduce the computation expense, and the results are illustrated in Figure 3-2.

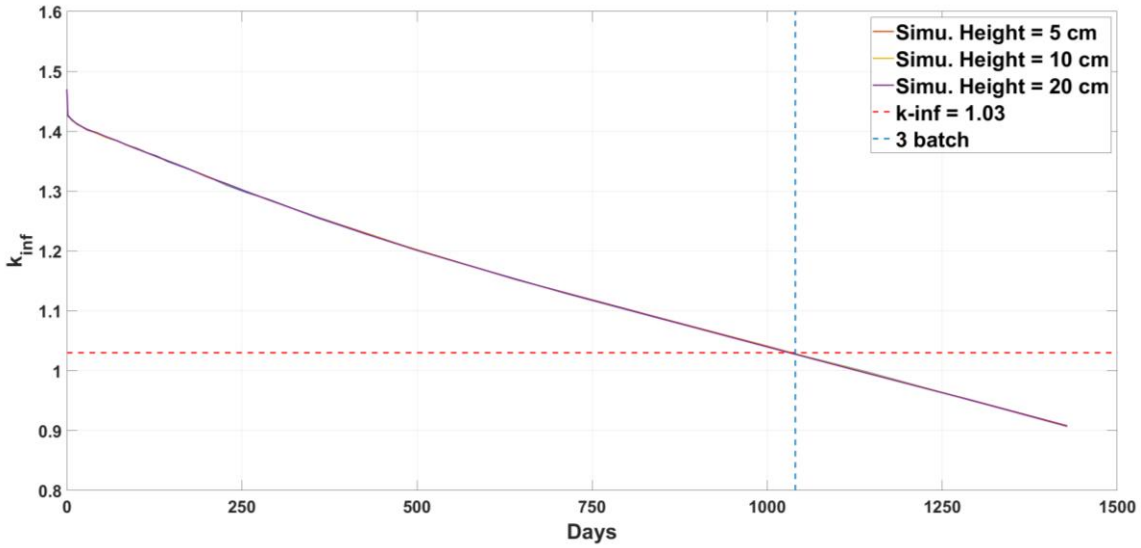

Figure 3-2. Sensitivity analysis of model height

Furthermore, a reduced model with a height of 5 cm and reflective boundary condition is employed in the assembly study. In full-core analyses, the vacuum boundary conditions are used outside the core reflector, and reflective boundary conditions are used

at the top and bottom of the core. This work is a 2-dimensional analysis, 3 % neutron leakage is assumed for the assembly calculations, and a 1.5 % margin on k_{eff} is left for full-core calculations.

Preliminary design sections (sections 3.3 and 3.4) used 100 active and inactive cycles for assembly calculation, and each cycle used 30,000 source neutrons. When performing the full-core calculation, the number of active cycles is increased to 600, and the source neutrons in each cycle are increased to 80,000. Results were checked, both settings are more than sufficient to produce reliable results. The variance in the assembly power distribution is smaller than 0.8 %. In each burnup step, the statistical error for k_{inf} /k_{eff} is always less than 30/10 pcm for assembly/full-core calculations. The nuclear cross-section data in these sections are derived from the ENDF-VII.0 library. For the detailed design of the 165 MWth small FHR core assembly (section 3.5), 200/100 active/inactive cycles are used, with each cycle utilizing 50,000 source neutrons. Therefore, the statistical error is reduced below 20 pcm. Moreover, the settings for full core remain unchanged. Each calculation used either 10 million or 48 million particle histories. In section 3.5, the nuclear cross-section data are from the ENDF-VII.1 library.

Due to the large volume of graphite in FHR, thermal scattering matrices $S(\alpha, \beta)$ are essential to be considered since the free gas assumption for low-energy neutrons becomes invalid, and bound atoms must be taken into account. In this study, Serpent's interpolation capability is utilized to interpolate matrices between library listings to accurately simulate the behavior of moderators under different temperatures. Thermal

neutron scattering sub-library ENDF-VII.0 and ENDF-VII.1 differ only in having SiO_2 data added to the latter [53].

3.3 Assembly Design

In this section, a brief introduction to the assembly design baseline is provided first. An examination of the optimization of the assembly size (AS) is then performed. An analysis of sensitivity is conducted in order to determine the radius of the coolant channel. Fuel channel pitches (FCPs) are examined with regard to its impact on the spectra and cycle length.

3.3.1 Assembly design baseline

Similar to the FHR DR, layouts of 180 fuel compacts (in black) and 109 coolant channels (in blue) within a hexagonal graphite block are shown in Figure 3-3. The radius of the fuel channels is 0.84 cm, determined by the consideration of power output, fuel loading, and neutron leakage (buckling). A thermal-hydraulic analysis must be conducted to determine the radius of the coolant channel. First, we assumed that the radius of the coolant channel is equal to that of the fuel channel to simplify the calculation. A summary of the basic parameters for assembly design is summarized in Table 3-3. A tight arrangement with a FCP of 1.78 cm is used to study the AS. The influence of the FCP is discussed in the following sections.

Table 3-3. Basic assembly parameters

Num. of fuel channels	180
Num. of coolant channels	109
Fuel and Coolant channel radius (cm)	0.84

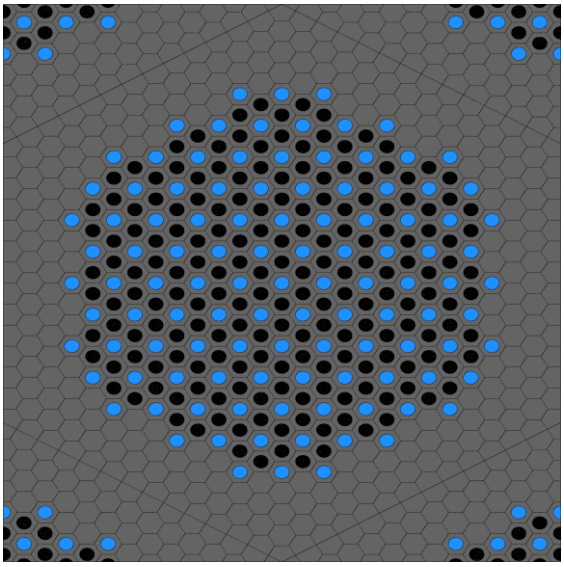

Figure 3-3. Distribution of fuel and coolant channels

3.3.2 Assembly size

In contrast to the FHR DR design, the fuel enrichment in this design is reduced from 15.5 to 9.5 %. Therefore, the AS must be adjusted accordingly to achieve the optimum fuel-to-moderator ratio. Assembly size with the longest cycle length is the optimized AS. Assembly parameters are calculated without considering the design of the burnable poison (BP) rods. An analysis of AS sensitivity, where the AS varied between 46 and 70 cm, is illustrated in Figure 3-4. Based on the linear reactivity theory, a full-core three-batch cycle length of 18 months required the multiplication factor of a fresh single assembly to remain above 1.03 before 1040 days (blue dashed vertical line in Figure 3-4).

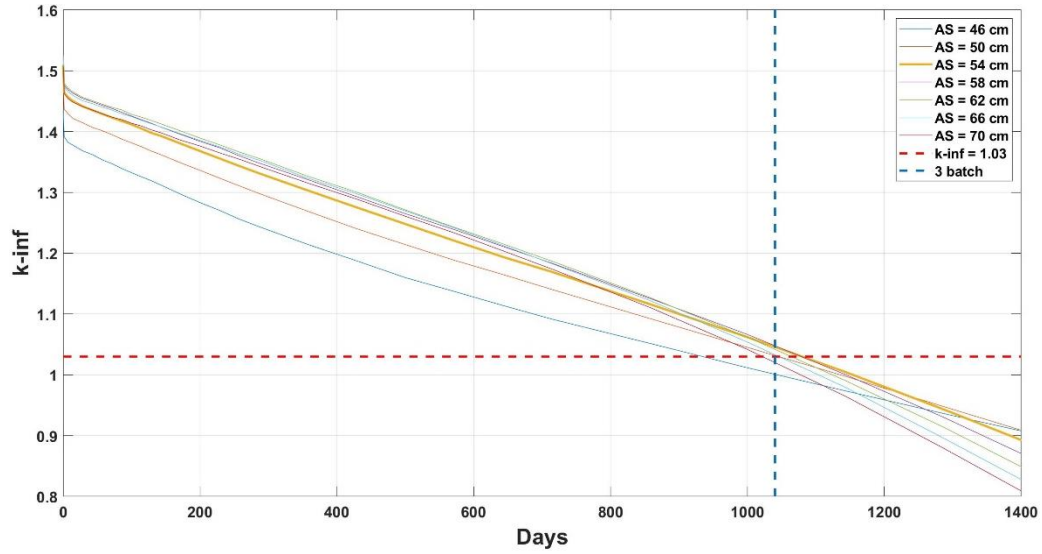

Figure 3-4. Sensitivity study of assembly size

Results indicate that an AS value between 53 and 56 cm exhibits the optimal reactivity, and a difference of fewer than three days is observed in their respective cycle lengths. Therefore, the AS of 54 cm is selected as the reference parameter for the assembly model due to its slight under moderation, which adversely affected the multiplication factor under the effects of thermal expansion.

3.3.3 Coolant channel radius

The calculation is performed by the assembly model that produced the optimal cycle length (AS = 54 cm). A sensitivity analysis of the coolant channel radius ranging from 0.80 to 0.88 cm is conducted. Figure 3-5 illustrates the results. The results show that the k_{inf} is not significantly sensitive to the radius of the coolant channel due to the relatively low average atomic mass of FLiBe, and the molten salt could act as a moderator. This fact

allows flexibility in determining the radius of coolant channels in thermal-hydraulic analysis, which can be performed in the future.

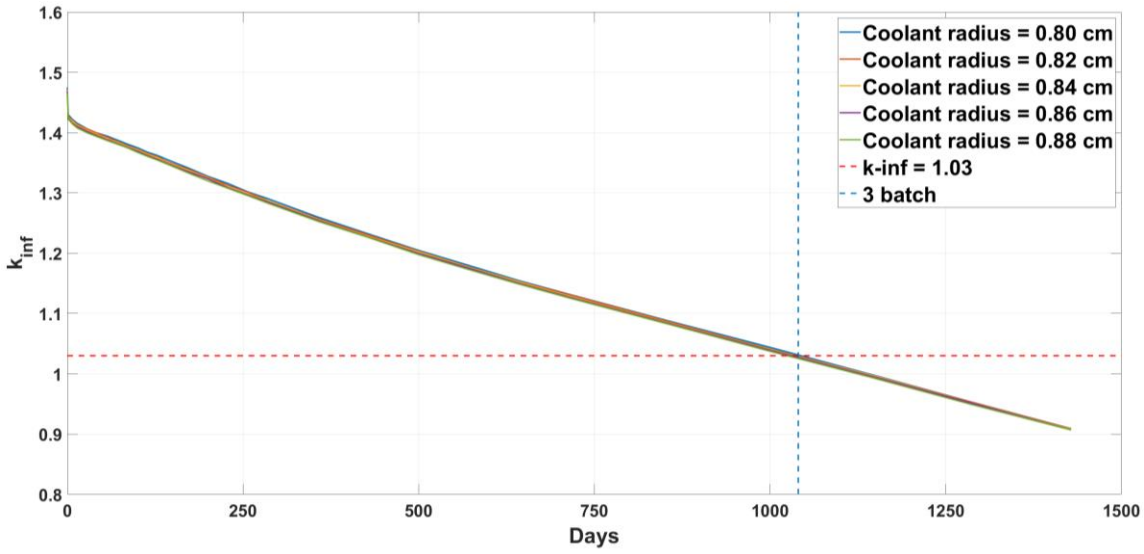

Figure 3-5. Sensitivity analysis of coolant channel radius

3.3.4 Fuel channel pitch (FCP)

Fuel channel pitch (FCP) must be analyzed in terms of its impact on neutronic performance. Four different FCPs, from 1.78 to 2.88 cm (shown in Figure 3-5), are selected to evaluate the impact on the neutron spectrum and the cycle length. Figure 3-6 (a) shows the spectra of the four cases, and Figure 3-6 (b) shows the change in k_{inf} as a function of time for each case. Major reactions, affecting neutron balance, are recorded in Table 3-4. As can be seen, a tighter configuration of the fuel channels resulted in a softer spectrum and shorter cycle length as there is less resonance capturing of U-238.

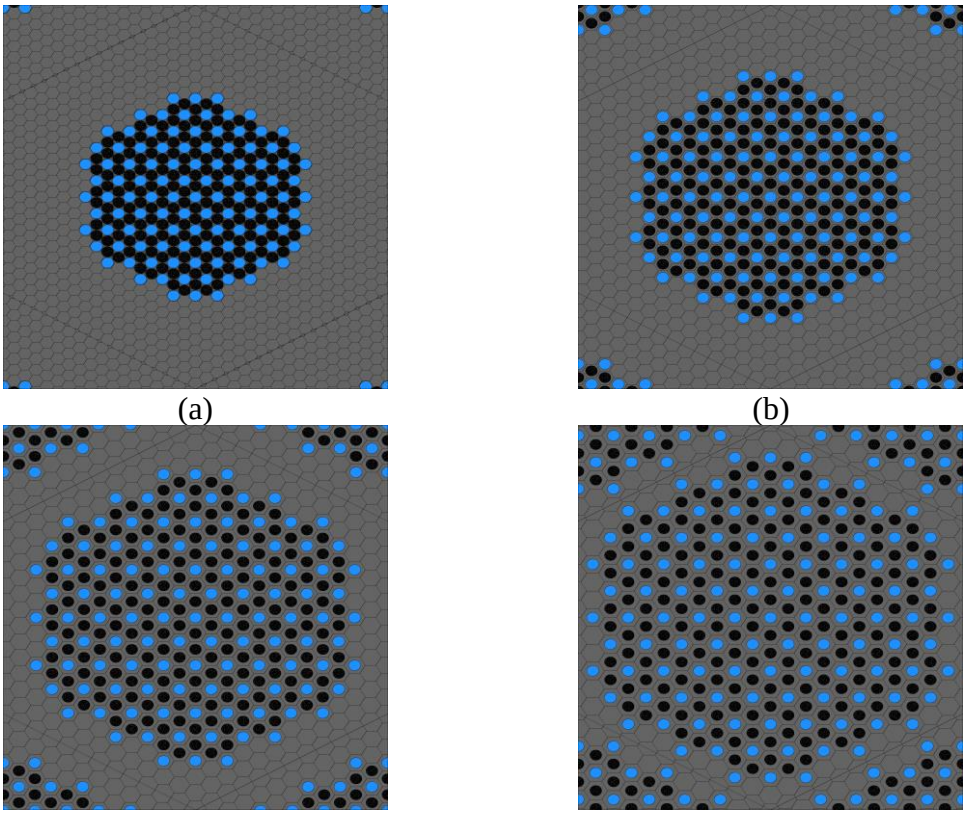

(a) (b)

(c) (d)

Figure 3-6. Fuel & coolant channels distribution of four scenarios (a) FCP = 1.78 cm; (b) FCP = 2.18 cm; (c) FCP = 2.58 cm; (d) FCP = 2.88 cm.

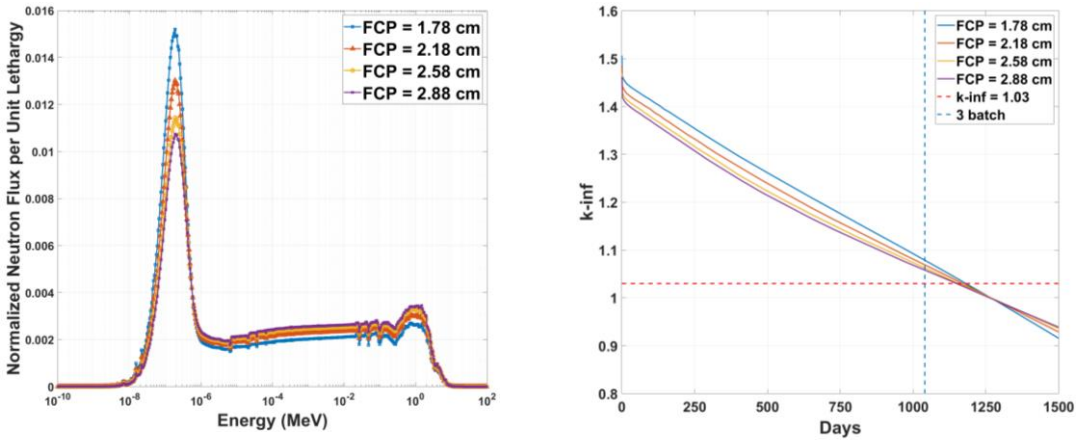

(a) Neutron Spectrum (b) k-inf

Figure 3-7. Neutron spectrum and cycle length

Table 3-4. Major reactions that affect neutron balance

Reactions	Reaction Rate			
	U-235		U-238	
	FCP=1.78 cm	FCP=2.88 cm	FCP=1.78 cm	FCP=2.88 cm
(n, 2n)	2.79E+10	1.72E+10	3.14E+11	2.10E+11
(n, 3n)	-	-	2.22E+09	1.16E+09
(n, fission)	2.06E+15	2.06E+15	1.08E+13	7.00E+12
(n, γ)	4.47E+14	4.57E+14	6.42E+14	7.85E+14

3.4 Core Design

In this section, three FHR core designs are presented with varying power. Preliminary analyses of the neutronics and fuel cycle are conducted. A full-core neutronic analysis is performed for each of the three core designs utilizing the three-batch refueling and shuffling strategy. The cases w/ and w/o BP are simulated in eight run-in cycles for each core design. The BP rods with 5 wt% Er_2O_3 can reduce the power peaking factor, hold down the k_{eff} during the entire operation period, and had a negligible impact on cycle length.

3.4.1 Reflector design

To mitigate radial neutron leakage, a sensitivity analysis is performed on the number of reflector layers. As shown in Figure 3-8, the k_{eff} changes as a function of time are compared for the reflector layer increasing from 0 to 4. Figure 3-9 shows that the k_{eff} curve converges when the number of reflector layers reaches two. Figure 3-8 (d) illustrates the final selected reflector.

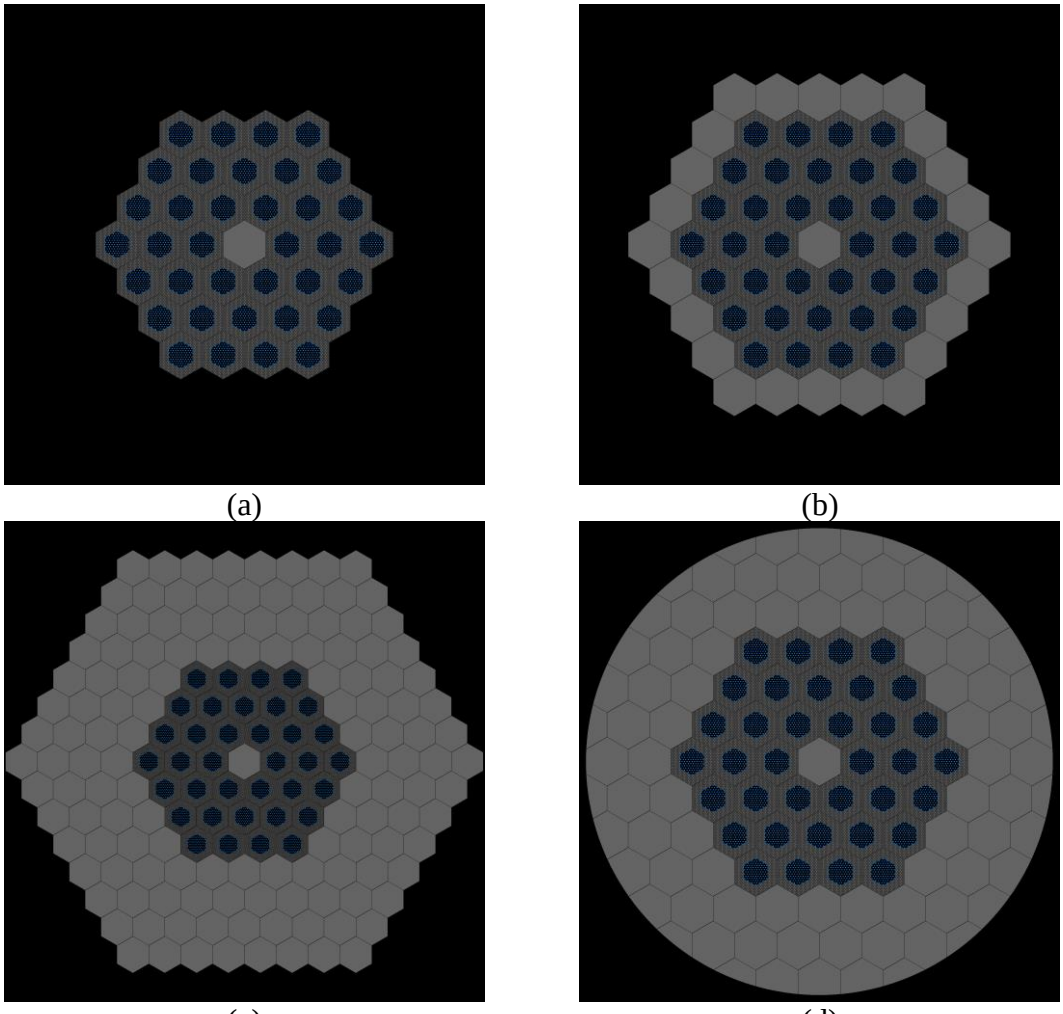

(a) (b)

(c) (d)

Figure 3-8. The number of reflector layers for the small core design (a) Layer = 0; (b) Layer = 1; (c) Layer = 4; (d) Final choice.

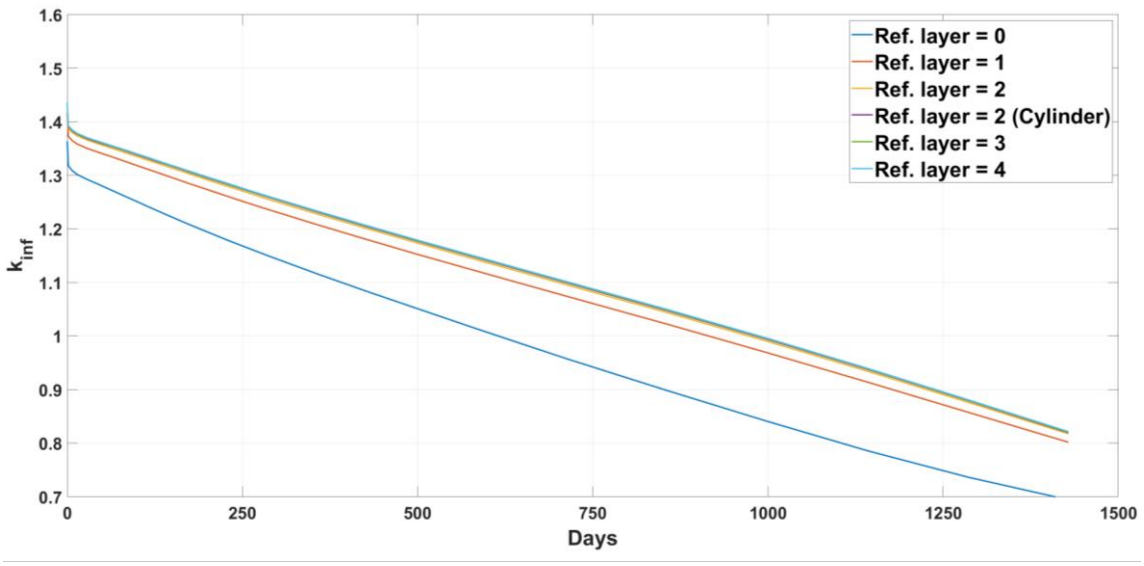

Figure 3-9. Sensitivity analysis of the number of reflector layers

3.4.2 Burnable poison design

The FHR full-core model is analyzed for both cases, w/ and w/o burnable poison. In the case of BP, six BP rods are placed at the corners of the fuel region, as shown in Figure 3-10. The radius of the BP rod is the same as that of the fuel channel (0.84 cm).

In BP rods, Er_2O_3 (density 8.64 g/cc) is homogeneously mixed with graphite. Pure Er-167 is assumed to be in the oxide. As shown in Figure 3-11, Er-167 has a large double absorption resonance peak near 0.5 eV. This feature can improve the negative moderator temperature coefficient (MTC) due to the location of the resonance at the high end of the thermal energy spectrum near the resonance in Pu-239 absorption. Furthermore, in contrast to gadolinium, erbium has a slower depletion characteristic as a burnable poison, releasing reactivity gradually over a longer period of fuel burnup [54].

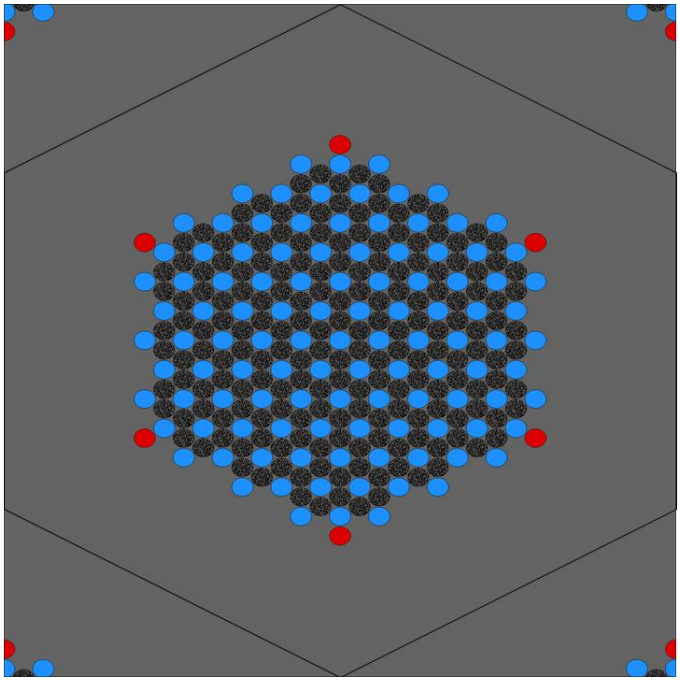

Figure 3-10. Distribution of fuel, coolant, and BP channels

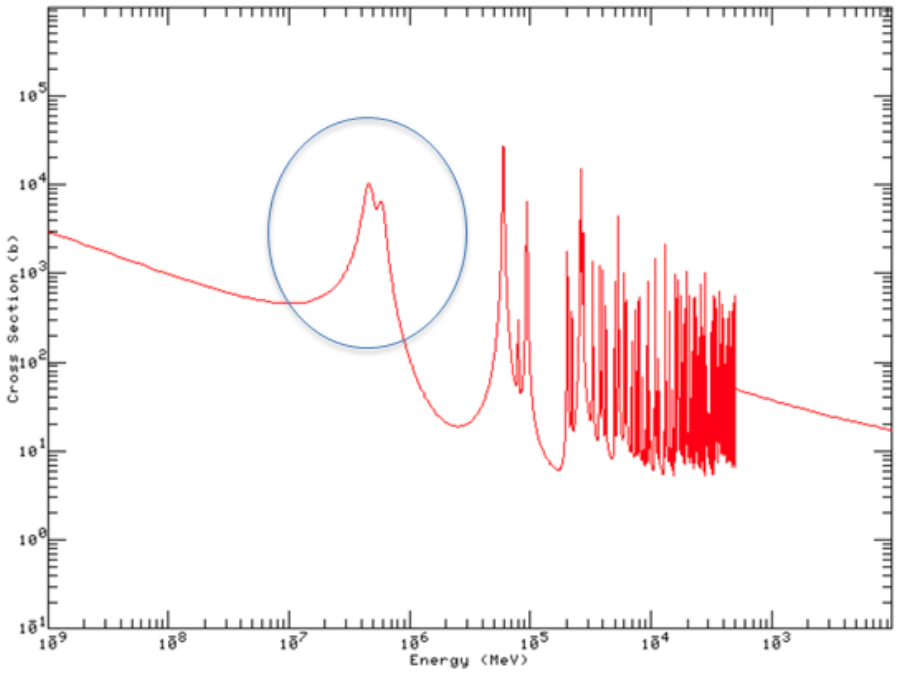

Figure 3-11. Er-167 absorption cross section

A sensitivity analysis is performed on the weight fraction of Er_2O_3 in the BP rod, and the results for the equilibrium cycle are shown in Figure 3-12. The weight percentage minimizing the impact on cycle length while holding down the k_{eff} as much as possible is considered optimal. A reference value of 5 wt% of Er_2O_3 is selected for the following calculations.

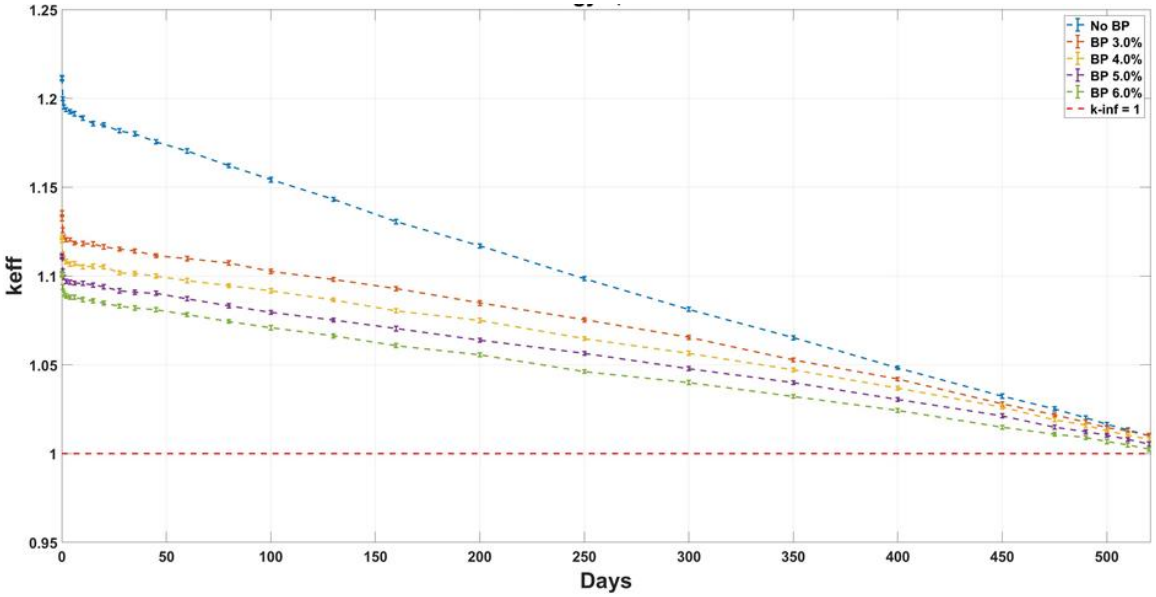

Figure 3-12. Sensitivity analysis of Er_2O_3 weight fraction

3.4.3 Three core design schemes

For the FHR design, a three-batch fuel cycle is selected. Several core designs with varying power levels are studied, as summarized in Table 3-5. The layout of each core is shown in Figure 3-13. The loading pattern of the different batches is denoted with light blue for batch 0 (fresh fuel), light yellow for batch 1 (once burned), and light pink for batch 2 (twice burned).

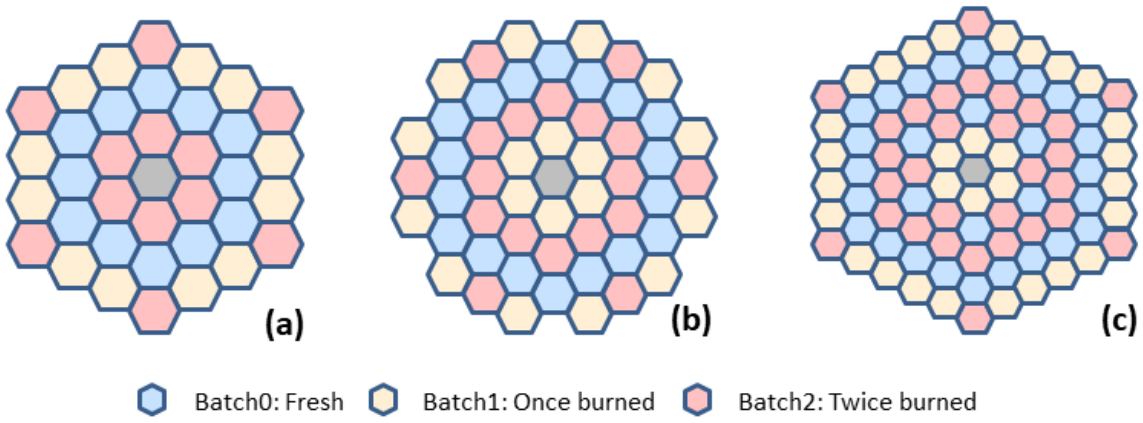

Figure 3-13. Three power levels of core design

Table 3-5. Core parameters

Core Parameters	**Small**	**Intermediate**	**Large**
Thermal power (MW)	**165**	**315**	**650**
Number of fuel assemblies	36	54	90
Num. of assemblies/batch (0/1/2)	12/12/12	18/18/18	30/30/30
Num. of batches	3		
Fuel cycle length (yrs)	1.5		
Core width D (cm)	378	486	594
Core height H (cm)	335	409	500
Fuel type	$UC_{0.5}O_{1.5}$		
Enrichment	9.5%		
Packing factor	0.35		
Capacity factor	95%		
Fuel loading (U tons)	2.6	4.77	9.72
Power density (kW/Ug)	0.0628	0.0660	0.0660
Primary coolant	$2LiF\text{-}BeF_2$ (or $NaF\text{-}ZrF_4$, $^7LiF\text{-}ZrF_4$, $NaF\text{-}BeF_2$) (^{7}Li enrichment: 99.995%)		
Core inlet temperature (^oC)	650		
Core outlet temperature (^oC)	700		
Mass flow rate (kg/s)	1366.4	2636.0	5370.8
Pressure drop (atm)	0.6759	0.8597	1.0986
Discharge BU (MWd/kgU)	98	103	103

At the end of each cycle, batch-2 assemblies (in light pink) are discharged and replaced with the assemblies in batch-1 zone (in light yellow). Fuel assemblies from batch-0 (in light blue) are shuffled to batch-1. Batch-0 is always filled with fresh fuel. Using the

refueling and shuffle scheme, the power distribution is expected to be flattened as much as possible.

The equilibrium cycle could be reached through a few run-in cycles. The calculation started with a completely fresh core and continued refueling and shuffling until a converged cycle length of 520.125 days. A 27.4-day outage interval is assumed between the cycles. After completing the eight run-in cycles, the model could reach its equilibrium state. For equilibrium, fuel composition in each batch should remain the same or differ slightly from the previous cycle.

3.4.3.1 Small core design

The small core design consists of 36 fuel assemblies with a thermal output of 165 MW, as illustrated in Figure 3-13 (a). A plot of k_{eff} as a function of time is shown in Figure 3-14 for the eight run-in cycles. Approximately three to four cycles are required for the reactor to reach its relative equilibrium state. It has also been demonstrated that the addition of 5 wt% of Er_2O_3 could effectively flatten the curve. After Cycle 8, only a 0.003 difference between the cases is observed w/ and w/o burnable poison, indicating that the BP has a negligible penalty on the cycle length.

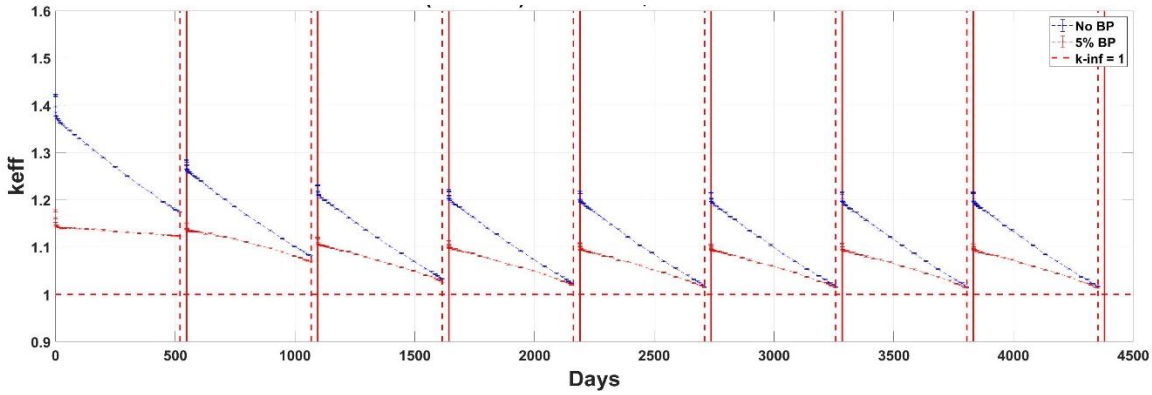

Figure 3-14. Small core run-in cycles for both w/ and w/o 5% BP cases

The power distribution at the beginning of cycle (BOC) of the small core is plotted in Figure 3-15. Numbers inside each cell are calculated as the ratio between the local and averaged core power densities. The assembly with the power peaking factor (PPF) is marked with a red edge. Furthermore, the BP could reduce the power peaking factor from approximately 1.5 to 1.35. Flattening the power distribution led to safer operating conditions and higher discharge burnup.

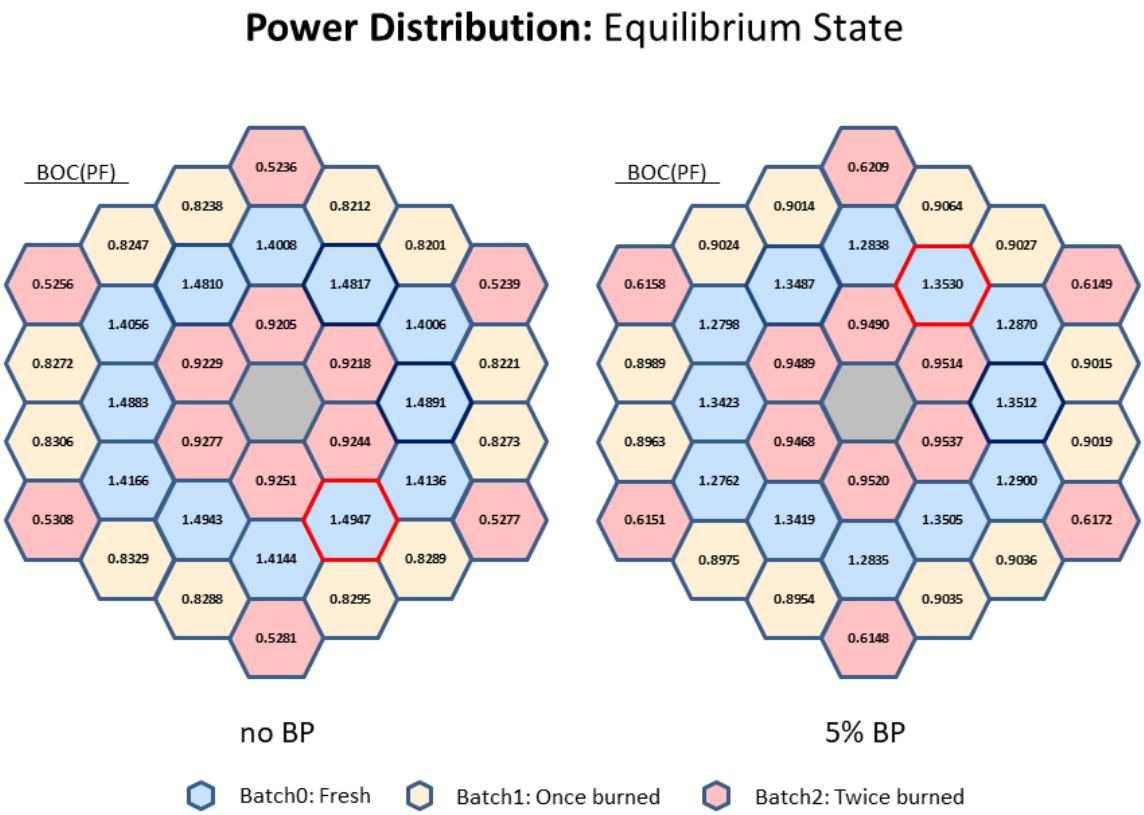

Figure 3-15. Power distribution of the small core design

3.4.3.2 Medium core design

On the periphery of the medium core, two additional rings of fuel assemblies are added compared to the small core. However, to balance the number of fuel assemblies in each batch, and to make the loading pattern rotationally symmetric, six fuel assemblies that are originally located in the corner of the reactor core, are removed and replaced with moderator assemblies, as shown in Figure 3-13 (b). Finally, the medium core design consisted of 54 fuel assemblies, and the thermal power of the medium core is increased to 315 MWth.

Similarly, eight run-in cycles are calculated for w/ and w/o BP cases for the medium core design, and the results are shown in Figure 3-16. At the equilibrium cycle, the difference of k_{eff} between the cases with BP and without BP is 0.00058, which is even smaller than that of the small core design. The power distribution at the BOC is shown in Figure 3-17. Power peaking factors for either w/ or w/o BP scenario are higher than those of the small core because the assembly with the PPF is immediately adjacent to the moderator and surrounded by relatively fresh fuel assemblies, resulting in relatively high-power levels.

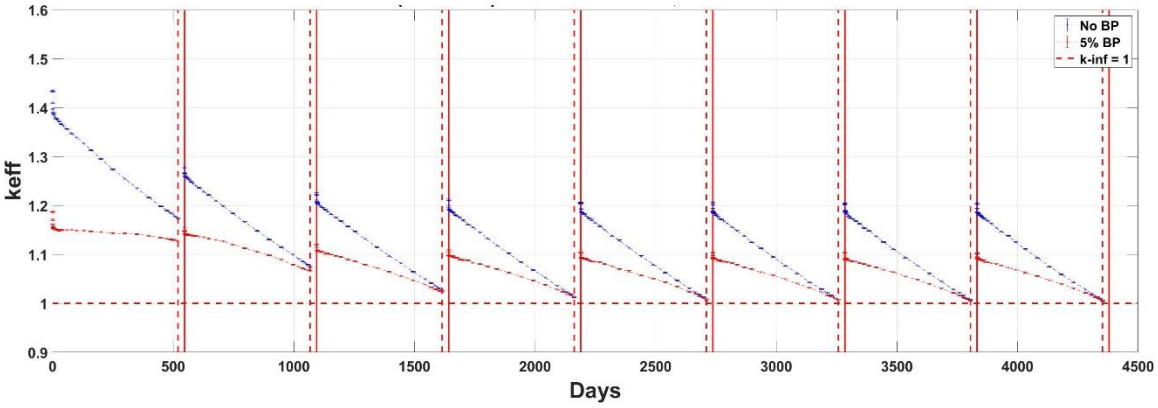

Figure 3-16. Medium core run-in cycles for both w/ and w/o 5% BP cases

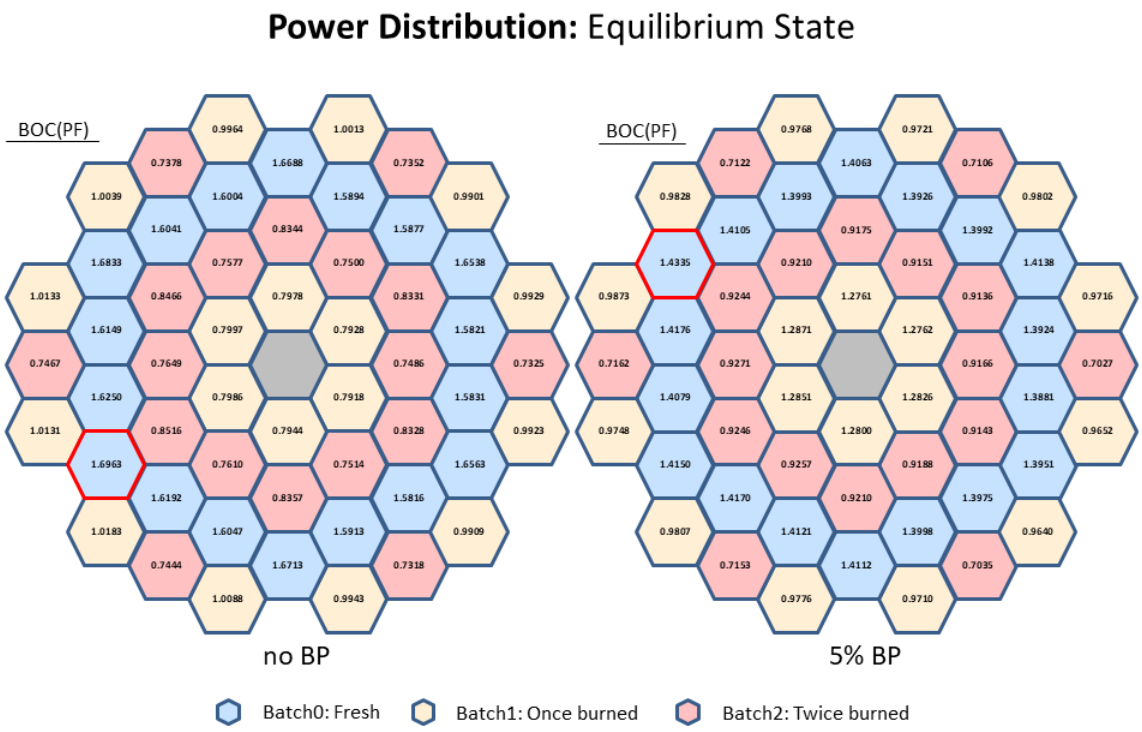

Figure 3-17. Power distribution of the medium core design

3.4.3.3 Large core design

Two more rings of assemblies are added on the periphery of the medium core, and the large core had 90 fuel assemblies. The thermal power output is increased to 650 MWth. The results of eight run-in cycles are calculated, and the results are plotted in Figure 3-18. Figure 3-19 shows the distribution of power. At the end of the equilibrium cycle, the difference in k_{eff} between the cases with BP and without BP is 0.0016, and the power peaking factor is reduced from 1.5390 to 1.3219.

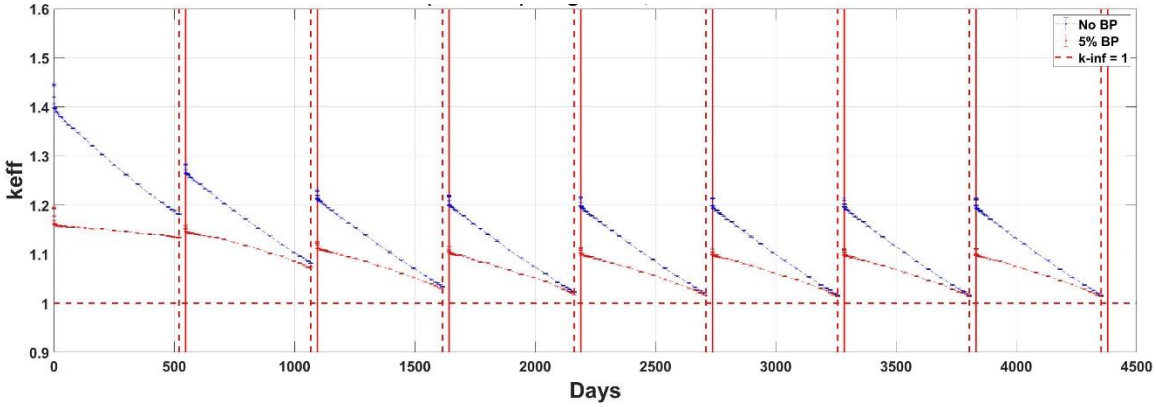

Figure 3-18. Large core run-in cycles for both w/ and w/o 5% BP cases

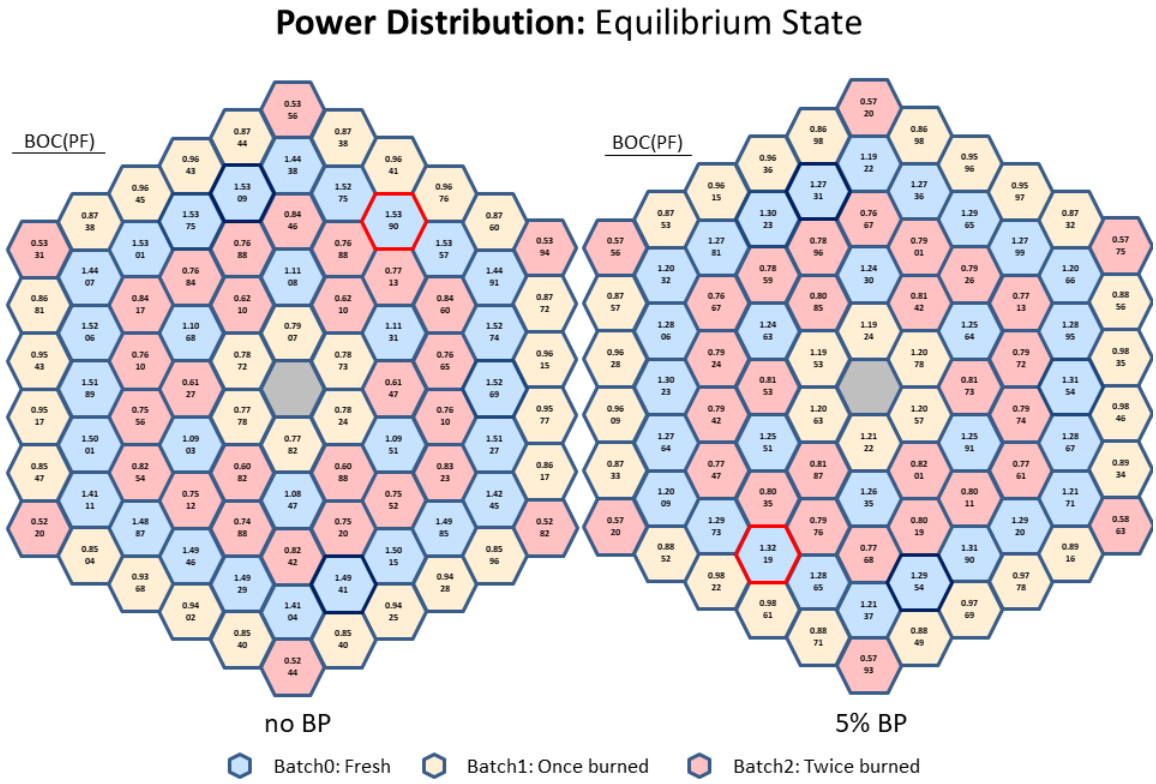

Figure 3-19. Power distribution of the large core design

3.5 165 MWth Small Core Design

This section provides a detailed analysis of the 165 MWth small FHR full-core model. Firstly, this section discusses a refueling and shuffling scheme specifically tailored for small cores in order to provide more accurate simulation results. Secondly, four aspects of the fuel cycle are addressed in depth: cycle length, power peaking factor, discharge burnup, and temperature coefficient. This section also provides the shutdown margin calculation for this FHR core design.

For the 165MWth small core model, moderator graphite density is adjusted from 1.75 to 1.89 g/cc [30], resulting in a reduction in assembly size from 54 to 53 cm. Both sensitivity analyses of AS and BP are re-evaluated, and the results are presented in Figure 3-20 and Figure 3-21, respectively. In the updated small core design, each BP rod is comprised of graphite, containing a 4 % weight fraction Er_2O_3. All the other parameters from the previous assembly design (i.e., the number of fuel or coolant channels, and channel radius) are preserved.

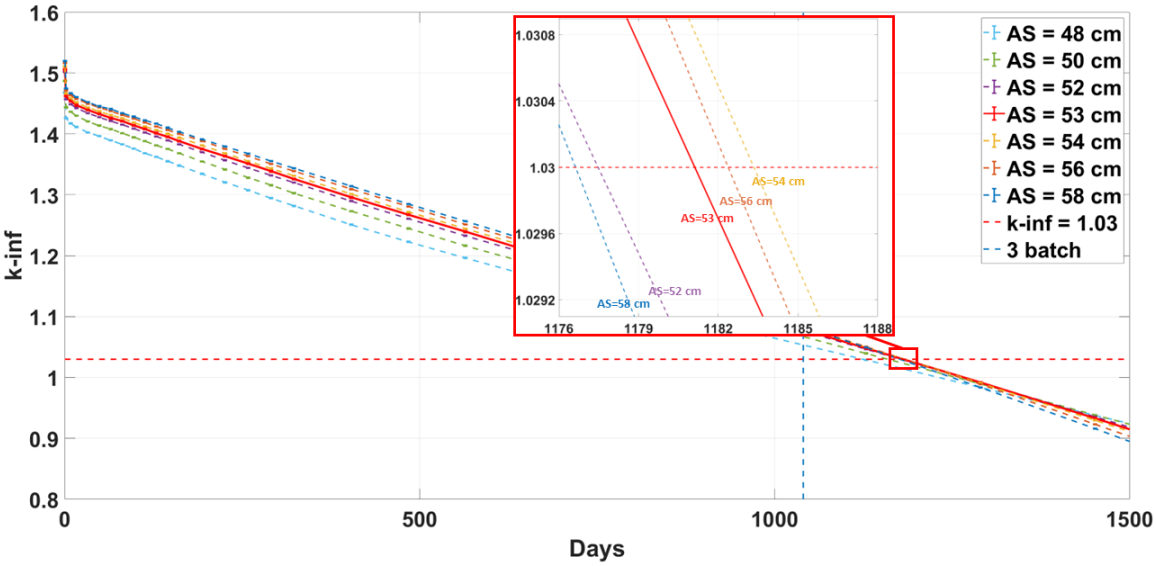

Figure 3-20. Updated sensitivity analysis of assembly size

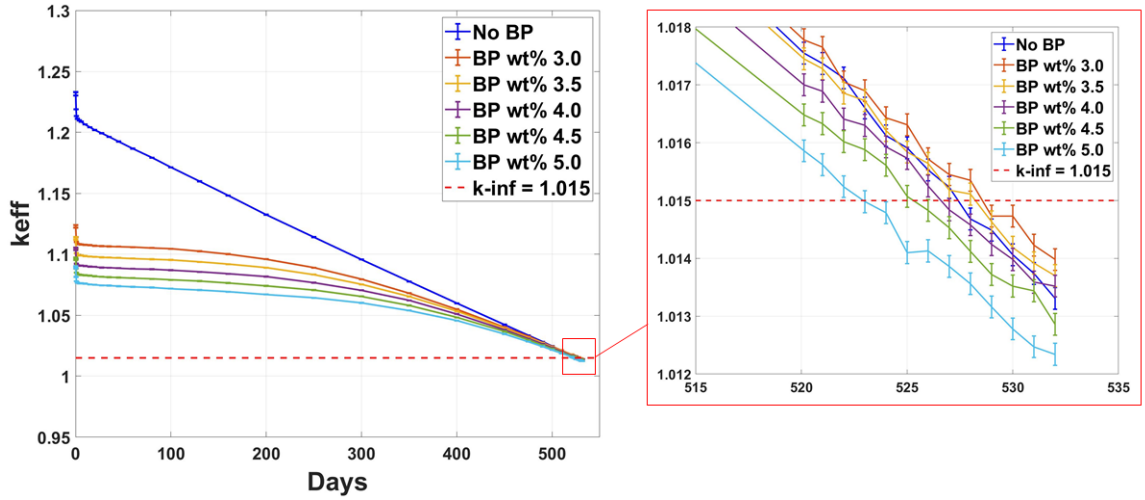

Figure 3-21. Updated sensitivity analysis of the weight fraction of Er_2O_3

Control blades in the shape of a "Y" are mounted at the corner of each fresh fuel assembly, following the similar design as the FHR DR [22], [23]. The control blade

material is composed of commercial molybdenum hafnium carbide (MHC) alloy with 1.4 wt % hafnium and 98.5 wt % molybdenum. The density of MHC alloy is 10.28 g/cc [7]. The control blade's dimensions are discussed in section 3.5.6.

The study examines the fuel channel pitch of the full-core model in the range of 1.78 to 2.88 cm. The case with FCP = 2.88 cm is shown in Figure 3-22 (a). Figure 3-22 (b) shows the layout of FHR core, consisting of 36 fueled hexagonal assemblies surrounded by reflector graphite blocks. The cycle length of the core is expected to be at least 18 months with a 95 % capacity factor. Detailed parameters of the core and assembly design are summarized in Table 3-6.

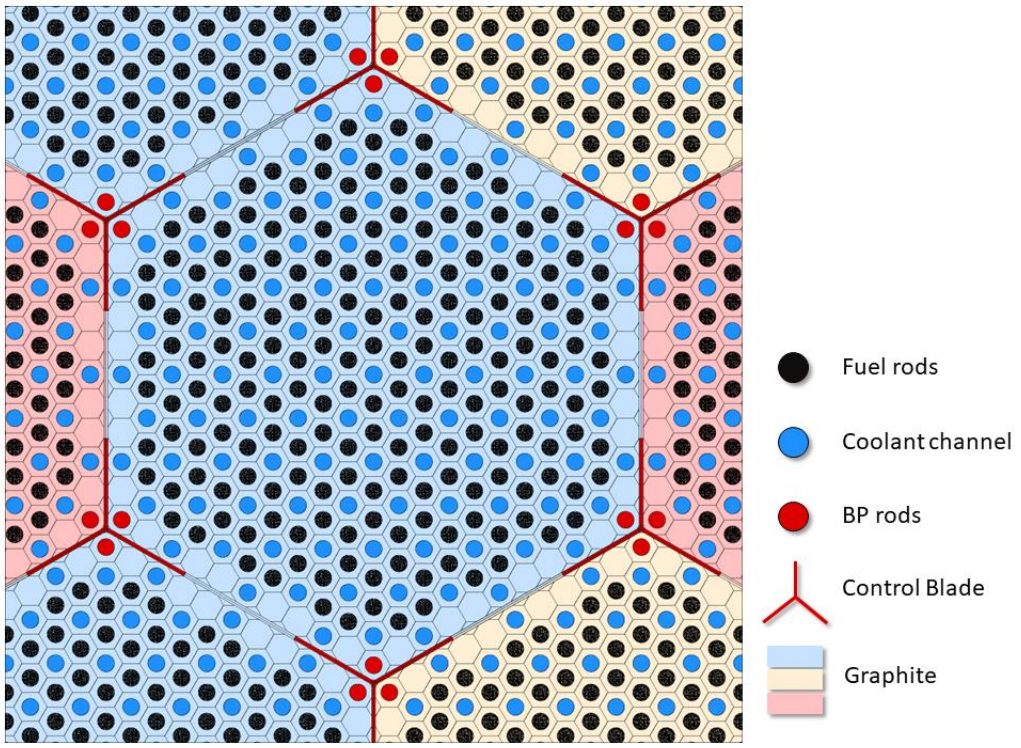

(a) Fuel assembly design (FCP = 2.88 cm)

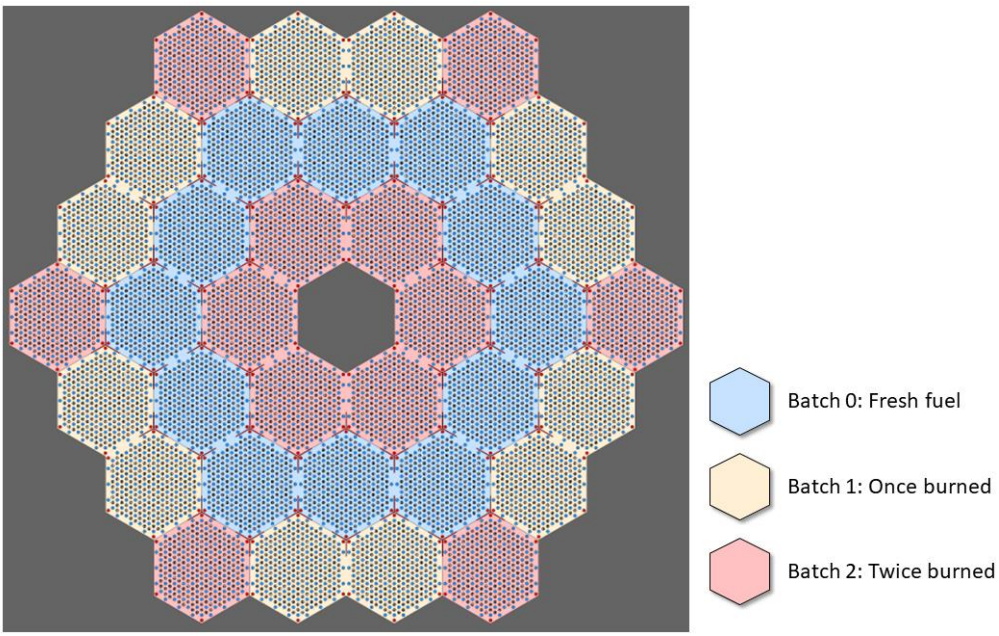

(b) Core design (FCP = 2.88 cm)

Figure 3-22. Fuel assembly and core design

Table 3-6. Small core design parameters

Core Parameters	
Thermal power (MW)	165
Num. of fuel assemblies	36
Num. of batches	3
Num. of assemblies for each batch (0/1/2)	12/12/12
Fuel cycle length (yrs)	1.5
Core width D/ height (cm)	371/342
Fuel type	$UC_{0.5}O_{1.5}$
Enrichment	9.5 %
Packing factor	0.35
Capacity factor	95 %
Fuel loading (U tons)	2.66
Power density (kW/Ug)	0.062
Primary coolant	2 ^{7}LiF-BeF_2 (^{7}Li enrichment 99.995%)
Core inlet/outlet temperature (℃)	650/700
Mass flow rate (kg/s)	1381
Pressure drop (atm)	0.6925
Assembly parameters	
# of fuel/coolant/BP channels	180/109/6
# of control blades	6 (Fresh fuel assembly only)
Fuel channel pitch (cm)	1.78 to 2.88
Radius of fuel/coolant/BP channels (cm)	0.84
BP rods	Graphite + 4 wt% Er_2O_3 (pure Er-167)
Control blades	MHC

3.5.1 Refueling and shuffling scheme

The layout of the different batches, shown in Figure 3-23, remains the same as described in section 3.4. It is evident from the figures of power distribution (Figure 3-15, Figure 3-17, and Figure 3-19) that even assemblies within the same batch might differ in their performance. For instance, batch-0 can be divided into two sub-groups based on the

location and the power output of the assemblies. Assemblies in the middle produced more power than those in the corners. Thus, a more detailed assembly shuffling strategy is adopted. Figure 3-23 shows arrows indicating the way assemblies moved between batches.

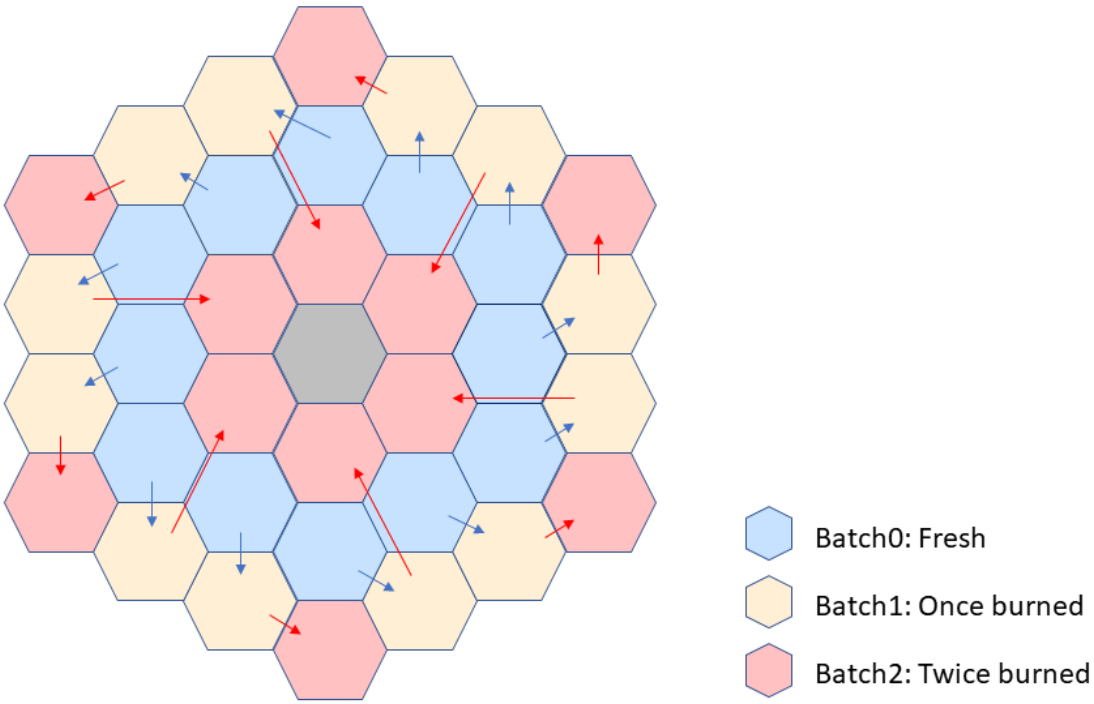

Figure 3-23. Three-batch refueling and shuffling scheme

3.5.2 Cycle length

To reach the equilibrium core, run-in cycle calculations are conducted (12 cycles in total). Analyses are performed for the cases w/ and w/o burnable poison. Calculations are divided into two stages. The first stage included the calculations spanning from a complete fresh core to a fixed cycle length of 520.125 days. The outage interval between each cycle is 27.4 days. Stage 1 reached equilibrium in seven run-in cycles. During the

second stage of the run-in calculations, the cycle is terminated when k_{eff} fell below 1.015 (the margin of 1.5% is considered for axial leakage). The calculation results for Stage 1 are shown in Figure 3-24, and the cycle lengths for Stage 2 are shown in Table 3-7.

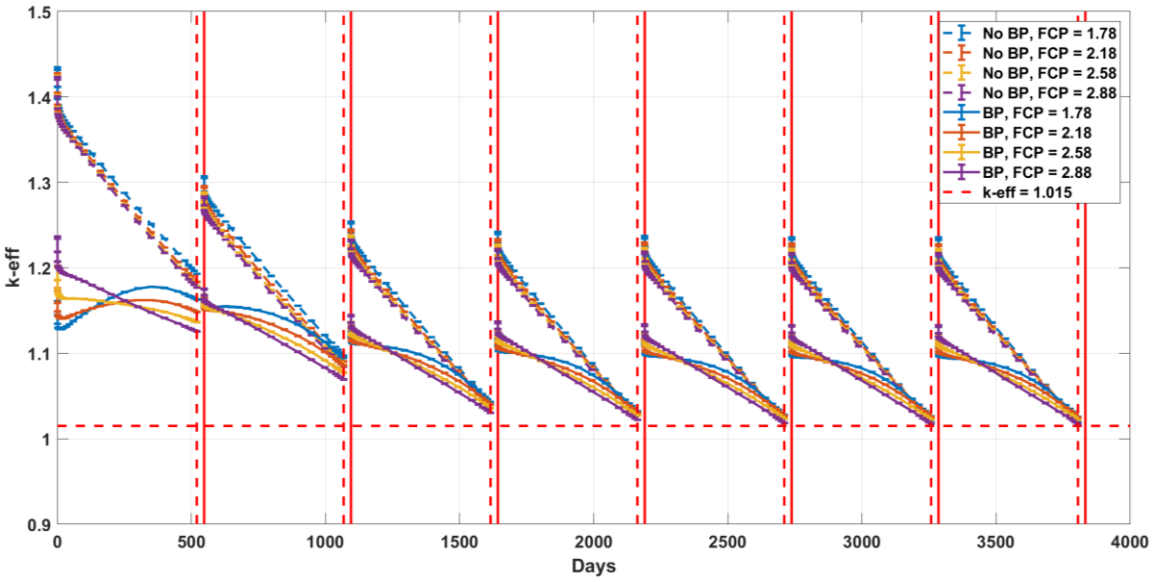

Figure 3-24. Refueling and shuffling of the first 7 cycles (Stage 1)

Table 3-7. Cycle length (days) for each scenario in stage 2

	Cycle Length (w/o BP) / (w/ BP)				
FCP (cm)	**Cycle 8**	**Cycle 9**	**Cycle 10**	**Cycle 11**	**Cycle 12**
1.78	536/552	526/532	526/532	528/537	527/534
2.18	544/557	530/534	531/534	532/538	531/538
2.58	549/549	531/529	533/531	534/535	534/532
2.88	550/529	532/523	532/524	535/524	535/524

Therefore, the larger FCP increased the cycle length, which is consistent with the findings in section 3.3.4. The tight fuel rod configuration produced a softer neutron spectrum, leading to a higher rate of fissile fuel depletion and a lower rate of Pu-239

production, resulting in a shorter cycle length. Burnable poison, Er_2O_3, is used to reduce excess reactivity. 4 wt% of Er_2O_3 in BP rods reduced k_{eff} during the entire operation period and had a negligible penalty on the cycle length.

3.5.3 Power peaking factor

Understanding power distribution in the core of a reactor is crucial for its safety. Power peaking factor (PPF) is defined as the ratio of the highest local assembly power density within the core to the average core power density. The PPF in this three-batch FHR design was observed in the blue-ring of the core (in Figure 3-23), which is the fresh fuel zone. Figure 3-25 shows the power distribution of the design with FCP = 2.88 cm. Additionally, the assembly with the PPF at the BOC is marked with the red edge of the hexagon, while marked with the green edge at the end of cycle (EOC). Table 3-8 summarizes the values of the power peaking factor for all the cases. The results show that BP could lower the PPF.

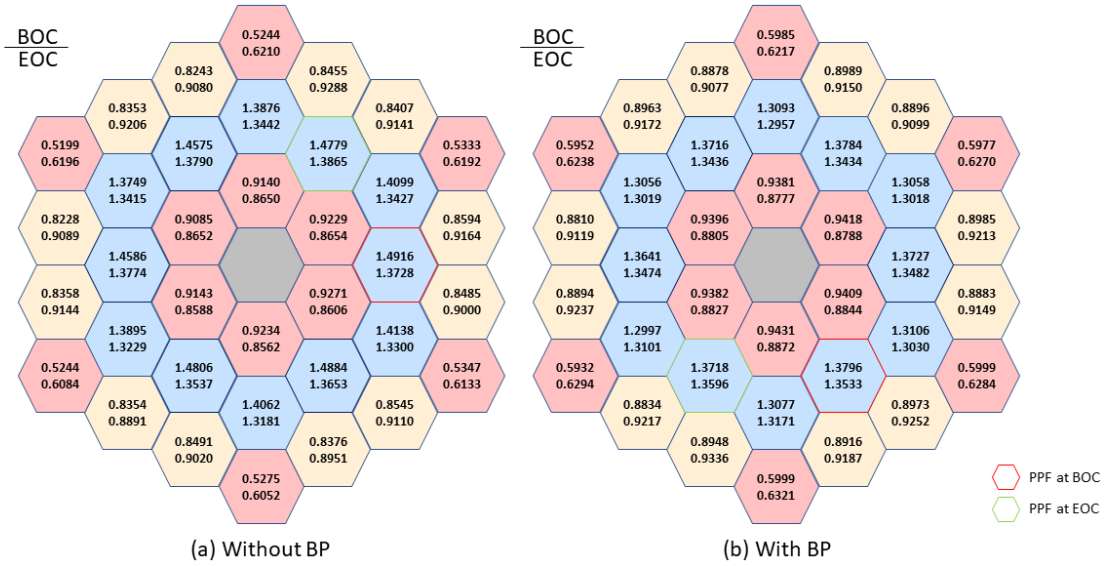

Figure 3-25. Power distribution of FCP = 2.88 cm

Table 3-8. Power peaking factors

FCP (cm)	w/o BP		w/ BP	
	BOC	EOC	BOC	EOC
1.78	1.5842	1.4621	1.3996	1.4644
2.18	1.5562	1.4348	1.3955	1.4311
2.58	1.5156	1.4034	1.3897	1.3935
2.88	1.4916	1.3865	1.3796	1.3596

3.5.4 Discharge burnup

An investigation is conducted into the discharge burnup of the FHR core design. Detailed results are presented in Table 3-9. We observed that FCP and BP had little impact on the discharge burnup. Furthermore, the difference between the internal and peripheral assemblies is approximately 10 MWd/kgHM, which is not trivial and should have been further reduced in future studies.

Table 3-9. Accumulated discharge burnup (MWd/kgHM)

FCP (cm)	w/o BP		w/ BP	
	Internal assemblies	**Peripheral assemblies**	**Internal assemblies**	**Peripheral assemblies**
1.78	101.96	92.21	103.25	93.93
2.18	102.89	93.14	103.73	94.45
2.58	103.21	93.78	102.74	94.09
2.88	103.09	94.12	100.91	92.87

3.5.5 Temperature coefficient

To ensure the safe operation of a reactor, it is essential that the temperature coefficients are designed to be negative. Four different temperature coefficients are examined in this section:

(1) fuel temperature coefficient (FTC), in which only the fuel temperature is varied.

(2) moderator temperature coefficient without burnable poison (MTC w/o BP), in which the moderator temperature is varied, meanwhile, the thermal expansion and thermal scattering matrices $S(\alpha, \beta)$ of the moderator graphite are considered.

(3) moderator temperature coefficient with burnable poison (MTC w/ BP), in which is basically the same as (2), but the temperature of BP rods is assumed to simultaneously change with moderator graphite since they are embedded in the moderator.

(4) fuel and moderator temperature coefficient (FMTC), in which the fuel and moderator temperature are varied and have been introduced with a same temperature perturbation.

A 50 K temperature perturbation is introduced to the 165MWth FHR core model. The changes in the fuel and BP density are ignored. The results for FTC w/ or w/o BP show no obvious difference, and the results against the operation time are plotted in Figure 3-26 (a). A relatively constant negative FTC are observed for all the cases, and loose fuel configuration (i.e., relatively large FCP) had a more negative FTC than the tight design.

The results for MTC are plotted in Figure 3-26 (b) and (c). For the cases w/o BP, it should be noted that the MTC became positive for small FCP (e.g., FCP = 1.78 cm and 2.18 cm). It also shows that larger FCP produced better MTC. When the FCP fell within the range of 2.58 to 2.88 cm, the MTC could stay negative during the entire operation period. Moreover, BP (Er_2O_3) could improve MTC significantly.

Figure 3-26 (d) depicts the FMTC of this FHR design. As can be seen, this FHR design could yield a negative FMTC under all the conditions discussed. In the calculation of FMTC, the fuel and moderator temperatures are assumed to increase simultaneously by the same amount. However, this assumption is somewhat unrealistic but conservative since when the core power is increased, the fuel temperature will always rise more and earlier than the moderator temperature.

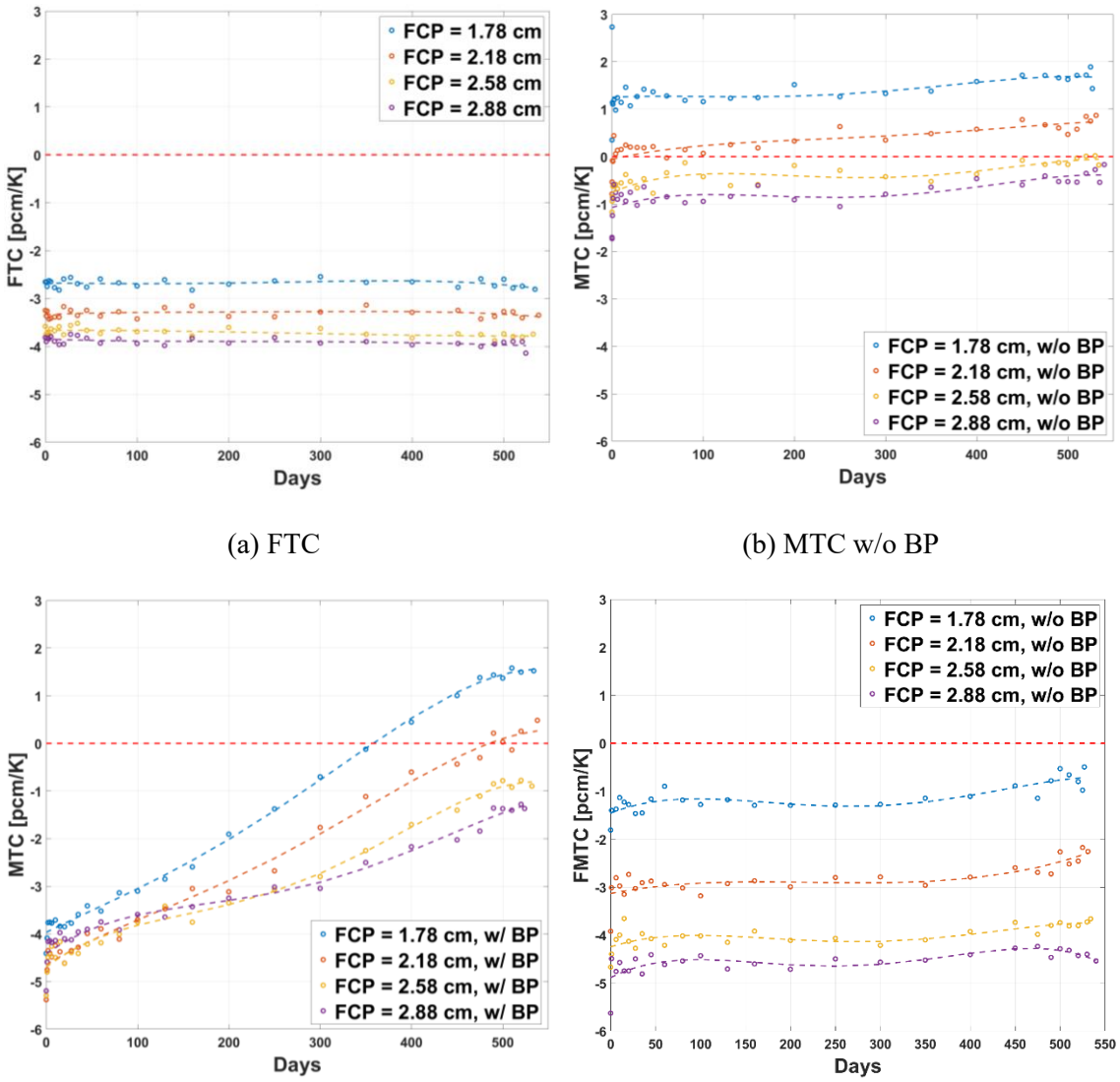

(a) FTC (b) MTC w/o BP

(c) MTC w/ BP (d) FMTC

Figure 3-26. Temperature coefficients of the 165MWth FHR design

For both the assembly model and full-core model, the impact of temperature perturbations on the MTC, is evaluated under 13 different moderator temperatures. The reference moderator temperature is 948 K, and delta T represents the difference between the moderator temperature used in a specific circumstance and the reference temperature.

Delta T varies from -300 K to +300 K at intervals of 50 K. No burnable poison is included in the calculations. Thermal expansion and thermal neutron scattering law $S(\alpha, \beta)$ of graphite change along with the temperature. The results of assembly k_{inf} change against the delta T are plotted in Figure 3-27, and changes in k_{eff} with delta T for the full-core model are plotted in Figure 3-28. Data points are plotted with an error bar, and the dashed lines represent the fourth-degree polynomial regression curves with $R^2 \geq 0.99$.

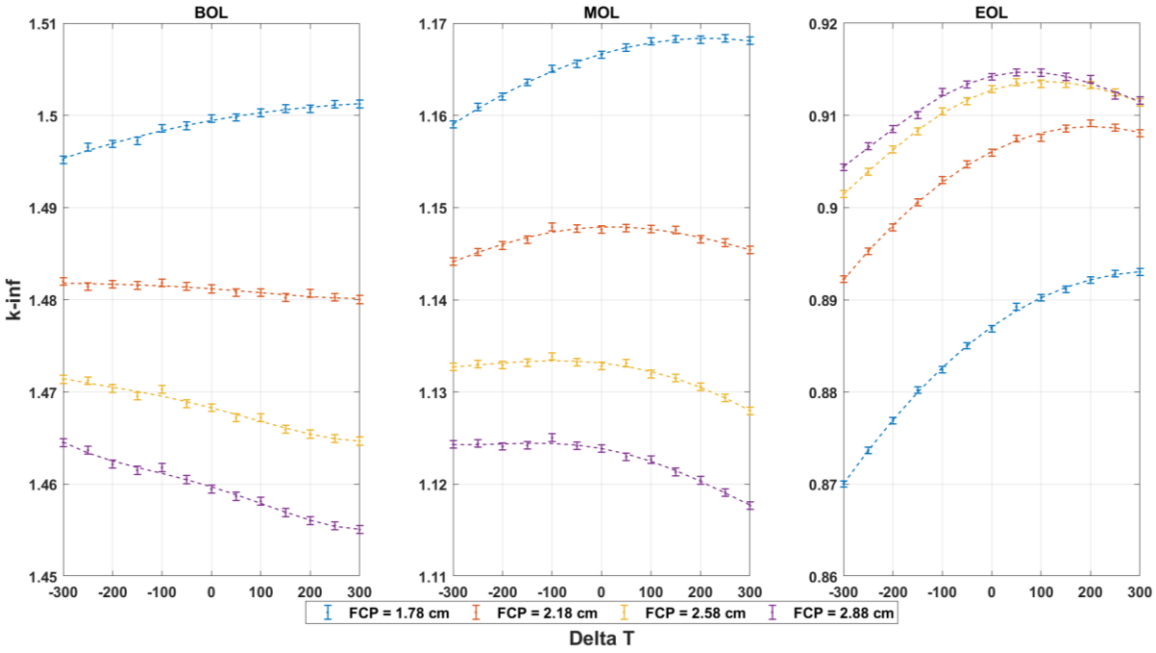

Figure 3-27. Assembly k_{inf} vs. delta T at different operating stages

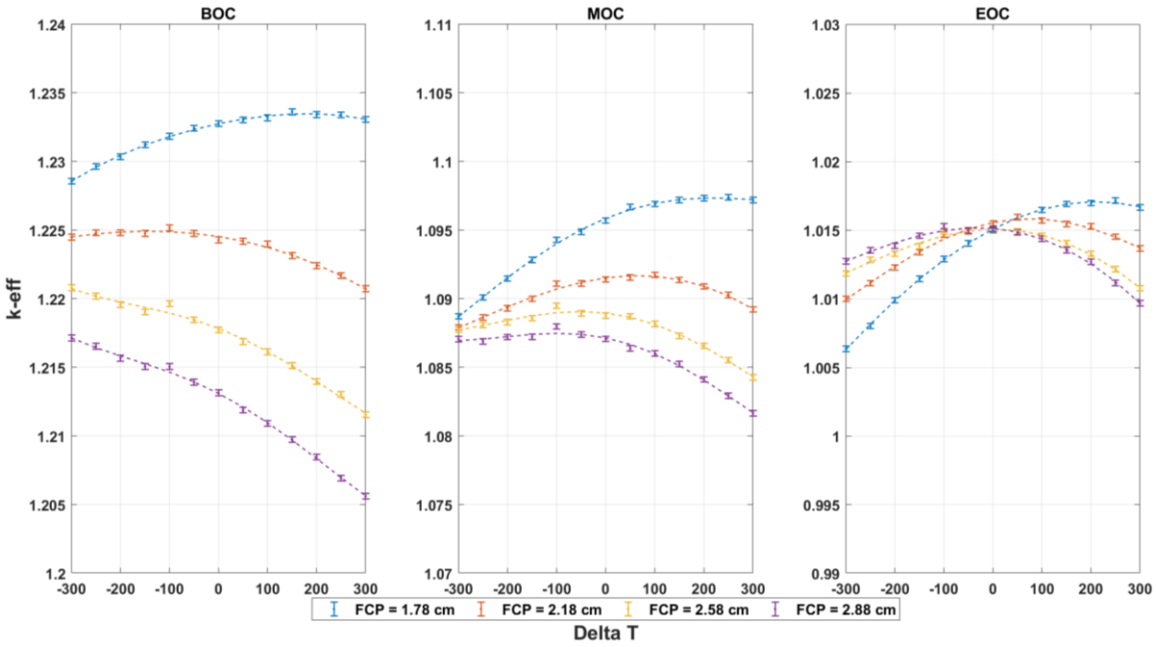

Figure 3-28. Full core k_{eff} vs. delta T at different operating stages

In general, the full core results are consistent with the assembly ones. A loose fuel channel configuration is desirable in terms of MTC.

3.5.6 Shutdown margin

Operation control rods are required during the reactor operation to adjust the reactivity that could not be canceled by burnable absorbers. In this small FHR design, reactivity control is provided by the "Y" shaped control blades (48 in total) mounted at the corner of the fresh fuel assemblies, as shown in Figure 3-22. Based on the run-in cycle calculations, BOC has the highest excess reactivity. In accordance with the Nuclear Regulatory Commission (NRC) regulations No. ML17311A755, the shutdown margin (SDM) during all modes of operation of nuclear power plants should be at least 1% $\Delta k/k$.

The most conservative condition for SDM is cold zero power (CZP) condition, which is defined as the temperature at which the fuel, coolant, and burnable poison are at 300 K [55]. Based on the assumption that all the control blades are inserted, Figure 3-29 displays the calculated results for the FHR design with FCP = 2.88 cm, at CZP conditions, comparing various sizes of control blades. The width of the control blade is fixed to 0.4 cm, while the length of each wing is varied. The results show that the control blade wing length should be at least 10 cm to achieve efficient activity control.

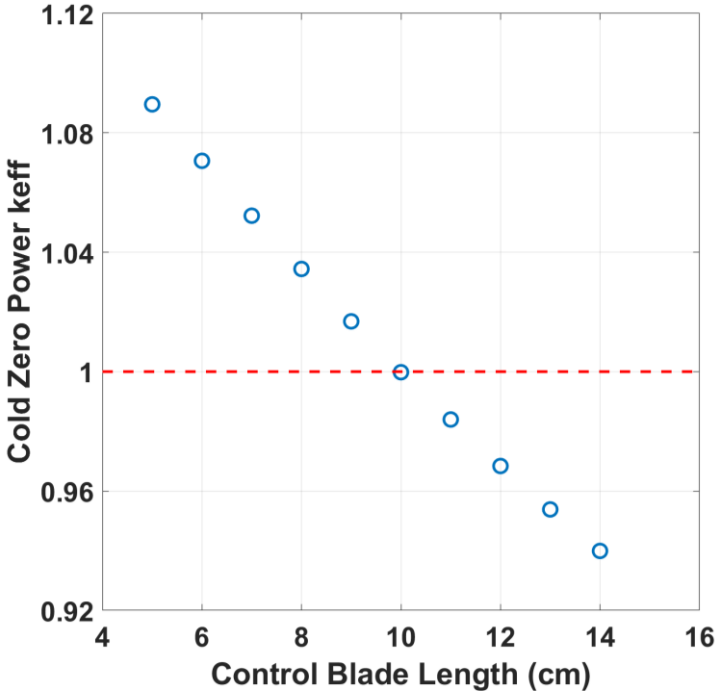

Figure 3-29. Cold zero power keff vs. control blade length

The Cold shutdown margin (CSDM) is the amount of reactivity required to make a reactor core in subcritical condition at CZP. The simulation is performed by inserting all

of the control rods, while leaving one of the highest worth control rods outside the active core. The CSDMs with a single failure of the highest control blade worth are summarized in Table 3-10.

Table 3-10. CSDM of different control blade length

Control Blade Length (cm)	11	12	13	14
CSDM (%$\Delta k/k$)	0.94	2.43	3.81	5.11

When the control blade width is 0.4 cm and the blade length is not shorter than 11 cm, the shutdown margin is sufficient at CZP conditions. Therefore, the control system designed is more than adequate for the current design of the FHR.

4. Design Alternatives

The objective of chapter 4 is to perform sensitivity and design-alternative studies to gain a better understanding of the FHR design space and facilitate better-optimized designs in the future. In section 4.1, a novel core design, which incorporated FIRM assembly, movable moderator, multi-batch strategy, and burnable poison management scheme, is proposed and analyzed in detail. Several other design alternatives are discussed and tested in sections 4.2 and 4.3, including molten salts, moderator materials, and fuel forms.

4.1 A Novel Core Design with Movable Moderator

The spectral shift is an innovative technique, which can increase both the cycle length and discharge burnup of FHRs. The basic idea of the spectrum shift technique is that by first removing partial moderator graphite from the active core at the early stage of the fuel cycle, a harder spectrum will be produced, and thus more Pu-239 will be bred as a result of increased resonance absorption by U-238. Later, the graphite structures will be inserted back into the core to increase moderation, allowing the extra accumulated Pu-239 to be burned, and eventually extending the cycle length. Former studies have mimicked the movement of the moderator either by varying the density of moderator graphite uniformly throughout the core [12], or by moving equal graphite volume around each fuel assembly

[13]. The novelty of our design is based on the FIRM fuel assembly design concept, which physically separates the fuel-bearing region from the central fuel cluster region, thereby providing the flexibility for adopting movable moderator design concept. For the purposes of reducing the reactivity in the fresh fuel region and minimizing neutron leakage, only the graphite blocks around the fresh fuel assemblies are moved out during operation, instead of removing moderator blocks from the whole core. The excess reactivity can be effectively suppressed when the moderator is partially removed, resulting in a reduction in the requirement for BP. The BP management scheme in conjunction with the movable moderator is also demonstrated in this work. The operating strategy of this novel core is divided into three stages, part of the removed graphite blocks will be reinserted into the core at the beginning of each stage to maintain a near-to-critical state. As the operation entered the final stage, all moderators will be reinserted back in, and then the reactor continues to operate until the end of the operation cycle. An extension of fuel cycle length of approximately 45 days can be achieved for an 18-month fuel cycle. It has also been found that important neutronics parameters, e.g., PPF, discharge burnup and temperature coefficients, have been improved in the novel core design when compared to the reference case.

To further enhance the neutronic performance of the 165MWth core, this section presents an innovative design that incorporates the flexible feature of the FIRM assembly with the movable moderator concept. A tight arrangement with a FCP of 2.0 cm is chosen as the reference case to demonstrate the superiority of the novel core design. The configuration of the movable moderator and burnable poison rods is introduced in section

4.1.1. Then, all four aspects: cycle length, PPF, discharge burnup, and temperature coefficient are re-evaluated.

4.1.1 Moderator and BP configuration

In the movable moderator design, the fuel assemblies in the fresh fuel zone are divided into a central hexagonal fuel cluster region and a peripheral movable moderator region, as shown in Figure 4-1 (a). The movable moderator configurations at different operation stages are plotted in Figure 4-1 (b). The strategy is divided into three stages:

- From 0 to 300 days: all moderators (12 blocks shown in shadow) outside the central hexagonal fuel cluster are removed from the active core.
- From 300 to 450 days: the moderator of the assemblies in the corners are moved back in.
- From 450 days to the end of the cycle: the rest of moderators are moved back in.

For the configuration of burnable poison, BP rods are divided into three groups. Group 1 BP rods are composed of 0.75 wt % Er_2O_3, designed to suppress the reactivity from 0 to 300 days. In contrast, groups 2 and 3 (composed of 1.5 wt % Er_2O_3) are designed to control the reactivity from 300 to 450 days and 450 days to the EOC. The detailed BP rod management scheme is listed as follows:

- From BOC to 200 days: all the BP rods are in the core.
- At 200 days: remove the BP rods of groups 2 and 3.
- At 300 days: insert back in group 2 and group 3 rods.
- At 400 days: remove group 3 rods.

- At 450 days: insert back group 3 rods.

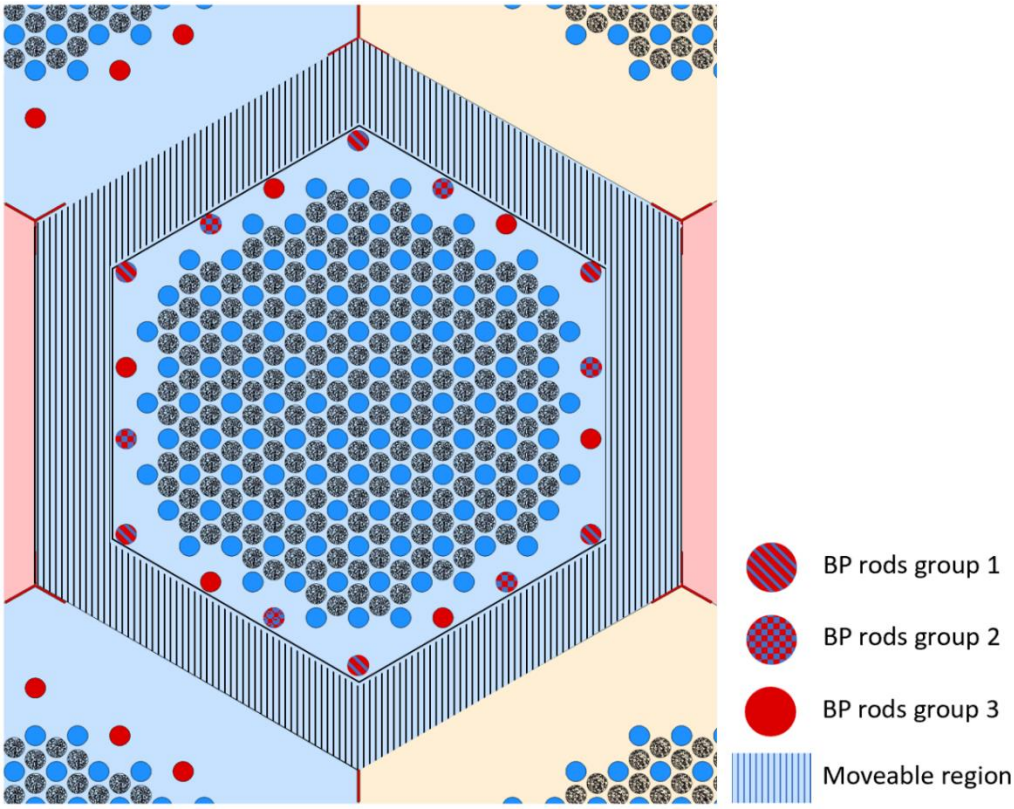

(a) Updated fuel assembly model

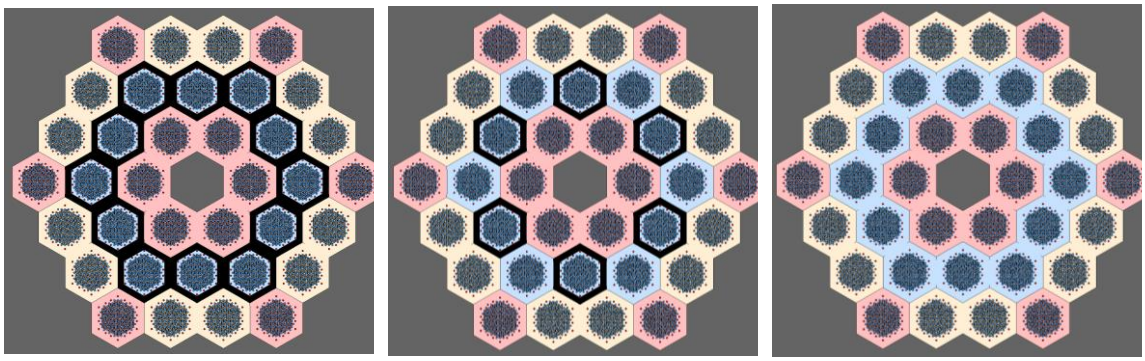

(b1) Stage 1 (b2) Stage 2 (b3) Stage 3

Figure 4-1. Movable moderator configurations (black regions indict moderator withdrawn)

4.1.2 Updated cycle length

Run-in cycle calculations are performed using the same procedures as applied in section 3.5. In the reference case, a FCP of 2.0 cm is selected without the presence of a burnable poison. The other two cases involved movable moderators w/ or w/o burnable poisons. Figure 4-2 shows the results of the equilibrium cycles of the three cases. In Figure 4-3, the mass density of U-235 and Pu-239 in the fresh fuel zone is plotted as a function of time.

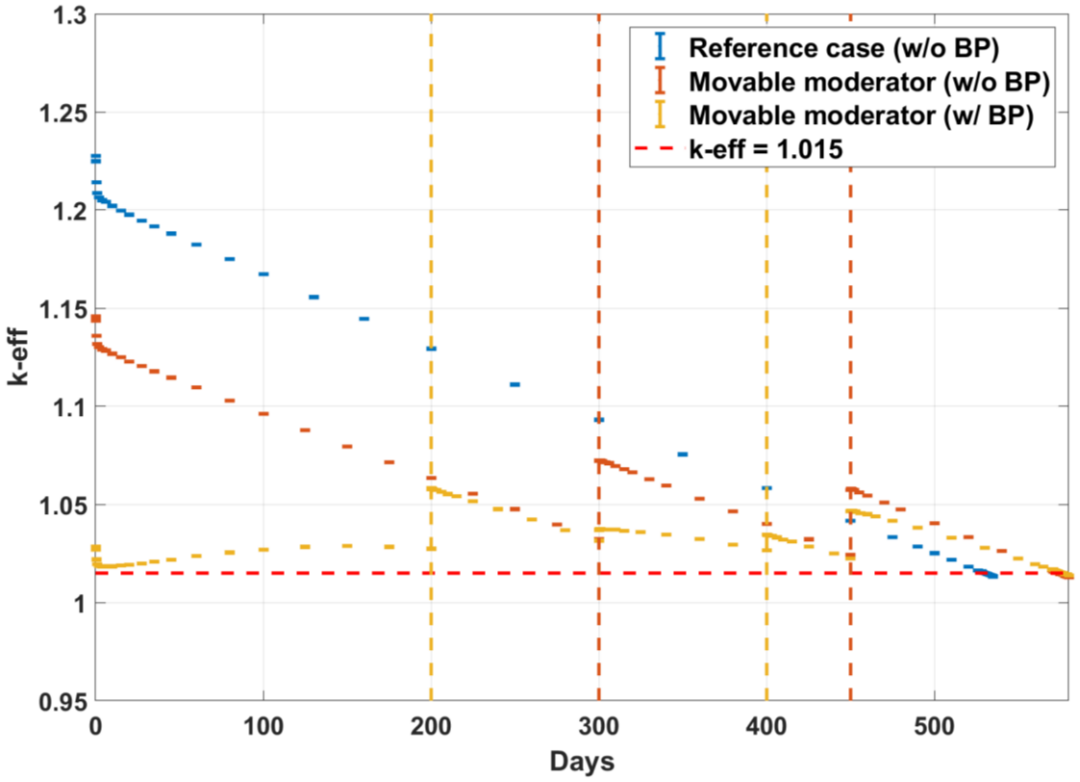

Figure 4-2. Comparing the k_{eff} vs. time for the equilibrium cycles

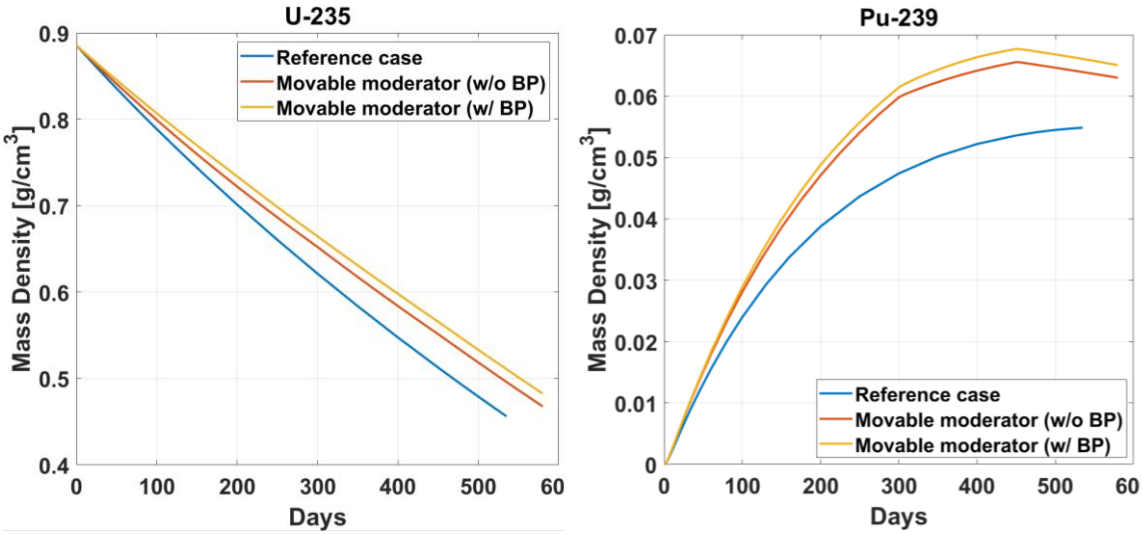

Figure 4-3. U-235 and Pu-239 mass density vs. time in fresh fuel assembly

It can be seen that the movable moderator design can effectively increase the cycle length by approximately 45 days for an 18-month fuel cycle. Moreover, moving the solid moderator (graphite) blocks out of the fresh fuel zone during the operation can effectively suppress the excess reactivity. The burnable poison, Er_2O_3, has almost no cycle length penalty and can further hold down the excess reactivity swing under 6% $\Delta k/k$ throughout the entire operation period. Through the management of the moderator in the fresh fuel zone, the depletion rate of U-235 is reduced, and the production rate of Pu-239 is increased.

4.1.3 Updated power peaking factor

A summary of the updated power peaking factors (PPFs) for the three cases is given in Table 4-1. It can be seen that the PPF can be greatly reduced by using movable moderators and BP only except near EOC.

Table 4-1. Updated power peaking factors

Cases	BOC	200-	200+	300-	300+	400-	400+	450-	450+	EOC
Ref. (w/o BP)	1.5725	1.4853		1.4855		1.4578		1.4586		1.4393
MM Design (w/o BP)	1.3624	1.3125		1.3036	1.3881	1.3808		1.3758	1.4796	1.4677
MM Design (w/ BP)	1.1927	1.2578	1.2988	1.2955	1.3250	1.3557	1.3724	1.3652	1.4569	1.4617

Note: MM: Movable Moderator. "-" denotes "before" and "+" denotes "after"

4.1.4 Updated discharge burnup

The movable moderator design is effective to improve the discharge burnup of the FHR core design, as shown in Table 4-2. The discharge burnups at both peripheral and internal assemblies are improved by approximately 8 MWd/kgHM. By flattening the power distribution with the help of movable moderator, the difference between the discharge burnups of the internal and peripheral assemblies is also slightly reduced.

Table 4-2. Updated accumulated discharge burnup (MWd/kgHM)

Cases	w/o BP		w/ BP	
	Internal assemblies	**Peripheral assemblies**	**Internal assemblies**	**Peripheral assemblies**
Ref.	102.5662	92.7716	103.6927	94.3523
MM Design	110.4873	101.1649	110.9949	102.2266

4.1.5 Updated temperature coefficients

Similarly, a 50 K perturbation to the temperature of the fuel and moderator is introduced to calculate the temperature coefficients. The results of FTC, MTC, and FMTC (w/o BP) change against time are plotted in Figure 4-4. In the reference case (FCP = 2.0

cm), the FTC is relatively constant, whereas in the movable moderator case, the FTC has improved when the moderator is partially removed from the active core. For the reference case, a positive MTC is observed with an FCP = 2.0 cm, which is in accordance with the findings in section 3.5.5. However, a combined negative temperature feedback can be achieved throughout the entire operation as shown in Figure 4-4 (c). In addition, the burnable poison Er_2O_3 can be applied to further improve the MTC.

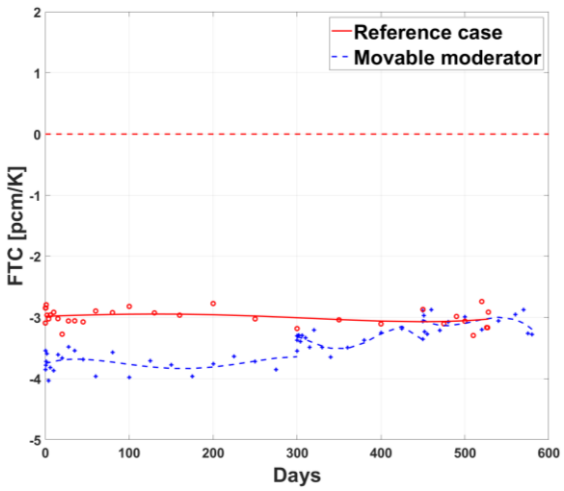

(a) FTC

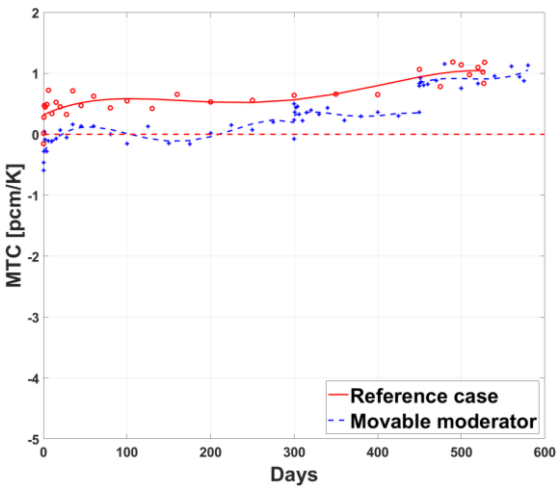

(b) MTC w/o BP

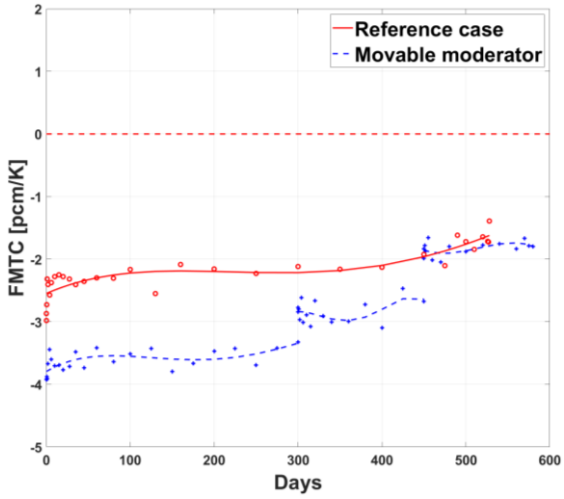

(c) FMTC

Figure 4-4. Updated FTC, MTC, and FMTC of the FHR design (FCP = 2.0 cm)

4.2 Alternative Coolant Salts

More than 10 potential molten salt compositions were evaluated in previous studies [47], [49], [56]. However, only a few meet the criteria for thermal-hydraulic properties, neutronic properties, and economic viability. This section provides an assessment of three alternative salts proposed as the primary coolants for the FHR design. An optimal coolant

not only provides excellent cooling capability, but also should has minimal impact on neutronics. Table 4-3 presents a summary of the properties of the standard coolant, FLiBe, and other three potential alternative coolant salts [47]. The density as a function of temperature for each salt is summarized in Table 4-4 [47]. The results of the neutronic performance of the four coolant salts are plotted in Figure 4-5.

Table 4-3. Properties of FLiBe and the potential alternative coolant salts

Salt	Melting point (°C)	Density (g/cc) (700 °C)	Volumetric heat capacity (cal/cc °C)	Thermal conductivity (W/m K)	Neutron capture relative to graphite	Moderating ratio
FLiBe	460	1.94	1.12	1.0	8	60
$NaF\text{-}ZrF_4$	500	3.14	0.88	0.49	24	10
$^7LiF\text{-}ZrF_4$	509	3.09	0.90	0.48	9	29
$NaF\text{-}BeF_2$	340	2.01	1.05	0.87	28	15

Table 4-4. Salt density equations

Salt	Density equation (g/cc)
$NaF\text{-}ZrF_4$	$3.650 - 0.00088 \cdot T\ (^{o}C)$
$^7LiF\text{-}ZrF_4$	$3.739 - 0.000924 \cdot T\ (^{o}C)$
$NaF\text{-}BeF_2$	$2.270 - 0.00037 \cdot T\ (^{o}C)$

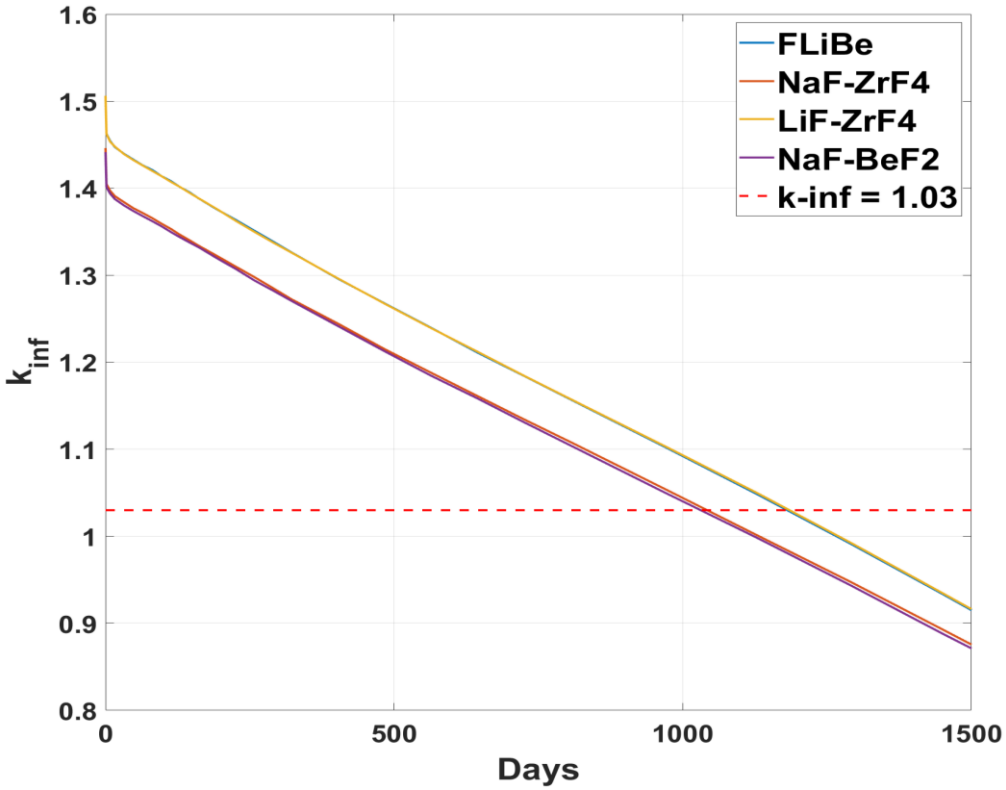

Figure 4-5. Neutronic performance of different coolant alternatives

4.2.1 $NaF\text{-}ZrF_4$

The molar composition of $NaF\text{-}ZrF_4$ (59.5 % NaF, 40.5 % of ZrF_4) is selected as the first alternative salts of the coolant. In comparison with FLiBe, $NaF\text{-}ZrF_4$ is a less expensive and low-performance salt, and its thermal conductivity is only half of that for FLiBe, and it has poorer neutronic performance than FLiBe [47], as shown in Figure 4-5. The neutron capture possibility of $NaF\text{-}ZrF_4$ is three times, and its thermal-spectrum moderating ratio is only one sixth of FLiBe. The high neutron absorption cross section for $NaF\text{-}ZrF_4$ might result in a positive coolant void coefficient and increased activation [49].

The price of $NaF\text{-}ZrF_4$ is approximately 20 times lower than FLiBe [49], since it does not require high purity lithium entichment.

4.2.2 $^7LiF\text{-}ZrF_4$

$^7LiF\text{-}ZrF_4$ (51 % LiF, 49 % of ZrF_4) is another backup alternative salt of FLiBe. Neutron capture of $^7LiF\text{-}ZrF_4$ is comparable to FLiBe, and its moderating ratio is three times higher than that of $NaF\text{-}ZrF_4$. The curve of $^7LiF\text{-}ZrF_4$, shown in Figure 4-5 nearly overlaps with that of FLiBe. However, in terms of volumetric heat capacity and thermal conductivity, $^7LiF\text{-}ZrF_4$ and $NaF\text{-}ZrF_4$ are nearly the same.

4.2.3 $NaF\text{-}BeF_2$

$NaF\text{-}BeF_2$ (57% NaF, 43% of BeF_4) is the third alternative coolant in this analysis. Compared to the other three molten salts listed in Table 4-3, $NaF\text{-}BeF_2$ has a relatively low melting point. This feature is desirable because it can simplify materials, components, and system requirements, as well as leave a relatively larger temperature margin for the reactor's safe operation [47]. Additionally, the volumetric heat capacity and thermal conductivity of $NaF\text{-}BeF_2$ are comparable to those of FLiBe. However, the neutron capture cross section and the moderating ratio of $NaF\text{-}BeF_2$ is a potential problem.

4.3 Alternative Moderator or Fuel Composition

Graphite has many excellent properties, such as high scattering cross section, low neutron absorption, good thermal conductivity, high melting temperature, and thermal

stability, making it very suitable to be used as a moderator material for FHR. However, high temperature graphite can react with oxygen and carbon dioxide in the reactor, and this can decrease its effectiveness and cause issues. In this section, we explore other possible moderator and fuel materials to be used in FHR. Silicon carbide [57] and metal hydride [58]–[62] are considered for the moderator. The fully ceramic micro-encapsulated fuel (FCM) [63], [64], which is more robust under irradiation and high temperature, is tested as well.

4.3.1 SiC

Due to their favorable neutronic and high-temperature properties, silicon carbide (SiC) materials have seen extensively studied for over half a century, and it has many advantages for nuclear reactor applications [57]:

- High decomposition temperature (over 2000 ℃)
- Swelling under irradiation is lower than 3 % for T > 200 ℃; and independent of the dose in the 200-800 ℃ range
- Mechanical properties are slightly affected by irradiation up to 1200 ℃
- Low creep under irradiation in the 200-1000 ℃ temperature range
- Low residual activity
- Good neutronic behavior
- Good air oxidation resistance up to 1500 ℃

SiC materials are commonly used as structural materials or cladding materials. In this study, we applied SiC as the reactor moderator for FHR design. The density of SiC matrix

used in this study is 3.1894 g/cc. The k_{inf} at BOC for different assembly sizes are summarized in the following Table 4-5.

Table 4-5. Replacing graphite with SiC, k_{inf} at BOC

Assembly Size (cm)	40	46	54	58	62	70	100
k_{inf} at BOC	0.9428	0.9212	0.8253	0.7666	0.7073	0.6019	0.3923

The results show that the moderator material with SiC has a significant adverse impact on criticality due to a relatively large capture cross-section, as shown in Figure 4-6.

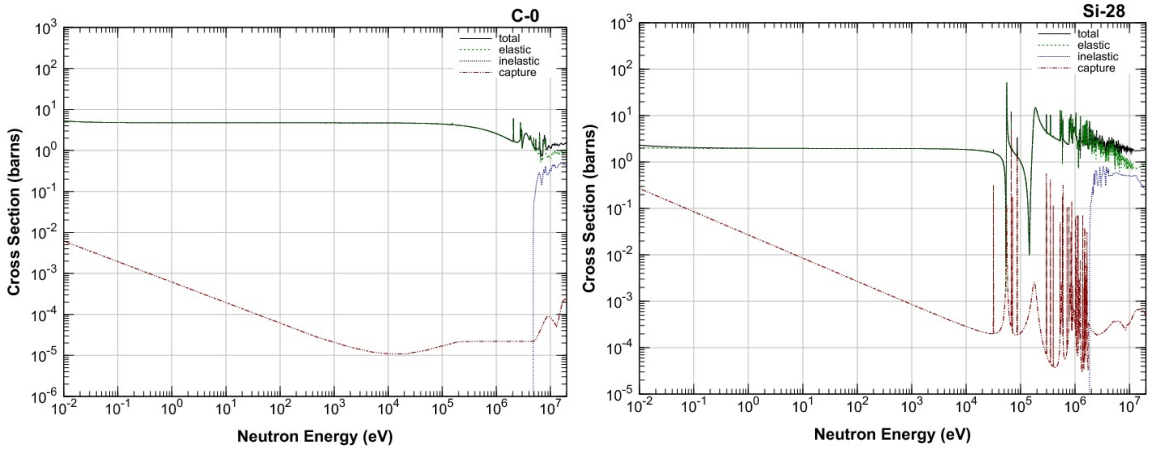

Figure 4-6. Cross-section of C-nat and Si-28

4.3.2 Metal hydrides

Hydrogen is an outstanding moderator material to be used in nuclear reactor applications due to the equivalent mass to the neutron, low neutron absorption cross-section, and high neutron scattering cross-section. Metal hydrides are uniquely suited for

high-temperature reactor systems. Table 4-6 lists the basic properties of selected hydrides that have potential application in our design [58]. H_2O on the last row of the table is included for comparison. The macroscopic slowing-down power (the product of the average logarithmic energy loss per collision and the macroscopic neutron scattering cross section) to the macroscopic cross section for neutron absorption is defined as the moderating ratio.

Table 4-6. Properties of metal hydrides have potential application in FHR design

Hydride	Attainable hydrogen density		Hydride density (g/cc)	Slowing down power	Moderating ratio
	10^{22} atoms H/cc	g H/cc			
ZrH_2	7.3	0.122	5.56	1.45	55
YH_2	5.8	0.097	4.24	1.2	25
H_2O	6.6	0.110	0.98	1.35	70

4.3.2.1 Zirconium dihydride

Zirconium hydride (ZrHx) alloy is produced by combining zirconium and hydrogen. In previous studies, ZrHx was employed as a neutron moderator in the systems nuclear auxiliary power (SNAP) program [59], training, research, isotopes, general atomic (TRIGA) reactors [60], nuclear thermal propulsion reactors [61], and Soviet TOPAZ-II or ENISY nuclear reactors. High moderator density and high thermal conductivity are the attractive attributes of this metal moderator. The disadvantage of ZrHx in nuclear reactor applications is that it necessitates careful temperature control and additional work to construct a hydrogen barrier to prevent hydrogen desorption at high temperatures.

In this study, we replaced the graphite moderator of the FHR fuel assembly model with ZrH_2. Various densities of ZrH_2 are considered. The purpose is to understand the influence of ZrH_2 on neutronic performance as reactor moderator. Calculation results are summarized in Table 4-7.

Table 4-7. The impact of ZrH_2 density on neutronic performance

ZrH_2 Density (g/cc)	5.56	2.78	1.39	0.695	0.3475	0.1
k_{inf} at BOC	0.7862	0.7399	0.9704	1.2732	1.4207	1.3234

The nominal value of the ZrH_2 density is 5.56 g/cc, which is the first column in the table. The results showed that when the density of ZrH_2 moderator dropped to approximately one-sixteenth (0.3475 g/cc) of the nominal value, the k_{inf} at BOC reached its maximum value. The cross-section of H-1 and Zr-90 are plotted in the following Figure 4-7.

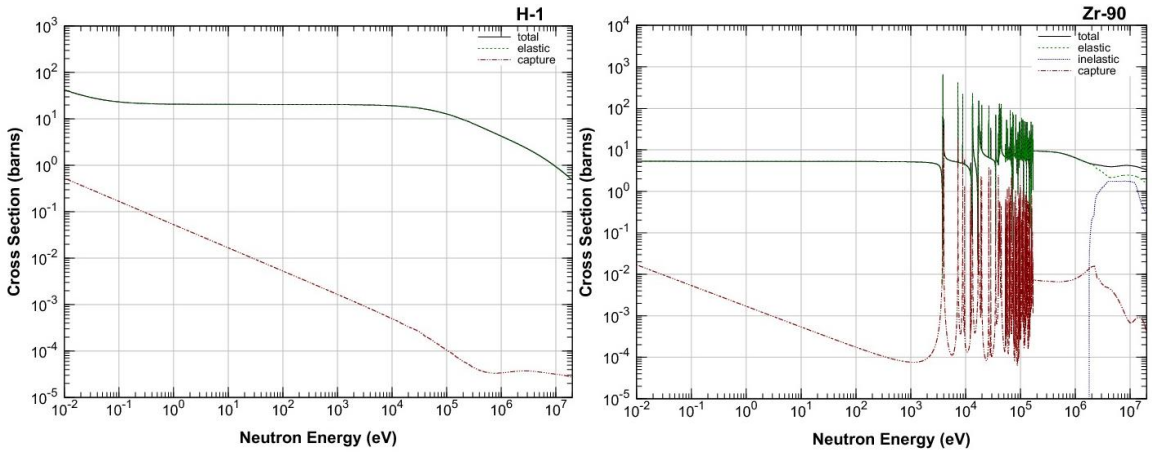

Figure 4-7. Cross-section of H-1 and Zr-90

Figure 4-7 indicates that replacing graphite with an equal volume of ZrH_2 makes the reactor over-moderated, thereby reducing the reactivity, as shown in Table 4-7. To achieve optimal moderation, the quantity of ZrH_2 should be reduced.

4.3.2.2 Yttrium dihydride

Yttrium hydride (YHx) is another type of metal hydride, appropriate for use in thermal reactor systems. YHx has excellent thermal stability, and its high hydrogen content at high temperatures makes it more suitable for high-temperature thermal neutron spectrum reactors [58].

Previously, yttrium was 30 times more expansive than zirconium [62], and due to this, yttrium was not widely used. Nowadays, affordable, and high-purity yttrium is readily accessible. Yttrium hydride is now being developed as a moderator for microreactors and small modular reactors under multiple DOE programs in the United States. One of these programs is the transformational challenge reactor (TCR) program, employing yttrium hydride as a moderator material.

In this study, the moderator graphite matrix is replaced with yttrium hydride ($YH_{1.92}$). The initial density of $YH_{1.92}$ is 4.1047 g/cc. Results are summarized in Table 4-8.

Table 4-8. The impact of $YH_{1.92}$ density on neutronic performance

$YH_{1.92}$ Density (g/cc)	4.1047	2.0524	1.0262	0.5131	0.2565	0.1
k_{inf} at BOC	0.5354	0.5145	0.7294	1.0344	1.2297	1.2460

As observed in Table 4-8, the trend of k_{inf} at BOC is approximately the same as that in Table 4-7. The maximum k_{inf} value is at the density 0.1 g/cc. However, the k_{inf} values of yttrium hydride are smaller than zirconium hydride because the absorption cross section of Y-89 is higher than that of Zr-90, as shown in Figure 4-8.

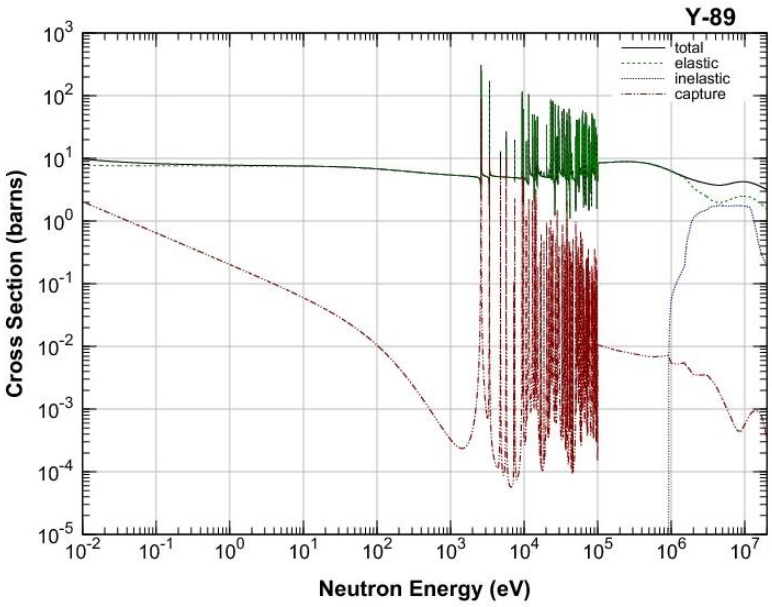

Figure 4-8. Cross-section of Y-89

4.3.2.3 Hybrid moderator design

In the previous sections, we showed that the neutron slowing down ability of a unit volume of metal hydride is much stronger than that of graphite. This feature may can help to reduce the size of the whole core.

In this section, a hybrid moderator design is investigated. ZrH_2 has a smaller neutron absorption cross section than that of $YH_{1.92}$, and it caused less penalty on k_{inf}. Thus, we used the former in combination with graphite for our FHR design. The graphite cells

are gradually replaced with the metal hydride cells, as shown in Figure 4-9. The blue regions are the coolant channels, the black regions are the fuel compacts, the dark gray region is graphite, and the light gray region is metal hydride. Results of k_{inf} at BOC are summarized in Table 4-9. With the hybrid moderator design, the assembly could be reduced from 53 to 38 cm.

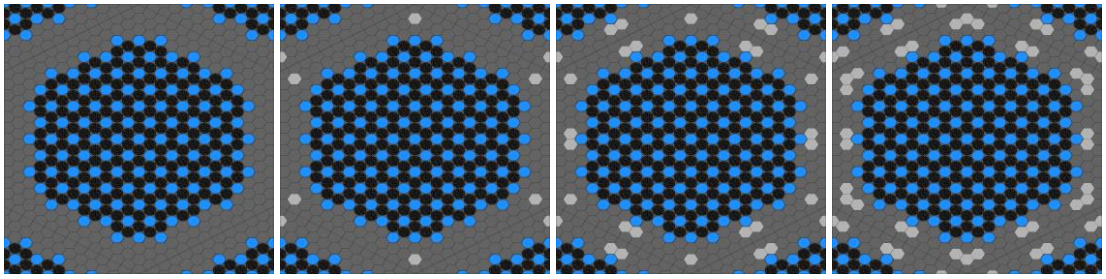

Figure 4-9. Combined moderator strategy (a) No replacement; (b) 6 cells replaced; (c) 18 cells replaced; (d) 30 cells replaced

Table 4-9. Combined moderator strategy

Num. of cells replaced	0	6	12	18	24	30
k_{inf} at BOC	1.2744	1.3416	1.3750	1.4063	1.4111	1.3919

After replacing the graphite cell with 24 ZrH_2 cells, the model could reach its maximum k_{inf} at BOC. However, the cycle length can be reduced by about 150 days, which is not desirable.

4.3.3 FCM

FCM is a fuel that encases the TRISO particles within a dense silicon carbide matrix [63]. Various thermal reactors such as light-water reactors [65]–[69] and salt-cooled

reactors [70] were envisaged as applications for this fuel form. The first reason for the effort was to use SiC as a stable matrix to host coated fuel particles because it had higher radiation resistance than graphite. Second, a more rugged fuel was required to withstand accidents, repository conditions, and other issues. Additionally, the silicon carbide matrix is more dimensionally stable than graphite compacts because dimensional swelling (as well as other properties such as strength and thermal conductivity) reached saturation at relatively low flux levels, as shown in Figure 4-10 [70]. Therefore, the silicon carbide compact is not subject to anisotropic swelling limitations.

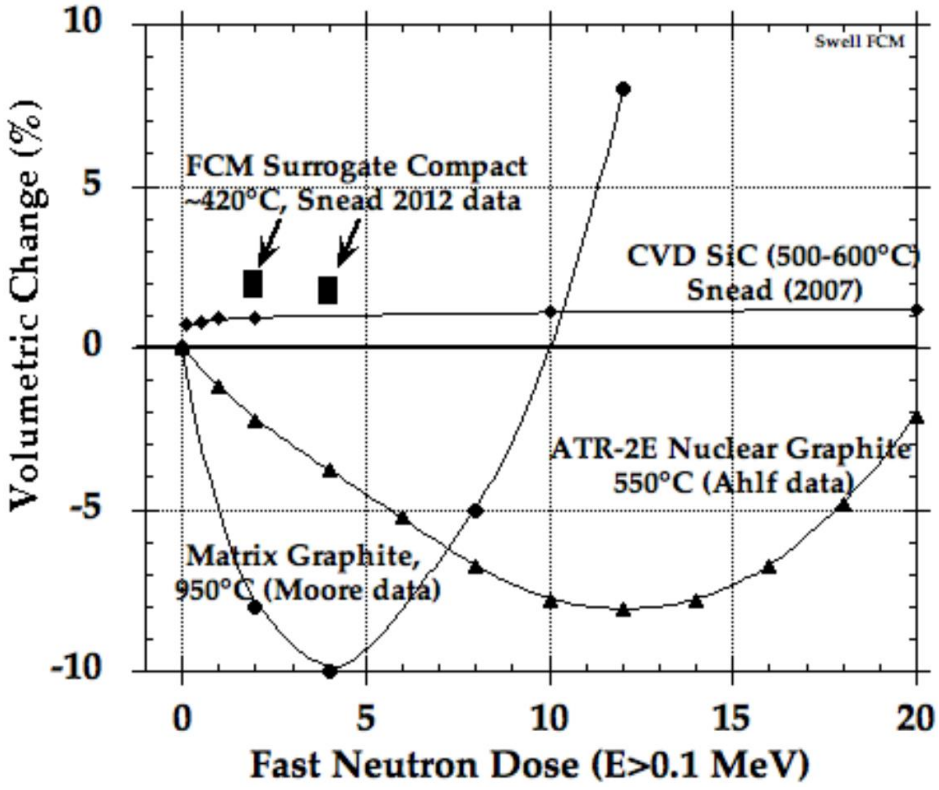

Figure 4-10. Dimensional change contrast of CVD SiC and FCM fuel with nuclear graphite ATR-2E and matrix graphite

This section explores the use of FCM for fuel compacts. The k_{eff} results for the FHR assembly model with different fuel channel pitches are plotted in the following Figure 4-11.

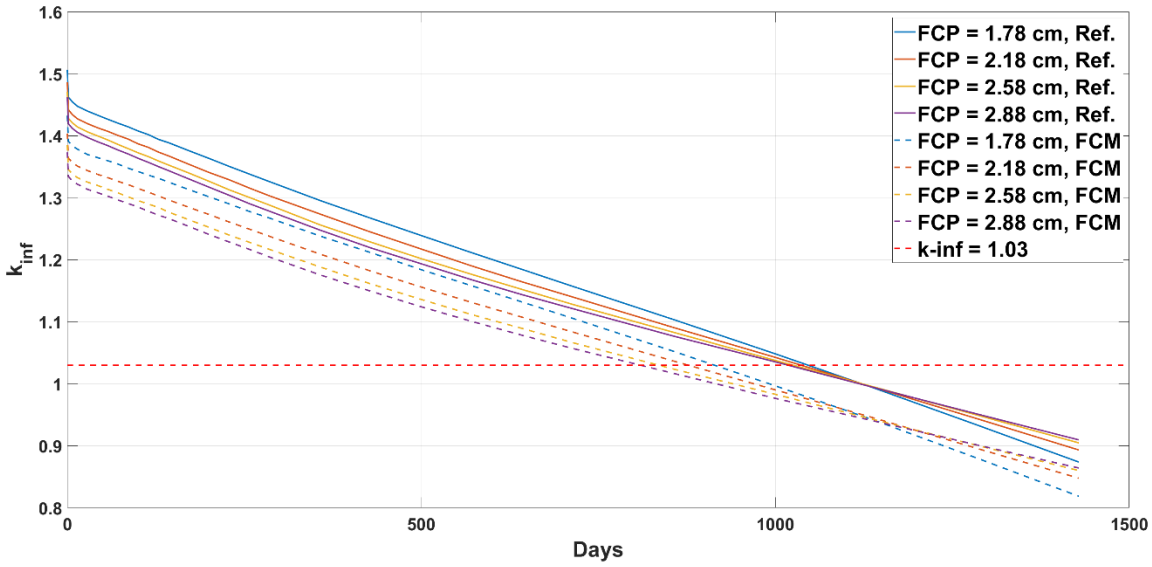

Figure 4-11. Neutronic performance of FCM fuel

The moderation of SiC is less than that of graphite. Moreover, SiC has a higher neutron absorption cross-section. Figure 4-11 shows that due to the relatively more significant absorption and poorer moderation of silicon carbide, the cycle length can be shortened by more than 100 days compared to the original design.

5. Conclusion

Chapter 5 concludes with a summary and recommendations for future research. In section 5.1, the research and the major findings of the dissertation are summarized. Section 5.2 offers recommendations for future efforts.

5.1 Summary

In this study, we have investigated the neutronic performance and fuel cycle characteristics of a commercial-scale prismatic block type of FHR design. The calculations were performed using the Monte Carlo code Serpent. Sensitivity analyses on various parameters were performed to optimize the cycle length and neutronic parameters. Based on that, this research proposed three feasible core designs with large, medium, and small core sizes (corresponding to different thermal outputs) to meet the market's requirements. Among the various design options, 165MWth small core design's fuel cycle was evaluated in detail. It was found that a larger fuel channel pitch (FCP) would have a relatively harder neutron spectrum, and yield a relatively longer cycle length, lower PPF, better fuel temperature coefficient (FTC), moderator temperature coefficient (MTC), and fuel and moderator temperature coefficient (FMTC). The full-core neutronic analyses of the proposed design utilizing the three-batch refueling and shuffling strategy were performed. To reach the equilibrium cycle, run-in cycle calculations were carried out for both cases w/

and w/o burnable poison (BP). The investigation was focused on the impacts of BP and FCP on fuel cycle length, power peaking factor, discharge burnup, and temperature coefficients. It was found that the burnable poison (Er_2O_3) is effective to hold down the excess reactivity, reduce the power peaking factor, and have a negligible penalty on the cycle length. More importantly, it can improve the MTC significantly. This core employs control blades located in the corners of the fresh fuel assemblies to control reactivity, a design that appears to be more than adequate for current FHR. At the CZP condition, the core shutdown margin (CSDM) was found to be sufficient when the control blade width is 0.4 cm, and the blade length is no shorter than 11 cm.

A novel core design which incorporating FIRM assembly, movable moderator, multi-batch strategy, and burnable poison management scheme was proposed and demonstrated in this study. During operation, only the graphite blocks surrounding the fresh fuel assemblies are designed to move out to reduce local excess reactivity and minimize neutron leakage, resulting in reduced BP requirement as well as a reduced PPF. A BP management scheme coupled with the movable moderator was also presented in this paper. The results indicate that such a scheme can suppress the excess reactivity swing under 6% Δk/k throughout the entire operation period with no penalty on the cycle length. Using the movable moderator results in an increase of approximately 8 MWd/kgHM in the discharge burnup and thus an extension of about 45-days in the cycle length. In addition, improvements were observed on all the calculated temperature reactivity coefficients (FTC, MTC, and FMTC). $NaF\text{-}ZrF_4$ and $NaF\text{-}BeF_2$ salts perform poorly in neutronic performance. $^7LiF\text{-}ZrF_4$ performs well in neutronics, which is comparable to the reference (FLiBe).

Three alternative moderators (SiC, ZrH_2, and $YH_{1.92}$) were studied, and they were found to be inferior to graphite. Fully ceramic micro-encapsulated fuel (FCM) was tested and observed to be not a desirable fuel form due to the relatively large neutron absorption of Si-28.

5.2 Recommendations for Future Work

Follow-on studies of the FHR design will have to include multiple aspects.

- Three-dimensional full-scale core calculations are required. On the current stage, the analyses were (assembly and full-core) based on a reduced model, a full-scale analysis will be required to validate the results and provide more design details, including axial burnup distribution, detailed power/temperature distribution, and etc.
- Thermal-hydraulic analyses coupling with neutronic results are needed. In spite of the fact that coolant salt (FLiBe) provides great flexibility in choosing the size of the coolant channel, it is still critical to perform a thermal-hydraulic analysis in conjunction with neutronic results to determine the final design.
- Dynamic system analyses must be performed for off nominal or accident scenarios. It is imperative to construct an FHR model for off nominal or accident analysis, which is important for ensuring that the transient behavior of the core demonstrates an adequate level of safety.
- The difference between spent fuel discharge burnup should be further reduced. The excessive difference in discharge burnup between the internal and peripheral

assemblies will result in unnecessary fuel waste, and this difference should be reduced in future work by further flattening the power distribution.

- More in-depth research about the novel design should be conducted, including an assessment of the engineering feasibility of utilizing movable graphite structures, replacement frequency of graphite components, and safety related analyses.
- Potential impact on the moderator temperature coefficient of the updated graphite thermal scattering law in the ENDF/B-VIII library.

Bibliography

[1] Briant, R. C., Weinberg, A. M., "Molten Fluorides as Power Reactor Fuels," *Nuclear Science and Engineering*, vol. 2, no. 6, pp. 797–803, Nov. 1957, doi: 10.13182/NSE57-A35494.

[2] Bettis, E. S., Cottrell, W. B., Mann, E. R., Meem, J. L., Whitman, G. D., "The Aircraft Reactor Experiment—Operation," *Nuclear Science and Engineering*, vol. 2, no. 6, pp. 841–853, Nov. 1957, doi: 10.13182/NSE57-A35497.

[3] Haubenreich, P. N., Engel, J. R., Prince, B. E., Claiborne, H. C., "MSRE Design and Operations Report. Part III. Nuclear Analysis," ORNL-TM-730, Feb. 1964. doi: 10.2172/4114686.

[4] Haubenreich, P. N., Engel, J. R., "Experience with the Molten-Salt Reactor Experiment," *Nuclear Applications and Technology*, vol. 8, no. 2, pp. 118–136, Feb. 1970, doi: 10.13182/NT8-2-118.

[5] Forsberg, C. W., Peterson, P. F., Pickard, P. S., "Molten-Salt-Cooled Advanced High-Temperature Reactor for Production of Hydrogen and Electricity," *Nuclear Technology*, vol. 144, no. 3, pp. 289–302, Dec. 2003, doi: 10.13182/NT03-1.

[6] Greene, S. R., Gehin, J. C., Holcomb, D. E., Carbajo, J. J., Ilas, D., Cisneros, A. T., Varma, V. K., Corwin, W. R., Wilson, D. F., Yoder, Jr, G. L., Qualls, A. L., Peretz, F. J., Flanagan, G. F., Clayton, D. A., Bradley, E. C., Bell, G. L., Hunn, J. D.,

Pappano, P. J., Cetiner, S. M., “Pre-Conceptual Design of a Fluoride-Salt-Cooled Small Modular Advanced High Temperature Reactor (SmAHTR),” Oak Ridge National Laboratory, ORNL/TM-2010/199, Feb. 2011. doi: 10.2172/1008830.

[7] Holcomb, D. E., Ilas, D., Varma, V. K., Cisneros, A. T., Kelly, R. P., Gehin, J. C., “Core and Refueling Design Studies for the Advanced High Temperature Reactor,” Oak Ridge National Laboratory, ORNL/TM-2011/365, Sep. 2011. doi: 10.2172/1025857.

[8] Wang, D., Yoder, G. L., Pointer, D. W., Holcomb, D. E., “Thermal Hydraulics Analysis of the Advanced High Temperature Reactor,” *Nuclear Engineering and Design*, vol. 294, pp. 73–85, Dec. 2015, doi: 10.1016/j.nucengdes.2015.08.017.

[9] Rahnema, F., Diamond, D., Serghiuta, D., Burke, P., “Phenomena, Gaps, and Issues for Neutronics Modeling and Simulation of FHRs,” *Annals of Nuclear Energy*, vol. 123, pp. 172–179, Jan. 2019, doi: 10.1016/j.anucene.2018.08.035.

[10] Ramey, K. M., Petrovic, B., “Monte Carlo Modeling and Simulations of AHTR Fuel Assembly to Support V&V of FHR Core Physics Methods,” *Annals of Nuclear Energy*, vol. 118, pp. 272–282, Aug. 2018, doi: 10.1016/j.anucene.2018.04.003.

[11] Huang, L. M., Petrovic, B., “Development of Methodology for Efficient Fuel Design Evaluation of the Advanced High Temperature Reactor (AHTR),” *Annals of Nuclear Energy*, vol. 121, pp. 646–660, Nov. 2018, doi: 10.1016/j.anucene.2018.07.001.

[12] Kotlyar, D., Lindley, B. A., Mohamed, H., “Improving Fuel Utilization in SmAHTR with Spectral Shift Control Design: Proof of Concept,” *Annals of Nuclear Energy*, vol. 104, pp. 53–63, Jun. 2017, doi: 10.1016/j.anucene.2016.12.037.

[13] Mehta, V., Kotlyar, D., "Core Analysis of Spectral Shift Operated SmAHTR," *Annals of Nuclear Energy*, vol. 123, pp. 46–58, Jan. 2019, doi: 10.1016/j.anucene.2018.09.013.

[14] Andreades, C., Cisneros, A. T., Choi, J. K., Chong, A. Y. K., Fratoni, M., Hong, S., Huddar, L. R., Huff, K. D., Krumwiede, D. L., Laufer, M. R., Munk, M., Scarlat, R. O., Zweibaum, N., Greenspan, E., Peterson, P. F., "Technical Description of the 'Mark 1' Pebble-Bed Fluoride-Salt-Cooled High-Temperature Reactor (PB-FHR) Power Plant," University of California, Berkeley, UCBTH-14-002, Sep. 2014.

[15] Andreades, C., Cisneros, A. T., Choi, J. K., Chong, A. Y. K., Fratoni, M., Hong, S., Huddar, L. R., Huff, K. D., Kendrick, J., Krumwiede, D. L., Laufer, M. R., Munk, M., Scarlat, R. O., Zweibau, N., "Design Summary of the Mark-I Pebble-Bed, Fluoride Salt–Cooled, High-Temperature Reactor Commercial Power Plant," *Nuclear Technology*, vol. 195, no. 3, pp. 223–238, Sep. 2016, doi: 10.13182/NT16-2.

[16] Forsberg, C., Wang, D., Shwageraus, E., Mays, B., Parks, G., Coyle, C., Liu, M., "Fluoride-Salt-Cooled High-Temperature Reactor (FHR) Using British Advanced Gas-Cooled Reactor (AGR) Refueling Technology and Decay Heat Removal Systems That Prevent Salt Freezing," *Nuclear Technology*, vol. 205, no. 9, pp. 1127–1142, Sep. 2019, doi: 10.1080/00295450.2019.1586372.

[17] Margulis, M., Shwageraus, E., "Advanced Gas-Cooled Reactors Technology for Enabling Molten-Salt Reactors Design - Estimation of Coolant Impact on Neutronic

Performance," *Progress in Nuclear Energy*, vol. 125, p. 103382, Jul. 2020, doi: 10.1016/j.pnucene.2020.103382.

[18] Forsberg, C., Richard, J., Pounders, J., Kochendarfer, R., Stein, K., Shwageraus, E., Parks, G., "Development of a Fluoride-Salt-Cooled High-Temperature Reactor (FHR) Using Advanced Gas-Cooled Reactor (AGR) Technology," *Transactions of the American Nuclear Society*, vol. 112, p. 566, Jun. 2015.

[19] Richard, J., Forget, B., Forsberg, C., Smith, K., "Neutronic Comparison of Liquid Salt Primary Coolants and Novel Assembly Design for a Fluoride Salt Cooled High-Temperature Test Reactor," *Transactions of the American Nuclear Society*, vol. 111, pp. 1076–1081, 2014.

[20] Richard, J., "Design Optimization and Analysis of a Fluoride Salt Cooled High Temperature Test Reactor for Accelerated Fuels and Materials Testing and Nonproliferation and Safeguards Evaluations," Doctoral thesis, Massachusetts Institute of Technology, 2016.

[21] Forsberg, C., Hu, L., Richard, J., Romatoski, R., Forget, B., Stempien, J., Ballinger, R., Sun, K., Carpenter, D., "Fluoride-Salt-Cooled High-Temperature Test Reactor (FHTR): Goals, Options, Ownership, Requirements, Design, Licensing, and Support Facilities," Massachusetts Institute of Technology, MIT-ANP-TR-154, Dec. 2014.

[22] Brown, N. R., Betzler, B. R., Carbajo, J. J., Wysocki, A. J., Greenwood, M. S., Gentry, C., Qualls, A. L., "Preconceptual Design of a Fluoride High Temperature Salt-Cooled Engineering Demonstration Reactor: Core Design and Safety Analysis," *Annals of Nuclear Energy*, vol. 103, pp. 49–59, May 2017, doi: 10.1016/j.anucene.2017.01.003.

[23] Qualls, A. L., Betzler, B. R., Brown, N. R., Carbajo, J. J., Greenwood, M. S., Hale, R., Harrison, T. J., Powers, J. J., Robb, K. R., Terrell, J., Wysocki, A. J., Gehin, J. C., Worrall, A., "Preconceptual Design of a Fluoride High Temperature Salt-Cooled Engineering Demonstration Reactor: Motivation and Overview," *Annals of Nuclear Energy*, vol. 107, pp. 144–155, Sep. 2017, doi: 10.1016/j.anucene.2016.11.021.

[24] Liu, Y., Yan, R., Zou, Y., Yu, S., Zhou, B., Kang, X., Hu, J., Cai, X., "Sensitivity/Uncertainty Comparison and Similarity Analysis Between TMSR-LF1 and MSR Models," *Progress in Nuclear Energy*, vol. 122, p. 103289, Apr. 2020, doi: 10.1016/j.pnucene.2020.103289.

[25] Ingersoll, D., "Status of Physics and Safety Analyses for the Liquid-Salt-Cooled Very High-Temperature Reactor (LS-VHTR)," Oak Ridge National Laboratory, ORNL/TM-2005/218, Dec. 2005. doi: 10.2172/885991.

[26] Forsberg, C. W., Peterson, P. F., Kochendarfer, R. A., "Design Options for the Advanced High-Temperature Reactor," *Proceedings of ICAPP*, vol. 8, pp. 8–12, 2008.

[27] Varma, V. K., Holcomb, D. E., Peretz, F. J., Bradley, E. C., Ilas, D., Qualls, A. L., Zaharia, N. M., "AHTR Mechanical, Structural, and Neutronic Preconceptual Design," Oak Ridge National Laboratory, ORNL/TM-2012/320, Sep. 2012. doi: 10.2172/1054145.

[28] Marsden, B., Mummery, A., Mummery, P., "Modelling the Coefficient of Thermal Expansion in Graphite Crystals: Implications of Lattice Strain Due to Irradiation and

Pressure," *Proc. R. Soc. A.*, vol. 474, no. 2218, p. 20180075, Oct. 2018, doi: 10.1098/rspa.2018.0075.

[29] DeHart, M. D., Ulses, A. P., "Benchmark Specification for HTGR Fuel Element Depletion," Nuclear Energy Agency of the OECD, NEA-NSC-DOC--2009-13, Jun. 2009.

[30] McEligot, D., Swank, W. D., Cottle, D. L., Valentin, F. I., "Thermal Properties of G-348 Graphite," Idaho National Laboratory, INL/EXT--16-38241, May 2016. doi: 10.2172/1330693.

[31] Swank, W. D., Valentin, F. I., Kawaji, M., McEligot, D. M., "Thermal Conductivity of G-348 Isostatic Graphite," *Nuclear Technology*, vol. 199, no. 1, pp. 103–109, Jul. 2017, doi: 10.1080/00295450.2017.1317530.

[32] Kim, E. S., No, H. C., Kim, B. J., Oh, C. H., "Estimation of Graphite Density and Mechanical Strength Variation of VHTR During Air-Ingress Accident," *Nuclear Engineering and Design*, vol. 238, no. 4, pp. 837–847, Apr. 2008, doi: 10.1016/j.nucengdes.2007.08.002.

[33] Forsberg, C. W., Peterson, P. F., "FHR, HTGR, and MSR Pebble-Bed Reactors with Multiple Pebble Sizes for Fuel Management and Coolant Cleanup," *Nuclear Technology*, vol. 205, no. 5, pp. 748–754, May 2019, doi: 10.1080/00295450.2019.1573619.

[34] Mohanty, S., Majumdar, S., "HTGR Graphite Core Component Stress Analysis Research Program–Task 1 Technical Letter Report," Nuclear Regulatory Commission, ML11276A009, Sep. 2011.

[35] Strydom, G., “IAEA Coordinated Research Project on HTGR Physics, Thermal-Hydraulics, and Depletion Uncertainty Analysis Prismatic HTGR Benchmark Specification: Phase II,” Idaho National Laboratory, INL/EXT--18-44815-Rev000, Apr. 2018. doi: 10.2172/1467563.

[36] McNally, K., Warren, N., Fahad, M., Hall, G., Marsden, B. J., “A Core-Monitoring Based Methodology for Predictions of Graphite Weight Loss in AGR Moderator Bricks,” *Nuclear Engineering and Design*, vol. 314, pp. 56–66, Apr. 2017, doi: 10.1016/j.nucengdes.2016.12.032.

[37] Tsang, D. K. L., Marsden, B. J., “The Development of a Stress Analysis Code for Nuclear Graphite Components in Gas-Cooled Reactors,” *Journal of Nuclear Materials*, vol. 350, no. 3, pp. 208–220, May 2006, doi: 10.1016/j.jnucmat.2006.01.015.

[38] Sun, Q., Ye, P., Peng, W., Yu, S., Zhou, H., Wang, J., “Wear of Graphite Pebbles Modeled Using a Macroscopic Particle Model in a Pneumatic Transport Lifting Pipe,” *Powder Technology*, vol. 361, pp. 581–590, Feb. 2020, doi: 10.1016/j.powtec.2019.11.075.

[39] Zhou, X., Tang, Y., Lu, Z., Zhang, J., Liu, B., “Nuclear Graphite for High Temperature Gas-Cooled Reactors,” *New Carbon Materials*, vol. 32, no. 3, pp. 193–204, Jun. 2017, doi: 10.1016/S1872-5805(17)60116-1.

[40] Pavlov, T. R., Lestak, M., Wenman, M. R., Vlahovic, L., Robba, D., Cambriani, A., Staicu, D., Dahms, E., Ernstberger, M., Brown, M., Bradford, M. R., Konings, R. J. M., Grimes, R. W., “Examining the Thermal Properties of Unirradiated Nuclear

Grade Graphite Between 750 and 2500 K," *Journal of Nuclear Materials*, vol. 538, p. 152176, Sep. 2020, doi: 10.1016/j.jnucmat.2020.152176.

[41] Yeo, S., Yun, J., Kim, S., Cho, M. S., Lee, Y.-W., "Fabrication Methods and Anisotropic Properties of Graphite Matrix Compacts for Use in HTGR," *Journal of Nuclear Materials*, vol. 499, pp. 383–393, Feb. 2018, doi: 10.1016/j.jnucmat.2017.11.055.

[42] Fukaya, Y., Goto, M., Nakagawa, S., Nakajima, K., Takahashi, K., Sakon, A., Sano, T., Hashimoto, K., "Reactor Physics Experiment in a Graphite-Moderation System for HTGR," *EPJ Web Conf.*, vol. 247, p. 09017, 2021, doi: 10.1051/epjconf/202124709017.

[43] Powers, J. J., Wirth, B. D., "A Review of TRISO Fuel Performance Models," *Journal of Nuclear Materials*, vol. 405, no. 1, pp. 74–82, Oct. 2010, doi: 10.1016/j.jnucmat.2010.07.030.

[44] Brown, N. R., "A Review of In-Pile Fuel Safety Tests of TRISO Fuel Forms and Future Testing Opportunities in Non-HTGR Applications," *Journal of Nuclear Materials*, vol. 534, p. 152139, Jun. 2020, doi: 10.1016/j.jnucmat.2020.152139.

[45] Marshall, D., "AGR-5/6/7 Fuel Specification," Idaho National Laboratory, INL/MIS-11-21423-Rev008, Mar. 2017.

[46] Marshall, D. W., "AGR-5/6/7 Fuel Fabrication Report," Idaho National Laboratory, INL/EXT--19-53720-Rev000, May 2019. doi: 10.2172/1512795.

[47] Williams, D. F., “Assessment of Candidate Molten Salt Coolants for the Advanced High Temperature Reactor (AHTR),” Oak Ridge National Laboratory, ORNL/TM-2006/12, Mar. 2006. doi: 10.2172/885975.

[48] Žáková, J., Talamo, A., “Analysis of the Reactivity Coefficients of the Advanced High-Temperature Reactor for Plutonium and Uranium Fuels,” *Annals of Nuclear Energy*, vol. 35, no. 5, pp. 904–916, May 2008, doi: 10.1016/j.anucene.2007.09.003.

[49] Richard, J., Wang, D., Yoder, G., Carbajo, J., Williams, D., Forget, B., Forsberg, C., “Implementation of Liquid Salt Working Fluids into TRACE,” *Proceedings of ICAPP*, vol. 2014, Apr. 2014.

[50] Leppänen, J., Pusa, M., Viitanen, T., Valtavirta, V., Kaltiaisenaho, T., “The Serpent Monte Carlo Code: Status, Development and Applications in 2013,” *Annals of Nuclear Energy*, vol. 82, pp. 142–150, Aug. 2015, doi: 10.1016/j.anucene.2014.08.024.

[51] Leppänen, J., “Serpent–A Continuous-Energy Monte Carlo Reactor Physics Burnup Calculation Code,” *VTT Technical Research Centre of Finland*, vol. 4, 2013.

[52] “Serpent - A Continuous-Energy Monte Carlo Neutron and Photon Transport Code.” https://serpent.vtt.fi/serpent/

[53] Cullen, D., “ENDF/B-VII.1 Versus ENDF/B-VII.0: What’s Different?,” Lawrence Livermore National Laboratory, LLNL-TR-548633, Mar. 2012. doi: 10.2172/1047779.

[54] Wang, D., “Optimization of a Seed and Blanket Thorium-Uranium Fuel Cycle for Pressurized Water Reactors,” Doctoral thesis, Massachusetts Institute of Technology, 2003.

[55] Qasim Awan, M., Cao, L., Wu, H., Shen, W., Li, Z., “Neutronic Design Study of a Small Modular IPWR Loaded with Accident Tolerant-Fully Ceramic Micro-Encapsulated (AT-FCM) Fuel,” *Nuclear Engineering and Design*, vol. 335, pp. 18–29, Aug. 2018, doi: 10.1016/j.nucengdes.2018.04.023.

[56] Williams, D.F., “Assessment of Candidate Molten Salt Coolants for the NGNP/NHI Heat-Transfer Loop,” Oak Ridge National Laboratory, ORNL/TM--2006/69, Jun. 2006. doi: 10.2172/1360677.

[57] Braun, J., Sauder, C., Lorrette, C., Gélébart, L., Loupias, G., Chaffron, L., “Processing and Properties of SiC/SiC Composites for Nuclear Power Plant Applications,” presented at the PACRIM 11, Jeju, South Korea, Aug. 2015.

[58] Hu, X., Schappel, D., Silva, C. M., Terrani, K. A., “Fabrication of Yttrium Hydride for High-Temperature Moderator Application,” *Journal of Nuclear Materials*, vol. 539, p. 152335, Oct. 2020, doi: 10.1016/j.jnucmat.2020.152335.

[59] Davies, N. F., Forrester, R. E., “Effects of Irradiation on Hydrided Zirconium--Uranium Alloy NAA 120-4 Experiment,” Atomics International Division, AI-AEC--12963, Jun. 1970.

[60] Simnad, M. T., “The U-ZrHx Alloy: Its Properties and Use in TRIGA Fuel,” *Nuclear Engineering and Design*, vol. 64, no. 3, pp. 403–422, Apr. 1981, doi: 10.1016/0029-5493(81)90135-7.

[61] Haslett, R. A., “Space Nuclear Thermal Propulsion Program,” Phillips Laboratory, PL-TR-95-1064, May 1995.

[62] Van Houten, R., “Selected Engineering and Fabrication Aspects of Nuclear Metal Hydrides (Li, Ti, Zr, and Y),” *Nuclear Engineering and Design*, vol. 31, no. 3, pp. 434–448, Jan. 1974, doi: 10.1016/0029-5493(75)90178-8.

[63] Terrani, K. A., Kiggans, J. O., Katoh, Y., Shimoda, K., Montgomery, F. C., Armstrong, B. L., Parish, C. M., Hinoki, T., Hunn, J. D., Snead, L. L., “Fabrication and Characterization of Fully Ceramic Microencapsulated Fuels,” *Journal of Nuclear Materials*, vol. 426, no. 1–3, pp. 268–276, Jul. 2012, doi: 10.1016/j.jnucmat.2012.03.049.

[64] Terrani, K. A., Kiggans, J. O., Silva, C. M., Shih, C., Katoh, Y., Snead, L. L., “Progress on Matrix SiC Processing and Properties for Fully Ceramic Microencapsulated Fuel Form,” *Journal of Nuclear Materials*, vol. 457, pp. 9–17, Feb. 2015, doi: 10.1016/j.jnucmat.2014.10.034.

[65] Terrani, Kurt A., Snead, L. L., Gehin, J. C., “Microencapsulated Fuel Technology for Commercial Light Water and Advanced Reactor Application,” *Journal of Nuclear Materials*, vol. 427, no. 1–3, pp. 209–224, Aug. 2012, doi: 10.1016/j.jnucmat.2012.05.021.

[66] Gentry, C., Maldonado, I., Godfrey, A., Terrani, K., Gehin, J., Powers, J., “A Neutronic Investigation of the Use of Fully Ceramic Microencapsulated Fuel for Pu/Np Burning in PWRs,” *Nuclear Technology*, vol. 186, no. 1, pp. 60–75, Apr. 2014, doi: 10.13182/NT13-75.

[67] George, N. M., Maldonado, I., Terrani, K., Godfrey, A., Gehin, J., Powers, J., "Neutronics Studies of Uranium-Bearing Fully Ceramic Microencapsulated Fuel for Pressurized Water Reactors," *Nuclear Technology*, vol. 188, no. 3, pp. 238–251, Dec. 2014, doi: 10.13182/NT14-3.

[68] Shapiro, R. A., Vincenzi, M. J., Fratoni, M., "Optimization of Fully Ceramic Micro-Encapsulated Fuel Assembly for PWR," Proceedings of PHYSOR 2014, JAEA-CONF--2014-003, 2014.

[69] Lee, Y., Cho, N. Z., "Three-Dimensional Single-Channel Thermal Analysis of Fully Ceramic Microencapsulated Fuel via Two-Temperature Homogenized Model," *Annals of Nuclear Energy*, vol. 71, pp. 254–271, Sep. 2014, doi: 10.1016/j.anucene.2014.03.039.

[70] Forsberg, C., Terrani, K. A., Snead, L. L., Katoh, Y., "Fluoride-Salt-Cooled High-Temperature Reactor (FHR) with Silicon-Carbide-Matrix Coated-Particle Fuel," *Transactions of the American Nuclear Society*, vol. 107, pp. 907–910, 2012.